

David Michael Sorger, BSc

**Fading Study and Optimization of a Time-Temperature Profile  
for the Routine Readout of a LiF:Mg,Ti  
Thermoluminescent Detector**

**MASTER'S THESIS**

to achieve the university degree of

Diplom-Ingenieur

Master's degree programme: Technical Physics

submitted to

**Graz University of Technology**

Supervisor

Assoc.Prof. Dipl.-Phys. Dr.rer.nat. Wolfgang Sprengel

Institute of Material Physics

Co-Supervisor: DI Dr. Hannes Stadtmann, MBA  
Seibersdorf Labor GmbH

## **AFFIDAVIT**

I declare that I have authored this thesis independently, that I have not used other than the declared sources/resources, and that I have explicitly indicated all material which has been quoted either literally or by content from the sources used. The text document uploaded to TUGRAZonline is identical to the present master's thesis.

---

Date

---

Signature

## **Acknowledgement**

At first I would like to thank Dipl.-Ing. Dr.techn. Hannes Stadtmann. As an expert in thermoluminescence dosimetry, it was a great honour to work in his group. His knowledge and support were of great value. Additionally, I want to thank Assoc.Prof. Dipl.-Phys. Dr.rer.nat. Wolfgang Sprengel for his grateful support and interesting discussions. His lecture in radiation physics inspired me to find my way into the field of radiation protection.

Finally I thank my beloved girlfriend Theresa for everything.

# Contents

<b>1. Introduction</b>	<b>6</b>
<b>2. Theory</b>	<b>8</b>
2.1. Ionising Radiation . . . . .	8
2.2. Radioactive Conversion . . . . .	8
2.3. Sources of ionising radiation . . . . .	10
2.4. Radiation Protection . . . . .	11
2.5. Luminescence Phenomena . . . . .	14
2.6. Basics of Thermoluminescence and General Model . . . . .	15
2.7. Glow Curves and Analysis Models . . . . .	17
2.8. Thermoluminescent Materials and their Lattice Defects . . . . .	21
2.9. Dose from the TL signal . . . . .	24
2.10. Fading . . . . .	24
<b>3. Materials and Methods</b>	<b>28</b>
3.1. TLD-100 Dosimeters . . . . .	28
3.2. Harshaw TLD Reader 8800 . . . . .	30
3.3. Responses . . . . .	31
3.4. Time-Temperature Profile . . . . .	32
3.5. Irradiation of TLDs . . . . .	36
3.6. Individual Calibration of TLD Cards . . . . .	39
3.7. Simulation of Glow Curves . . . . .	40
3.8. Fading Study . . . . .	42
3.9. Readout-Optimization . . . . .	45
<b>4. Results and Discussion</b>	<b>48</b>
4.1. Individual Calibration . . . . .	48
4.2. Fading Study under Routine Conditions . . . . .	50
4.3. Fading Function . . . . .	66
4.4. Fading Study with different TTPs . . . . .	75
4.5. Readout-Optimization . . . . .	81
4.6. Validation of new TTPs . . . . .	90
<b>5. Conclusion</b>	<b>97</b>
<b>A. Appendix</b>	<b>104</b>
A.1. Time-Temperature Profiles of the Experiments . . . . .	104
A.2. Additional Details to the Fading Study . . . . .	105
A.3. Additional Details to the Readout-Optimization . . . . .	110
<b>B. Abbreviations</b>	<b>119</b>

## Abstract

LiF:Mg,Ti thermoluminescent dosimeters (TLDs) are frequently used for personal dosimetry by individual monitoring services (IMS) all over the world. Ionizing radiation leads to a signal storage in the TLD which can be deduced as the absorbed dose. The readout is performed with the controlled heating of the detector element according to a defined time-temperature profile (TTP). The output of this procedure is a time dependent light signal, called glow curve (GC). The fading in LiF:Mg,Ti is an influencing problem and leads to higher uncertainties. The main effects of fading are Pre-irradiation-fading and Post-irradiation-fading. Pre-irradiation-fading is characterized by the spontaneous collapse of the available energy gaps in the crystal at storage temperature. Post-irradiation-fading appears after irradiation due to the loss of the trapped electrons. In some IMSs preheating the LiF:Mg,Ti detector element is performed to reduce the fading. The application of different Time-Temperature-Profiles and the influence of fading in the routines of the individual monitoring services were investigated at Seibersdorf Labor GmbH. Several Harshaw TLD-100 dosimeters have been irradiated and fully read out after different periods of storage. A following fading study with an optimization of the standard procedure was performed. As a result a mathematical fading-function could be introduced and the TTP could be optimized.

# 1. Introduction

Radiation protection is a multidisciplinary field with a wide range of applications. Since radiation research started in the last century, technologies were developed to utilize the complex effects of ionising radiation for advantage. Whether X-ray tubes are used for computer tomography or radioactive sources were applied in the quality control for material defects and food control in the industry; the use of ionising radiation is established in today's applications. However, the frequent contact with ionising radiation leads to an ensemble of regulations and laws to decrease, monitor and control the exposure. "Radiation protection and nuclear safety denotes the protection of people and the environment against radiation risks, and the safety of facilities and activities that give rise to radiation risks." [1] According to the handling of ionising radiation a safe work with ionising radiation has to be guaranteed. Due to this, a field of monitoring and the evaluation of the exposure was established - the dosimetry. Several dosimetric techniques to measure ionising radiation have already been developed. This includes active and passive dosimetric methods. The most frequent monitoring procedure is called thermoluminescence dosimetry, which is a passive method. It is specifically applied to monitor people on workplaces (personal dosimetry) and monitor on locational use (environmental dosimetry). The thermoluminescence dosimetry is based on using an item, that holds a card with thermoluminescent crystals that represent the functional unit inside, i.e., the detectors. These small thin crystals are engraved into optical transparent Teflon<sup>TM</sup> in so called thermoluminescent dosimeters (TLDs). During irradiation the crystals store tissue-equivalent signals, which can be extracted by controlled heating in form of a light output. This simple system allows an affordable, fast and full determination of several dose quantities. Therefore an accurate readout system is needed. The way the readout system heats the crystal belongs to a predefined profile with defined heating rate, preheat and maximum temperature over time, called the time-temperature-profile (TTP). The output of the readout procedure is a time dependent light signal, called glow curve (GC). This study concentrates on a thermoluminescent material made of lithium fluoride doped with magnesium and titanium (LiF:Mg,Ti). The readout procedure was designed to be fast, which is important for the practical readout of several thousands of TLDs every month. This study deals with the questions, whether the glow curve is really of highest quality and how reproducible the light signal is. According to this, two main problems were pointed out, which were targeted to solve:

- The first problem refers to the quality of the glow curve, that implicates the investigation of the optimization of the time-temperature profile.
- The second problem is the influence of a material effect, called fading, which has impact on the reproducibility of the glow curve. Fading is a time dependent effect that appears in two forms: The pre-irradiation fading before the exposure with ionising radiation occurs and the post-irradiation fading after the exposure. The first one is determined by the loss of sensitivity and the second one by the loss of

the signal.

The aim of this thesis is to answer the upper two questions and additionally focus on an introduction of a fading function and optimal TTPs with lower fading exposure.

## 2. Theory

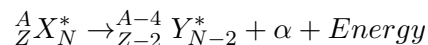
### 2.1. Ionising Radiation

Radiation in general is a common denotation for any kind of electromagnetic energy- or particle-transfer. It is called *ionising* radiation, if this transport in form of a wave is able to remove electrons from the atomic shell. For this, the radiation has to overcome the so called binding energy  $E_B$  of the electrons in the atomic shell, which is between  $10^{-19}$  and  $10^{-16}$  J. Furthermore, ionising radiation is considerable into *direct* and *indirect* ionising radiation. The *direct* ionising radiation includes all types of electrical charged particles like electrons, protons or alpha particles (helium nucleus), which causes immediate ionisation of atoms due to collisions. *Indirect* ionising radiation covers the types without electrical charge and which transfers the collision energy into an electrical charged collision partner, e.g., an electron. Then this partner causes ionising of other particles. Examples for this type of radiation are neutrons (collision with protons) and photons. [2]

### 2.2. Radioactive Conversion

Atomic nuclei are called *radioactive*, if they pass from an instable state to a stable configuration under the spontaneous emission of radiation and the release of energy. The conversion is stochastic. Because of that it depends on coincidence and is not foreseeable for the individual nucleus. There are several kinds of radioactive conversions and decay: (referred to Krieger et.al. [2])

- **Alpha decay:** Alpha particles are batches of two protons and two neutrons, which are emitted from a mother nucleus; e. g. they are double ionised  ${}^4\text{He}$ -atoms. Due to this evidence the proton number and the neutron number <sup>1</sup> of a mother nucleus decrease each by two. The interaction only takes place according to the strong force. They have the following decay equation:



- **Beta conversion:** A radionuclide with an isobar neighbour of low binding energy (in the common N-Z diagram) often leads to a  $\beta$  conversion. This is a conversion of nucleons with a following  $\beta$  emission. On the one hand there is a  $\beta^-$  conversion where neutrons are converted into protons with an electron emission (the  $\beta^-$  particle) and an emission of an positron-anti-neutrino  $\bar{\nu}_e$ . On the other hand there is a  $\beta^+$  conversion where protons are converted into neutrons with an positron-neutrino (the  $\beta^+$  particle) and an emission of an electron-neutrino  $\nu_e$ . The conversion equations are:

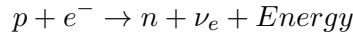


---

<sup>1</sup>N is the neutron number, Z is the proton number, A is the number of all nuclei

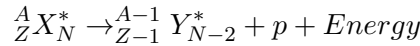


- **Electron Capture:** The electron has a small probability to be present in the nucleus of the atom. If it happens it is possible that the electron gets captured in the nucleus and interacts with a proton. This reaction occurs to set the atom in a more stable state.



- **Gamma conversion:** During radioactive decays and conversions it is sometimes not possible to create particles, because of the lack of excitation energy. In this case the present conversion energy is transformed into an high energetic photon - the gamma quantum.

- **Proton- and Neutron decay:** These decays are very rare, because usually alpha- or beta-emission are of higher probability to take place. The nuclei-equation for a proton emission is



- **Spontaneous fission:** It happens for heavy nuclei in very unstable configurations. The fission-parameter  $s$  gives a value for the probability:

$$s = \frac{Z^2}{A}$$

Due to instabilities in the deformation coulomb repulsion of between two parts of the heavy nuclei appears. Due to that the nuclei deformed more and more, till the fission takes place (figure 1 right).

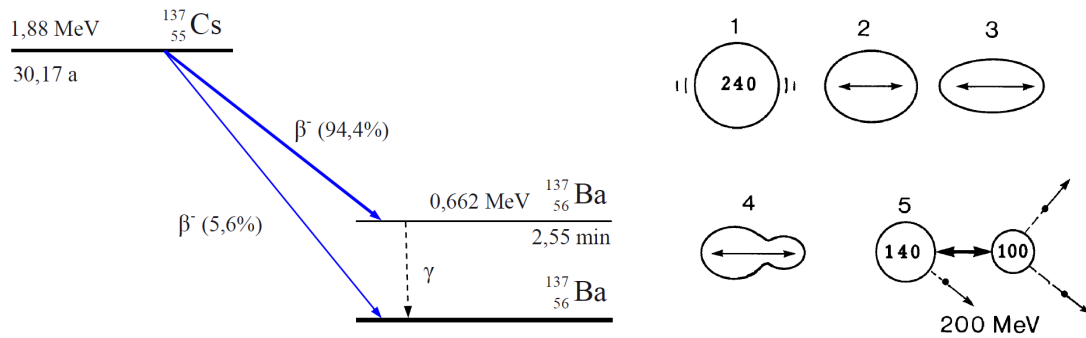


Figure 1: Left: Decay-scheme of  ${}^{137}\text{Cs}$ . Right: Spontaneous fission of a heavy nucleus. [2].

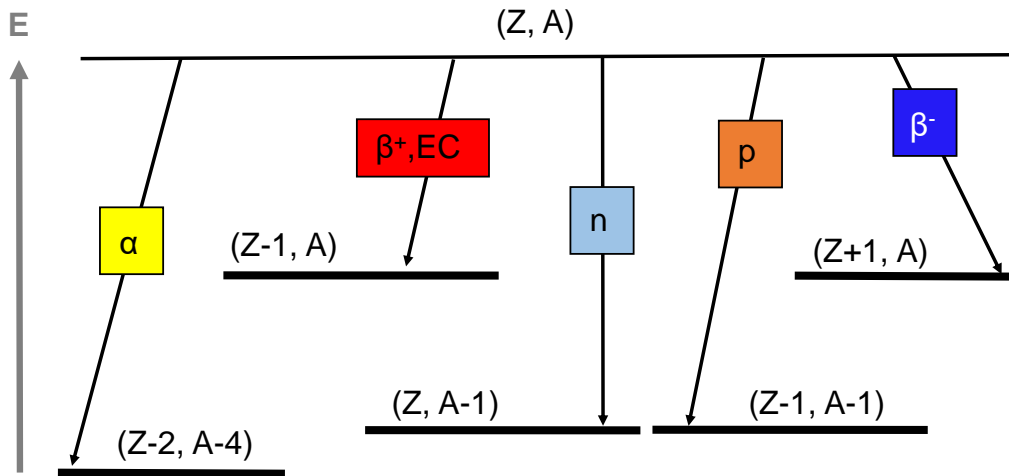


Figure 2: Radioactive conversions. The vertical axis describes the energy scale [2].

### 2.3. Sources of ionising radiation

The most common dosimetric relevant sources of ionising radiation are listed below:

- **X-ray tube:** The X-ray tube is a construction with an anode and a cathode which requires a heating voltage. The electrons get accelerated by an induced electric field and interact on the anode surface. Due to this the electrons release a part of their energy in continuous x-rays and in addition produce characteristic x-rays.
- **Radioactive conversion:** There are several radioactive isotopes, which are used in medical and industrial applications. Some examples of these isotopes are  $^{60}\text{Co}$ ,  $^{137}\text{Cs}$  and  $^{90}\text{Sr}$ . The applications of these materials are the radiation therapy, the material testing with gammamats and the quality control of food.
- **Accelerators:** There are several types of accelerators in medical use. The classical linear accelerator is applied in radiation therapy to extinguish cancer cells. These accelerators could be applied for  $\gamma$ -ray production. [3] Furthermore cyclotrons are used to accelerate heavy ions (e. g. Carbon-dioxide).
- **Cosmic radiation:** It consists of a solar component (H-nuclei, He-nuclei and heavy nuclei) and a galactic component (protons and heavy nuclei). [4]
- **Terrestrial radiation:** This radiation is composed of the natural radionuclides of the decay chain (decay chain of uranium and thorium) and the primordial radionuclides (long half lives e.g.  $^{40}\text{K}$ ,  $^{87}\text{Rb}$ ). [4]

## 2.4. Radiation Protection

### 2.4.1. Dose Quantities

Radiation protection is defined by the International Atomic Energy Agency (IAEA) as "The protection of people from harmful effects of exposure to ionizing radiation, and the means for achieving this". [1] To achieve this aim, methods were established to measure the exposure of ionising radiation on the human body. Materials and detectors were developed and dose quantities were introduced.

There are three categories of dose quantities which were defined by the International Commission on Radiological Protection (ICRP) and the International Commission on Radiation Units and Measurements (ICRU):

- **Physical Quantities:** These quantities are directly measured and consider only the interaction of ionising radiation with the detector.

- The *absorbed dose*  $D$  is the quotient of  $d\bar{\epsilon}$  by  $dm$ , where  $d\bar{\epsilon}$  is the mean energy imparted to matter of the mass  $dm$  by ionising radiation, which is

$$D = \frac{d\bar{\epsilon}}{dm} \quad (1)$$

and the SI unit is  $\text{J kg}^{-1}$  with the special unit gray (Gy). [5]

- The *KERMA*  $K$  (*K*inetic *E*nergy *R*elaxed per unit *M*Ass) for ionizing uncharged particles, is another energy quantity in  $\text{J/kg}$  with the special unit gray (Gy). It is the quotient of the mean sum of the initial kinetic energies of all charged particles  $dE_{\text{tr}}$  by the mass of a material  $dm$ . [6]

$$K = \frac{dE_{\text{tr}}}{dm} \quad (2)$$

- **Protection Quantities** [5]: Including the biological effects of ionising radiation there are defined protection quantities:

- The *equivalent dose* in an organ or tissue  $H_{\text{T}}$  is defined as the average absorbed dose  $D_{\text{T,R}}$  times the radiation weighting factor  $w_{\text{R}}$  in the volume of an organ or tissue T.

$$H_{\text{T}} = w_{\text{R}} \cdot D_{\text{T,R}} \quad (3)$$

The values of  $w_{\text{R}}$  are dimensionless and differ from the type of radiation (e. g. photon: 1,  $\alpha$ -particle: 20). The quantity is equivalent to the SI unit  $\text{J kg}^{-1}$  and its special name is Sievert (Sv) that considers biological effects.

- The *effective dose* is a complex dose quantity. The unit is Sv and it considers the tissue damages. It is in relation to the organ equivalent dose. [7] "In radiation protection, the mean value of the absorbed dose averaged over the

specified organ or tissue is correlated with the detriment due to stochastic effects. The averaging of absorbed doses in organs and tissues, and the summing of weighted mean doses in different organs and tissues comprise the basis for the radiation protection quantity." [8] According to that the effective dose is defined as

$$E = \sum_{\text{T}} w_{\text{T}} \cdot H_{\text{T}}. \quad (4)$$

where  $\sum w_{\text{T}} = 1$  and is defined by the ICRP 103 [5].

- **Operational Quantities** [9]: There are three kinds of the operational quantities. The ambient dose equivalent and the directional dose equivalent were defined at a point in a radiation field. They are the dose equivalent that would be produced by the corresponding expanded and aligned field, in the ICRU sphere at a depth,  $d$ .
  - The *ambient dose equivalent*,  $H^*(d)$  is defined on the radius opposing the direction of the aligned field. [9]
  - The *directional dose equivalent*,  $H'(d, \Omega)$ , is defined on the radius in a specified direction,  $\Omega$ . [9]
  - "The personal dose equivalent,  $H_p(d)$ , is the dose equivalent in soft tissue, at an appropriate depth,  $d$ , below a specified point on the body." [9]

All quantities are used to estimate the protection quantities and have the unit  $\text{J kg}^{-1}$  with the special name Sievert (Sv). They are based on the concept of dose equivalent:  $H = Q \cdot E$ . [10]

#### 2.4.2. Radiation Protection Dosimetry

The dosimetry has the purpose to detect ionising radiation and evaluate the dose. Furthermore there are standards and regulations to keep the population below the defined dose limits. People who work with radioactive substances or with x-ray tubes are more exposed and therefore they are classified with higher dose limits in category A and B for exposed persons. They are monitored with dosimeters during the exposure and have a maximum dose limit of 20 mSv per year for category A and 6 mSv per year for category B.

In radiation protection two types of effects on the human body are distinguished [5], [11]: **Stochastic effects**: These are all biological effects with a random influence to the human body. Only the interaction probability to the tissue depends on the dose, not the severity of the exposure. If stochastic damages appear, it can cause cancer or genetic defects.

**Tissue reactions**: By this reaction the severity of the exposure depends on the dose. In general it is a local effect on a body region. Furthermore, these reactions can cause the radiation sickness and the radiation dead.

The dosimetric detection of ionising radiation is performed by

- active dosimeters and
- passive dosimeters.

*Active dosimeters* immediately display the value of the dose. For these dosimeters electronic methods are the common way to detect ionising radiation. The advantage of these dosimeters is an immediate display of the exposure on ionising radiation. [12]

*Passive dosimeters* just track the absorbed dose and need to be read out by an active readout process. Basically during exposure they absorb a dose-equivalent signal and can be read out at a certain time. The application of such dosimeters is in the environmental dosimetry, where the evaluation of the dose values takes place in certain time periods and the personal monitoring, where people get their dose tracked once per month or in extended time periods. [13]

### 2.4.3. Thermoluminescence Dosimetry

Thermoluminescence dosimeters (TLDs) are passive dosimeters, which are common for the monitoring use in personal dosimetry. Widespread applications take place in medicine and industry. Nowadays the TLD systems are the most widespread monitoring systems in Europe (Eurados Report 2018 [14]). The effects of thermoluminescence are utilized with TLDs, which is introduced in section 2.6. Basically ionizing radiation leads to a signal storage of the absorbed dose by irradiation. Heating the TLD material leads to the emission of light, which can be measured. With all their advantages and disadvantages lithium fluoride was chosen, according to the kind of application and the research outcomes of the last decades. [15]

The analysis and methods of the TLD signal are described in section 2.7.3.

## 2.5. Luminescence Phenomena

The phenomenon of luminescence is described by the process of emission of optical radiation from a material, i.e., it exhibits the emission of light. Luminescent materials have the ability to absorb the energy and convert a fraction into optical radiation. The glow of micro-organisms, insects and heated minerals were probably the first luminescence phenomena observed (McKinlay, 1981 [16]). The first documented observation was in 1664; Sir Robert Boyle discovered the luminescence behaviour of a diamond by holding it above a candle or heating it with body heat to see the 'glimmering light'. (Boyle, 1664 [17])

The most occurring effects in application research are fluorescence (prompt emission) and phosphorescence (delayed emission) with its special case, the thermoluminescence (thermally accelerated emission). The means of excitation are various. The principles of these effects are depicted in figure 3. [16]

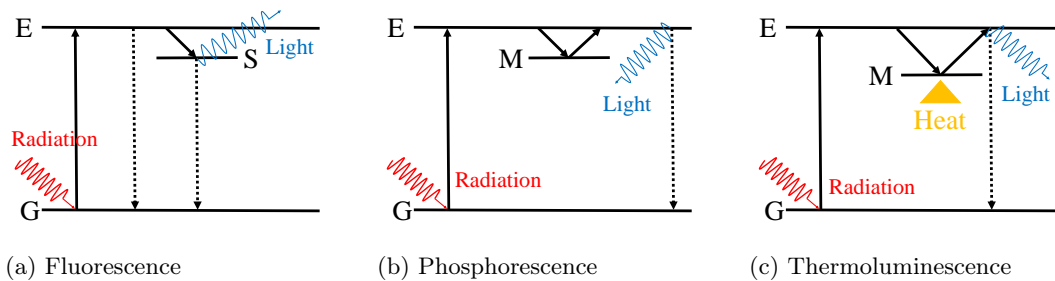


Figure 3: Simple examples of luminescence processes with G to be the ground state, E to be the excited state, M to be the metastable state and S to be the intermediate state (McKinlay, 1981 [16]).

- (a) Fluorescence describes "the prompt return of an electron from an excited state either directly to the ground state or via an allowed transition from an intermediate state S (relaxation)" [16]. The luminescence photons are of longer wavelength than the photons that provided the excitation. [16]
- (b) Phosphorescence describes the "return of an electron from an excited state to the ground state and is delayed by the metastable state M. Direct transition of an electron from the metastable state to the ground state is forbidden." [16]
- (c) Thermoluminescence is physically "the return of electrons trapped in the metastable state" [16] - like Phosphorescence. The difference is, that these traps are more stable and heat is required for accelerating the process. [16]

Examples of other luminescence effects occur through other means of excitation, like the release of chemical energy (chemiluminescence) or the occurrence of electric fields (electroluminescence) - further effects are listed in McKinlay et al., 1981 [16].

In this work it was focused on thermoluminescence (TL). The term of TL was coined by Wiedmann and Schmidt in 1895; thus pioneer work has been done for the following decades in the research of radioactivity. [16]

## 2.6. Basics of Thermoluminescence and General Model

Beside the effects of luminescence, thermoluminescence (TL) is one of the so called Thermally Stimulated Phenomena. Included in the TL-family, as described by Chen and Kirsh (1981) [18], in addition to TL there are Thermally Stimulated Conductivity (TSC), Thermally Stimulated Capacitance (TSCap), Thermally Stimulated Polarisation (TSPC) and Depolarisation Currents (TSDC). [16]

Several models for TL materials have been developed, especially for the common material lithium fluoride doped with magnesium and titanium - abbreviated LiF:Mg,Ti. This is one of the most applied materials in TL dosimetry. It is one of the most investigated TL materials. LiF:Mg,Ti and its isotopic variants are the end products of a dozen of studies. Even already in the early 1980s it turned out that there are few TL materials which are comparable with LiF:Mg,Ti, according to its practical applicability and signal stability in dosimetry. [16]

Another example of an well applicable material in TL dosimetry is LiF:Mg,Cu,P. The big advantage of this material is that the phenomena of fading (described in section 2.10) has no significant presence. In an extensive study of 17 months, no significant fading occurred (Luo, 2008 [19]). However, the disadvantage is the higher sensitivity to high temperatures, which requires more sophisticated handling.

Other well applicable TL materials are listed in table ??.

**General Model** A simple model (resumed by McKinlay et. al., 1981 [16]) describes the TL production with the band model and considers, for the exposure to ionising radiation, two stages to divide in:

- ionisation and electron trapping,
- electron and hole recombination with photon emission.

Impurities within the lattice and structural defects, which occur in a crystal, make it possible for electrons to occupy energy states which are forbidden in a perfect crystal. Illustrated in figure 4 an energy band configuration for each stage shows the process in the band model. The following steps refer to McKinlay et.al., 1981 [16].

**Step 1:** Ionising radiation is absorbed by the material and thereupon free electrons are produced, i.e., transfer electrons from the valence band to the conduction band over the Fermi level.

**Step 2:** The electrons are free and move through the crystal.

**Step 3:** If the trapping levels near the conduction band (such as E) are present (obvious in all TL materials), electrons may become trapped with a certain probability (see the Boltzmann equation (5)). Electron trap centres are lattice defect centres.

**Step 2':** Induced by ionising radiation, the production of free electrons causes the production of free positive holes, which are free moving in the valence band.

**Step 3':** The holes may become trapped by hole trapping levels (like H) near the valence band. (also see the Boltzmann equation (5)).

**Step 4':** Hole centres are thermally unstable and may decay rapidly at normal room temperature.

**Step 4 and 5:** Trapped electrons remain in their traps until they are provided energy to escape. The electron traps have a specific energy depth  $\Delta E$  and they need thermal stimulation, which comes from the addition of thermal energy from ambient temperature. Then the electrons may be released from the trap E and recombine with holes at the luminescence centre L. The excess energy is then released as visible light or ultraviolet photons.

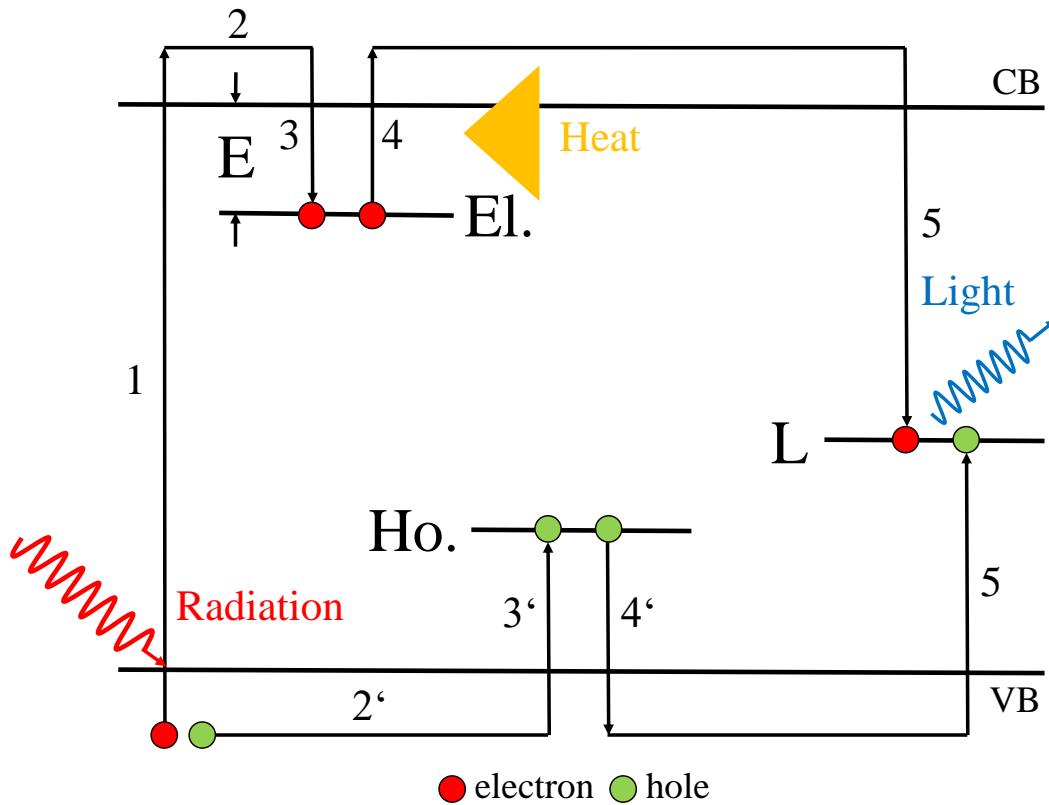


Figure 4: Simple energy band model of thermoluminescence, (McKinlay, 1981 [16]).

## 2.7. Glow Curves and Analysis Models

The radiative transitions that are monitored when recording the TL emission are called Glow Curves (GC). The release of the stored energy in the form of luminescence is stimulated by an increase in the temperature of the sample. Thus, there is the thermally stimulated return of the system from its metastable state to equilibrium, with a portion of the excess energy being released as light. The peak in figure 5 shows that the luminescence emission increases with rising the temperature. As the temperature increases further, the luminescence intensity decreases rapidly. Usually several glow peaks are observed to contribute to the complete glow curve. Each glow peak within the glow curve corresponds to the release of electrons, holes or interstitial atoms from different defect species, each characterised by its own value for  $E$  and  $s(T)$  (for detail information about the parameters see section 2.7.1)(Mc Keever, 1995 [20]).

An example of a glow curve is depicted in figure 6.

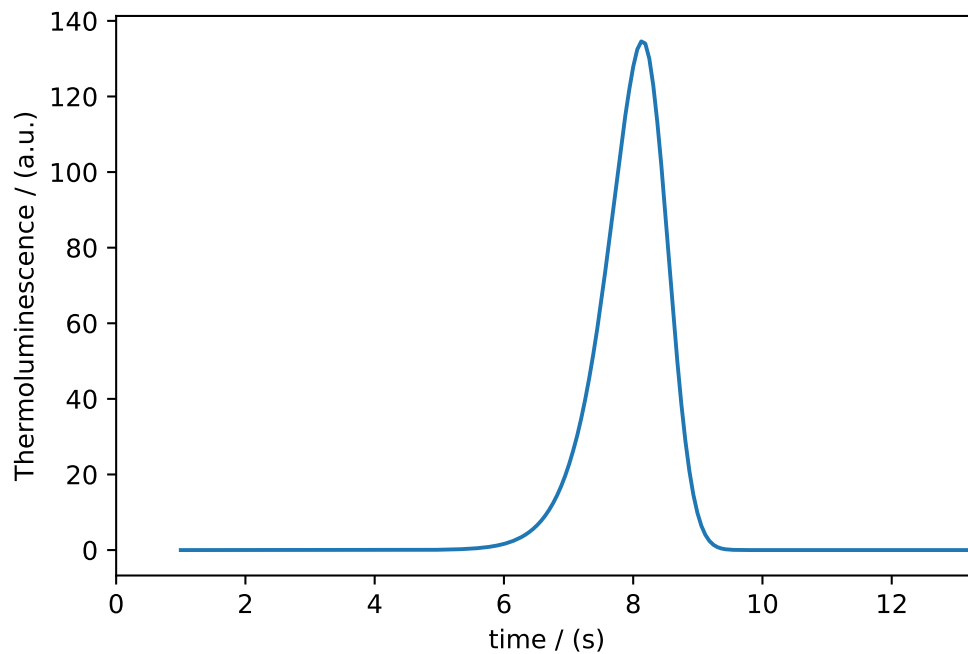


Figure 5: Schematic TL glow peak.

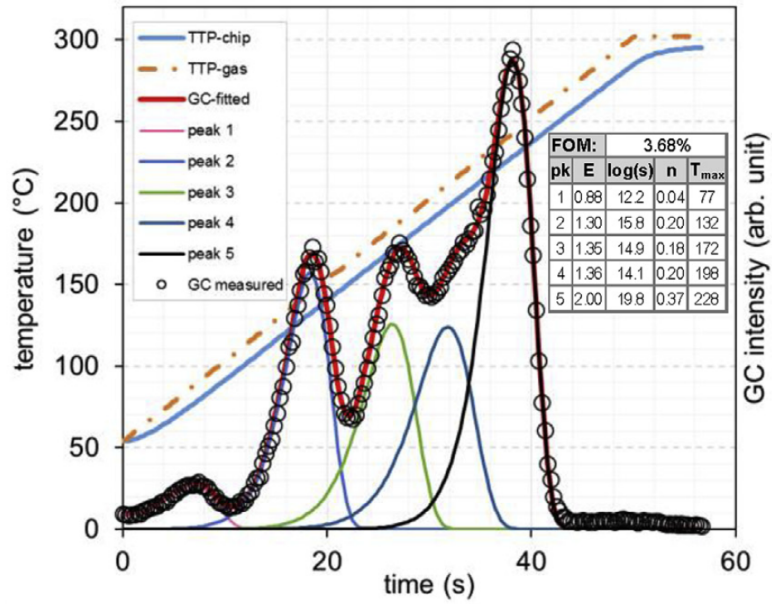


Figure 6: TL glow curve with linear heating profile. Example of a fitted GC with linear TTP, based on the analysis of a CGCD spreadsheet application using Microsoft Excel 2013, applied on GC measurement data; the spreadsheet application was written by Stadtmann and Wilding in SL [21].

### 2.7.1. A kinetic first Order Model

For an accurate mathematical description of the GC-shape (TL signal versus temperature), there is the need to make assumptions on the physical procedure. There is considered

- a single electron-hole pair,
- a single electron-hole recombination with a related probability,
- material containing defects which give rise to a single electron trap and one type of recombination centre and
- the probability of charge retrapping is neglected.

This is the so-called "first-order" description by Randall and Wilkins, 1945 [22]. As described in the simple band-gap model in section 2.6 where there is a probability per unit time to release an electron from the trap; it is assumed to be described by the Boltzmann equation

$$p(T) = s(T) \cdot \exp \left[ -\frac{E}{k_B T} \right], \quad (5)$$

"where  $p(T)$  is the probability per unit time,  $k_B$  is the Boltzmann constant,  $T$  is the temperature,  $E$  is the depth of the electron-trap and  $s(T)$  is the so called frequency factor (weekly temperature dependent). This is related to the local lattice vibrational frequency and the entropy change associated with the charge release." (Mc Keever et al., 1995 [20])

To come to the formulation of the first order kinetics, the following rate equation is introduced:

$$-\frac{dn}{dt} = n \cdot s \cdot \exp\left[-\frac{E}{k_B T}\right], \quad (6)$$

with  $n$  to be the concentration of the trapped electrons. It is assumed that  $s$  is approximately temperature independent ( $s(T) \approx s$ ).

The core of the first order kinetic model is that there is no retrapping, as considered above. The TL signal  $I$  (e. g. the intensity of TL emission) depends on three rates:

- the rate of photon emission
- the rate of the trapped electrons which are released and
- the rate of arrival at luminescence centres.

The following equation (referring to Mc Keever, 1995 [20]) considers these aspects:

$$I = -\Phi \frac{dn}{dt} = \Phi \cdot n \cdot s \cdot \exp\left[-\frac{E}{k_B T}\right], \quad (7)$$

$\Phi$  is a constant - the so called luminescence efficiency.

The essential part for the temperature in this formulation is the assumption of a linear heating rate  $\beta$  in the form of

$$\beta = \frac{dT}{dt},$$

and is rewritten as

$$\frac{dn}{dt} = \frac{dn}{dT} \cdot \frac{dT}{dt} = \beta \cdot \frac{dn}{dT}. \quad (8)$$

With the substitution of equation (6) to (8) it follows

$$\frac{dn}{dT} = -\frac{1}{\beta} \cdot n \cdot s \cdot \exp\left[-\frac{E}{k_B T}\right],$$

or

$$\frac{dn}{n} = -\frac{s}{\beta} \cdot \exp\left[-\frac{E}{k_{\text{B}}T}\right] \cdot dT, \quad (9)$$

which can be integrated to get the following equation:

$$\ln\left(\frac{n}{n_0}\right) = -\int_{T_0}^T \frac{s}{\beta} \cdot \exp\left[-\frac{E}{k_{\text{B}}T'}\right] \cdot dT'. \quad (10)$$

$n_0$  is introduced as the number of electrons present in the trap at starting time  $t_0$  and the starting temperature  $T_0$ . Finally the substitution of equation (10) in (7) leads to the formulation of the first order kinetics (derivation based on McKinlay, 1981 [16]):

$$I(T, t) = n_0 \cdot \Phi \cdot s \cdot \exp\left[-\frac{E}{k_{\text{B}}T}\right] \cdot \exp\left[-\frac{s}{\beta} \cdot \int_{T_0}^T \exp\left[-\frac{E}{k_{\text{B}}T'}\right] \cdot dT'\right]. \quad (11)$$

The intensity of the GC  $I_{(T,t)}$  is introduced as dependent on the heating-temperature and the readout-time. A linear heating rate  $\beta$  is assumed in the first Order kinetic model.

### 2.7.2. Other Models

**Second Order kinetic model** In the first order kinetic model only a system of single electron - hole recombination was considered. The introduction of retrapping of one electron in the first Order model leads to the second order model. [16]

**General Order kinetic model** The generalisation of the retrapping leads to the general Order model. It came out that this is a useful framework in the analysis of TL glow curves. [23] In this assumption  $m$  and  $n$  are the occupation densities of the recombination centres and trapping centres respectively. The case of  $m = n$  is highly unlikely in a complex material with many overlapping glow peaks. [24]

**Localised transition model** The localised transition model is another example for TL calculation. It allows "charge recombinations which occur by transitions through an excited state common to a trap and luminescence centre pair." [25] The model has been applied by Templer to fit anomalous fading. He came up with the result: when thermal activation energies are low, the tunnelling transitions become dominant. [25]

### 2.7.3. Analysis and Methods

In GC-analysis, various methods are used to make statements about the quality of the GC. To estimate the TL signal value of a GC, a series of methods were reviewed by Horowitz in 2013 [26]. These common methods are listed here:

- **Peak height method:** The peak heights in the GC are measured. The disadvantage here is that at low TL signals, the peak height maximum is influenced by statistical fluctuation and not always valid.
- **Measure the integral of the emitted light** over the whole temperature interval  $\Delta T$ .
- **Range of interest (ROI) method:** It is to integrate the TL-signal between two pre-determined temperatures and define the ROI. In addition there could be added more than one ROI. Its statistical fluctuations appear because of the overlap of several peaks and of the subjective choice of the temperature-points.
- **Computerised glow curve deconvolution (CGCD):** "It delivers the greatest amount of information, but the time and effort involved may not be justified in practical situations or when precision/accuracy are not an important requirement." [26]

However, CGCD takes the GC signal and with the first order kinetic formulation it fits the GC near to the measured curve. In addition it splits the GC into its glow peaks. It should be mentioned that this procedure is a mathematical conception to evolve the signal.

The big challenge to handle with, is indeed that in complex GCs a single peak can have a large number of different configurations. The aim is to get the best figure of merit (FOM). [27] Several ways lead to a physical proper FOM.

## 2.8. Thermoluminescent Materials and their Lattice Defects

The most common TL material in personal dosimetry is lithium fluoride (LiF). Other less widely used materials are lithium borate ( $\text{Li}_2\text{B}_4\text{O}_7$ ), calcium sulphate ( $\text{CaSO}_4$ ) and calcium fluoride ( $\text{CaF}_2$ ). TLD crystals are produced in different varieties of shapes and thicknesses.

The *European Radiation Dosimetry Group* (Eurados) performs frequent intercomparisons for personal dosimeters. The current data from the Eurados Report 2018 shows a high use of commercial TLD systems with different TLD materials and combinations. [20]

Table 1: Number of systems per TL detectors with different materials and combinations, Eurados Report 2018 [14]

TLD	Number of systems
LiF	2
LiF:Mg,Ti	44
LiF:Mg,Cu,P	14
Li <sub>2</sub> B <sub>4</sub> O <sub>7</sub> /CaSO <sub>4</sub>	15
CaSO <sub>4</sub> :Dy	2
CaSO <sub>4</sub> :Dy/PTFE	1
LiF/Li <sub>2</sub> B <sub>4</sub> O <sub>7</sub> :Mn,Si	1

### 2.8.1. LiF:Mg,Ti

Lithium fluoride in form of LiF:Mg,Ti is one of the most widespread TL materials on the market. The big advantage of LiF materials is the tissue-equivalence of the effective atomic number  $Z_{eff}$ . "Ideally, the atomic number,  $Z$ , of the dosimetric material should match that of the biological tissue ( $Z_{eff} = 7.42$ ) as much as possible so the measurement becomes independent of the incident energy of the photons." [28] The physical forms differ from its application: One can produce it with single cristal, extruded rods, hot pressed chips, powder or impregnated PTFE (McKeever, 1995[20]).

Described by McKeever the lattice defects in LiF have a massive influence to the TL properties. LiF consists of two interpenetrating fcc lattices - one for Li<sup>+</sup> ions and one for F<sup>-</sup> ions, where thermal defects appear. Magnesium enters the lattice in form of Mg<sup>2+</sup> substitutionally for Li<sup>+</sup> with charge neutrality being preserved by the presence of excess Li<sup>+</sup> vacancies. Titanium enters the LiF lattice substitutionally for Li<sup>+</sup> in either the Ti<sup>3+</sup> or Ti<sup>4+</sup>. The manufacturers produce TL materials in many kinds and shapes which are labeled. LiF:Mg,Ti has also labels according to the isotope composition. [20]

Table 2: LiF:Mg,Ti and its labels according to the manufacturers Thermo Fisher Scientific Inc., 2007 [29] and TLD Poland, 2019 [30]

Special name	Manufacturer	Isotop composition
TLD-100	Thermo Fisher	Li natural
MTS-N	TLD Poland	Li natural
TLD-600	Thermo Fisher	Li-6 isotope
TLD-700	Thermo Fisher	Li-7 isotope

### 2.8.2. Properties of TL Materials

**Dose response** "The dose response  $F(D)$  is defined as the functional dependence of the intensity of the measured TL signal upon the absorbed dose. The ideal dosimetric

material would have a linear response. However, there appear a variety of non-linear effects. In particular, one often finds with increasing dose that the response is linear, then supra-linear and then sub-linear." (MacKeever et.al., 1995 [20]) The relative normalised dose response function  $f(D)$  is defined as

$$f(D) = \frac{F(D)/D}{F(D_1)/D_1} \quad (12)$$

"where  $F(D)$  is the dose response at a dose  $D$ , and  $D_1$  is a low dose at which the dose response is linear." [20]

An ideal dosimeter has a dose response of  $f(D) = 1$  over a wide dose range. [20]

**Sensitivity** As described by Mc. Keever [20], the sensitivity of a particular TLD material is formally defined as the TL signal strength per unit of absorbed dose. Because of the parameters depending on the TL readout system, the definition is quite difficult. Sensitivity now is defined in a relative way referring to the dose response of TLD-100 as reference value.

$$S(D) = \frac{F(D)_{\text{material}}}{F(D)_{\text{TLD-100}}} \quad (13)$$

$F(D)_{\text{material}}$  is the dose response, measured with the same TL readout system as TLD-100. Furthermore,  $S(D)$  is also a function of the heating rate  $\beta$ .

**Fading** This property is of great importance. Fading is described in detail in chapter 2.10.

### 2.8.3. Lattice Defects

Lattice defects are responsible for trapping the excited electrons in different energy levels. They are distinguished between three kinds of lattice defects (McKinlay, 1981 [16]):

1. **Thermal or intrinsic defects:** In a (hypothetically) pure crystal this defects would appear. The higher the temperature of the lattice the higher is the number of defects. With a fast decrease of the temperature, one can 'freeze' the number of the defects. This defects appear in two ways: [16]
  - *Frenkel defect:* Displaced atoms occupy an interstitial position.
  - *Schottky defects:* In ionic crystals it could appear that pairs (i. e. anions and cations) are missing.

2. **Extrinsic defects:** These defects are caused by doping the crystal with traces of different materials. For example TLD-100 is doped with traces of titanium and magnesium. McKinlay, 1981 [16]
3. **Radiation-induced defects:** The electrons stored in the lattice itself build this defects and displaced lattice atoms (caused by ionizing radiation) as well. (McKinlay, 1981 [16])

A general model, that includes the theory of the lattice defects - energy levels for the electron-hole pairs - was introduced in chapter 2.6.

## 2.9. Dose from the TL signal

The absorbed dose  $D$  can be expressed from the light emission, obtained during the readout, by

$$D = M \cdot F_c \quad (14)$$

with  $D$  to be the absorbed dose,  $F_c$  to be the individual calibration factor of the detector and  $M$  to be the TL signal, measured with the integral under the GC. Equation 14 is a simple expression. Several parameters can influence the dose, which leads to a general expression. Examples are the influences of the individuality of the crystals, the experimental conditions, the difference of the exposure beam to the calibration beam and the influence of the non-linearities in the TL signal. [27]

## 2.10. Fading

It was noted that one of the most problematic features of LiF:Mg,Ti dosimetry is the occurrence of reactions between defects in the crystal. During the time intervals of pre-irradiation annealing and the irradiation there occur sensitivity changes and charge transfer/release at all stages of the irradiation - which leads to fading. (Horowitz and Moscovitch, 2013 [26])

### 2.10.1. Principle in TLD-100

Electrons get trapped after irradiation of the TL material. The old definition of fading consists of the unintentional release of these electrons before the readout. There fading can have a thermal or an optical stimulated release. [16] The major parts are the low energy peaks (the first three). Fading has been described and observed in various studies ([19], [26], [31], [32], [33] and many more). The principle in the old definition has always been the same: After irradiation the fading is high, because the low energy peaks 1 and

2 fade. Peak 3 is unstable. In a modern definition, this would be one part of the phenomenon - called the *signal loss*. [19]

B. Ben and Y.S. Horowitz came up with a fading study [34] that shows that peak 4 grows over the first nine months of storage and then starts to decay, while the peak 5 decays rapidly in the first six months and then stays constant and begins to increase slowly. However, peak 4 and 5 in one range of interest (ROI) give the best equivalent of the irradiated dose. Moreover there is a fading-dependence on the ambient temperature. An investigation from 1983 [35] showed that the field dosimeters exhibit higher fading rates during the summer months.

According to the first Order kinetic model (described in section 2.7.1), the signal loss is mathematically described as preheating at storage temperature over a long period of time.

A modern definition of fading has been done by Luo, 2008: "Fade is the process of gradually reducing the capability of producing the response due to radiation exposure." [19] It is distinguished between signal loss and sensitivity loss. The fading rate of LiF based TL materials depends on many experimental parameters: ([19],[31], [32])

- storage temperature
- heading profile (TTP)
- annealing (TTP)
- radiation type
- time (post- and pre-irradiation intervals)

An interesting aspect is, according to the study of Doremus and Higgins [31] that there is no significant difference in fading between photon and high LET exposure. LET is the linear energy transfer and describes the energy transfer per distance in the absorber.

Another aspect, which is often neglected (and not important in practical use) is the effect of athermal fading. This effect is described by the quantum mechanical tunneling of the trapped charge to the recombination site [36], and the localised transition which do not take place via the delocalised bands [25].

### 2.10.2. Signal Loss and Sensitivity Loss - the modern Description

Based on the storage time before or after radiation, fading has two components (the modern description refers to Luo, 2008 [19]):

- **Signal loss:** Also called post-irradiation fading, it is the reduction of the response signal after the material has been irradiated. It appears due to the spontaneous recombination of electrons and holes in the low energy gaps at storage temperature.
- **Sensitivity loss:** Also called pre-irradiation fading, it is the reduction of the capability to produce the response before the material is irradiated. It appears due

to the spontaneous collapse of the energy gaps in the crystal at storage temperature.

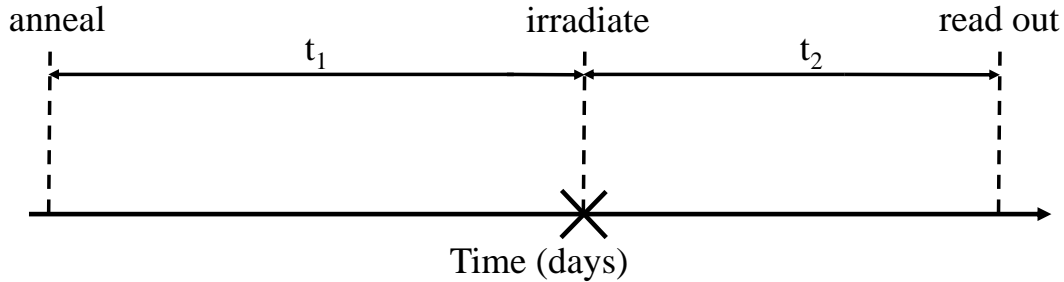


Figure 7: Graph with  $t_1$  to be the time between anneal and irradiation, that causes the loss of sensitivity and is called pre-irradiation time. The  $t_2$  to be the time between irradiation and the readout, that causes the loss of signal and is called post-irradiation fading. The concept of the irradiation scheme is based on [31]

In the study of Harshaw on fading, Ling Lou et. al. [19] came to some interesting conclusions about the relationship between the signal loss and the sensitivity loss for LiF materials: The signal loss and the sensitivity loss do not fade at the same rate and are dependent of the storage temperature. At low temperatures, signal loss is faster than the sensitivity loss due to the preservation of low temperature peak 2. In relation to that peak, the degeneration of the higher energy peaks occur faster. There is a transition period, when peak 2 is completely faded. At that point, the sensitivity starts to fade faster than the signal, which was stated by Luo in the experiment as beyond 60-80 days. A readout TTP, with preheat, is able to reduce the fading. Different material isotopes, sizes and forms have insignificant effects on fading.

**Fading Function** A fading function describes the process in a mathematical formulated way. It can be a function of time and storage temperature. The parameters in the function are experimentally estimated. Usually it shows a exponential behavior. [19]  
A good approximation of a fading function considers the physical accuracy. This could be archived using several parameters in the function with physical meanings and units.

**Comparison between LiF:Mg,Ti and LiF:Mg,Cu,P** The LiF:Mg,Ti is compared to the second common material in use <sup>2</sup>: LiF:Mg,Cu,P:

<sup>2</sup>see the intercomparison of Eurados, 2018 [14]

Table 3: Comparison between two common TL materials according to Luo et. al. [19].

	<b>LiF:Mg,Ti</b>	<b>LiF:Mg,Cu,P</b>
<b>Fading</b>	Typical fading characteristics	No significant fading detectable
<b>Thermal stability</b>	heatable to $T > 300^{\circ}\text{C}$	irreversible damage for $T > 250^{\circ}\text{C}$

LiF:Mg,Cu,P shows a big advantage according to its fading behavior. As described in section 2.6, there was no significant fading during a 17 months period. On the other hand LiF:Mg,Cu,P does not have the high thermal resistivity than LiF:Mg,Ti. The big advantage of LiF:Mg,Ti is that the signal shows no supralinearities according to the estimation of the dose. LiF:Mg,Cu,P is a more sensitive material, which is better for low energy exposure. But the disadvantage in the handling with LiF:Mg,Cu,P is that calibration needs more attention due to faster changing calibration coefficients. [19]

## 3. Materials and Methods

### 3.1. TLD-100 Dosimeters

The TLD-100 system used in this work is a thermoluminescence dosimeter for personal dosimetry. For people who work with radioactive substances, or in related environments, where they are exposed to ionising radiation, wearing dosimeters is obligatory. The main applications of TLDs are in medicine and in industry. The predefined time-period of wearing a dosimeter is one month for dosimeters in Seibersdorf Laboratories. The dosimeters pass through a cycle: At the first month they are sent back to the IMS, where the dosimeters will be read out. Then they get assigned to a new person and after one month of wearing the dosimeter, they are sent back to the IMS and read out again. The central part of the dosimeter is a LiF:Mg,Ti crystal, which is manufactured as chip with a size of 3.2 mm x 3.2 mm and a thickness of 0.38 mm. The chips are encased in transparent Teflon<sup>TM</sup> between two aluminium sheets that form the TLD card. They are manufactured with up to four chips inside. For the application of personal dosimetry, cards with two chips are commonly used. As depicted in figure 8, TLD cards are sealed in personalized packages and worn in a card holder. One of the chips in the holder is shielded by an aluminium disc, which makes it possible to distinguish between high energy and low energy ionising radiation.



Figure 8: On the left side a TLD-100 card with two LiF:Mg,Ti chips encased in Teflon™ (orange circles) is shown. A sealed card for the customer is depicted in the middle. On the right side the card is placed in a badge. In the green circle there is an aluminium disc which shields one of the two elements. ©Seibersdorf Laboratories

### 3.2. Harshaw TLD Reader 8800

The overall experiments of this studies were performed using the Harshaw TLD Reader 8800. The TLD System 8800 consists of a card reader and a personal computer (PC). The PC controls the operation of the card reader, i.e. the Time-Temperature Profile (TTP). The TTP controls the readout process and is responsible for the structure of the glow curve (GC). The principle of the hardware mechanism is described as follow: Nitrogen is received from an external supply. Solenoid valves stops the gas flow to the detectors on the TLD card which are not to be read out. The gas is heated in the form of the TTP in electrical resistance heating tubes. Four nozzles located within 3 mm of each detector guarantees a focused hot gas beam. Then four photomultiplier tubes (PMTs) detect the TL emitted light signal. Charge integration accumulates the PMT signal, digitised and reported to the PC as 200 ordered pairs (channels) of the TL signal; a GC is recorded. In addition, the TTP information is also digitised with the TL signal. Finally the system converts the TL signal into an element value in nano Coulomb (nC). [37]



Figure 9: TLD Reader 8800 with four photomultipliers, heater nozzles, heating tube, depots for TLD cards and internal irradiation source.

### 3.2.1. Dose calculation of the TLD System 8800

The general procedure to estimated the dose out of the TL signal is described in section 2.9. In contrast to equation (14), the formula for the output data is

$$D_{\text{system}} = M \cdot k \cdot F_{\text{st}} \quad (15)$$

with  $D_{\text{system}}$  to be the detector dose in  $\mu\text{Sv}$ ,  $M$  to be the TL signal in nC,  $k$  to be the individual calibration factor of the detector (described as  $F_c$  in section 2.9) and  $F_{\text{st}}$  to be a specific parameter of the readout system in  $\mu\text{Sv}/\text{nC}$ . It includes the influence of the TTP as well as the noise of the high voltage and the photomultiplier. The term  $k$  is a calibrated to 1 correction for the reference glow curves. A batch of average GCs is used as reference to calibrate the  $k$  values.

### 3.3. Responses

The TL signal value unit is in nano Coulomb (nC). Values in nano Sievert (nSv) were calculated by using a calibrated TTP, which gives the TLD signal multiplied with  $F_{\text{st}}$ . However, it does not matter whether the values are estimated in nC or in  $\mu\text{Sv}$ , because the irradiation reference dose during all irradiation experiments was equal.

The procedure to get relative responses was as follows:

The element values  $M$  in nC were measured. The irradiations took place in the dosimetry laboratory (DEL) with an equal dose for all samples. Every measurement was evaluated with the following response equation:

$$r_i = \frac{M_i}{D} \quad (16)$$

with  $r_i$  to be the response of one measurement  $i$  in  $\text{nC}\mu\text{Sv}^{-1}$ ,  $M_i$  to be the element value of one measurement  $i$  in nC and  $D$  to be the dose in  $\mu\text{Sv}$ . Then the average of all measurements of one time combination of  $t_1$  and  $t_2$  (see section 2.10.2) is

$$M = \frac{1}{N} \sum_i^N M_i, \quad (17)$$

with  $N$  to be the number of measurements. Relative responses  $R$  were then calculated with one response  $r_{\text{ref}}$  as reference in a time combination of  $t_1$  and  $t_2$ . That followed

$$R_k = \frac{r_k}{r_{\text{ref}}} = \frac{M_k \cdot D}{D \cdot M_{\text{ref}}} = \frac{M_k}{M_{\text{ref}}} \quad (18)$$

for one relative response  $R_k$  of  $k$  relative responses.  $M_k$  is one average element value of one time combination and  $M_{\text{ref}}$  is the reference for all time combinations.

**Adaptation coefficients** In this work adaptation coefficients  $\alpha$  were introduced to handle with the fact that for the fading study several experiments were necessary. To handle with the different readout times these coefficients were estimated for each experiment to get comparable relative responses  $R$ . The adaptation coefficients  $\alpha$  were estimated with an overlap process. Finally the coefficients could be multiplied by each individual element value  $M_j$ . The equation is

$$R_j = M_j \cdot \alpha \quad (19)$$

with  $R_j$  the relative response for one individual measurement. The average of the measurements for one time combination leads to the relative response for one time combination.

$$R = \frac{1}{N} \sum_i^N R_i \quad (20)$$

### 3.4. Time-Temperature Profile

The Time-Temperature profile (TTP) is the reader specific temperature per time combination. The concept was developed by Harshaw and described by Moscovitch. [37] It is a concept with the following main parameters.

- the preheat temperature  $T_{\text{Ph}}$ ,
- the preheat time  $t_{\text{Ph}}$ ,
- the heating rate on the temperature ramp  $\beta$ ,
- the maximum temperature  $T_{\text{max}}$  and
- the acquisition time  $t_{\text{aq}}$ . [37]

This procedure has direct effects on the shape and size of the GC. A scheme of such a TTP is depicted in figure 10.

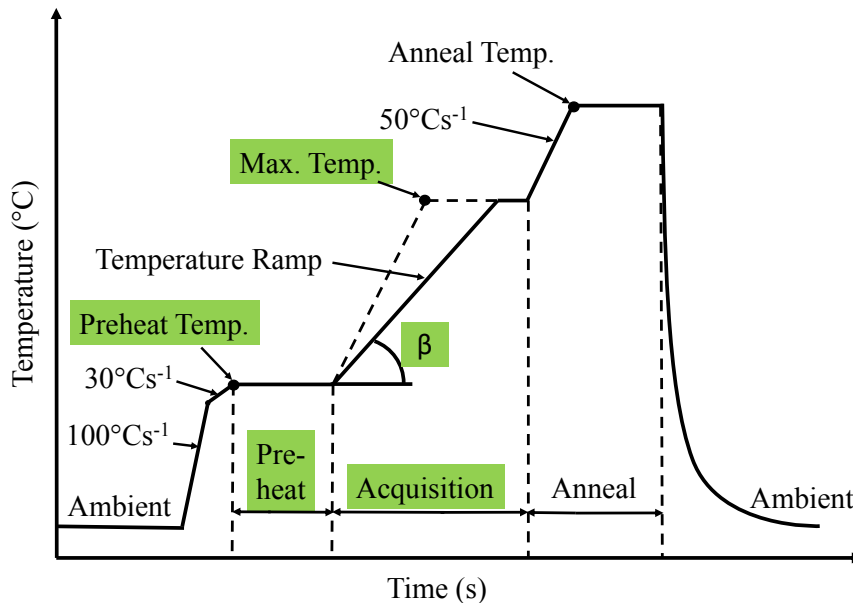


Figure 10: Linearly controlled time-temperature profile, characteristic for a Harshaw system [37].

In a Harshaw gas heating system the TTP concept is as follows: At first, the nitrogen temperature starts at ambient temperature; before preheat, the programmed temperature with a heating rate of  $100\text{ }^{\circ}\text{C}\text{s}^{-1}$  rises and slows down to  $30\text{ }^{\circ}\text{C}\text{s}^{-1}$  before the preheat temperature  $T_{\text{Ph}}$  is reached. After the preheat is done the detection of the TL signal starts by heating the TLD crystal. At this point the adjustable heating rate  $\beta$  is used during acquisition time  $t_{\text{aq}}$ . If the maximum temperature  $t_{\text{max}}$  is reached, the heating rate directs to zero and the temperature is constant for the rest of  $t_{\text{aq}}$ . Then the anneal starts with a heating rate of  $50\text{ }^{\circ}\text{C}\text{s}^{-1}$  up to the maximum anneal temperature until the annealing time is reached. Finally the TLD crystal is cooled down to ambient temperature. [37]

The five main parameters have a big influence on the glow curve shape, which targets its quality and reproducibility.

- **Heating rate  $\beta$ :** The heating rate has the biggest influence on the GC. Horowitz and Moscovitch [26] reviewed that high heating rates generally lead to increasing values of  $T_{\text{max}}$  for the various glow peaks. The peaks merge together and create a glow curve shape that is far harder to deconvolve. In addition, higher heating rates lead to non-linearities in the heating profile.
- **Maximum temperature  $T_{\text{max}}$ :** The importance of a wise chosen maximum temperature is owed by the fact, that with too low  $T_{\text{max}}$ , not all charges are released

from the traps and the TL signal is not complete. With a too high  $T_{\max}$  the Teflon<sup>TM</sup> could be damaged. Furthermore the TL light signal would be influenced by an increasing IR-signal of the heat. Horowitz discussed 2008 [38] that there are no glow peaks beyond 400 °C. But at very high levels of dose (or following HCP) irradiation, there are TL peaks beyond. To come over this problem it is possible to reread the cards, and if the residual-dose is too high, the card falls out of the routine. [39]

- **Preheat temperature  $T_{\text{Ph}}$  and time  $t_{\text{Ph}}$ :** Preheat is performed to extinguish the low energy peaks that relate to the fading phenomenon. With an adequate preheat period that consists of high  $T_{\text{Ph}}$  and long enough  $t_{\text{Ph}}$ , the low energy peaks could be fully extinguished.
- **Acquisition time  $t_{\text{aq}}$ :**  $t_{\text{aq}}$  describes the recording time of the GC. Ideally  $t_{\text{aq}}$  is long enough to record the whole GC with up to five dosimetric relevant glow peaks in TLD-100 and the TTP reaches  $T_{\max}$ . In addition, the acquisition time should be short enough to decrease the IR-background signal.

### 3.4.1. Non-linearities in the Heating Profile

"In routine monitoring [...] many dosimeters need to be annealed within a short time period and the maximum read out temperature is sometimes restricted due to the dosimeter design, i.e., the use of Teflon<sup>TM</sup>. In this case the real heating profile of the detector is not always linear and sometimes not constant from one readout to the next." ([40] Stadtmann et al. 2006, S. 310)

The computer controlled linear heating profile of a hot nitrogen gas reader is equal with detector temperature  $T_{\text{LiF}}$  for slow heating rates. Unfortunately for higher heating rates  $T_{\text{LiF}}$  varies within the so called temperature lag. An adequate formulation and a theoretical description of these non-linearities in the heating profile has been performed by Stadtmann, Delgado and Gomez-Ros in 2002 [41].

Three physical heat transfers - conduction, forced convection and radiative loss - were considered. It follows a differential equation for  $T_{\text{LiF}}$ :

$$\frac{dT_{\text{LiF}}(t)}{dt} = A [T_{\text{gas}}(t) - T_{\text{LiF}}(t)] + B [T_{\text{reader}}^4(t) - T_{\text{LiF}}^4(t)]. \quad (21)$$

$A$  is an experimental estimated parameter with the unit  $\text{s}^{-1}$  and  $B$  is of theoretical origin, with the unit  $\text{s}^{-1}\text{K}^{-3}$  (Stadtmann, 2002 [41]) and own the characteristic of a heating frequency.

Equation 21 can be described in a more comprehensive way, based on the thermodynamic model by van Dijk [42]. Considering the mass of the LiF chip  $m_{\text{LiF}}$  and the surface  $S_{\text{LiF}}$  leads to the following equation [40]:

$$\frac{dT_{\text{LiF}}(t)}{dt} = \frac{A^*}{m_{\text{LiF}}} \cdot [T_{\text{gas}}(t) - T_{\text{LiF}}(t)] + \frac{B^*}{S_{\text{LiF}}} \cdot [T_{\text{reader}}^4(t) - T_{\text{LiF}}^4(t)]. \quad (22)$$

with  $A^*$  to be the experimental estimated parameter with the unit  $\text{kg s}^{-1}$  and  $B^*$  is of theoretical origin, with the unit  $\text{kg s}^{-1}\text{K}^{-3}$ . Summing up, the LiF chip has no linear heating profile at higher heating rates.

Figure 11 describes the numerical solution of the differential equation (22) and leads to a valid simulation of real glow curves. Therefore, the peak heights decrease, and the GC delays to a longer readout time.

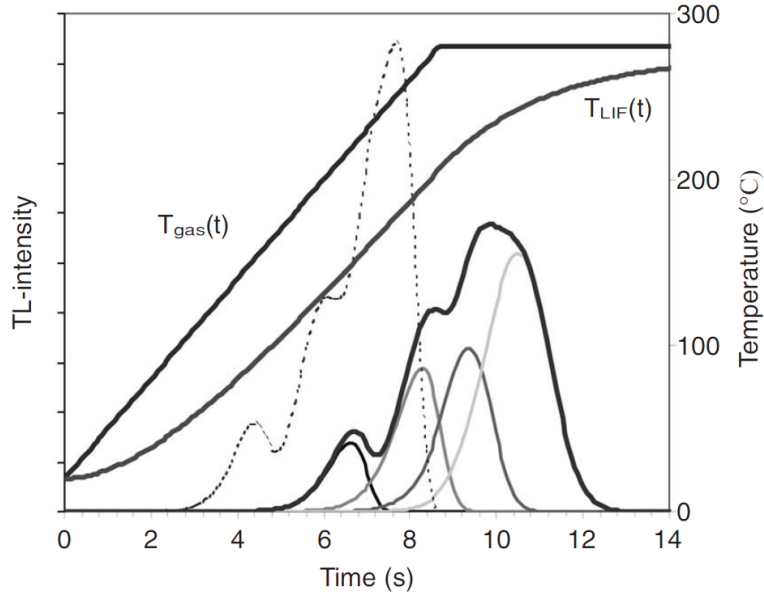


Figure 11: Calculated glow curve (solid line) on the basis of the non-linear modelled  $T_{\text{LiF}}(t)$  in comparison with a glow curve (dotted line) resulting in the linear time temperature profile  $T_{\text{gas}}(t)$  ( $\beta_{\text{gas}} = 30 \text{ }^\circ\text{Cs}^{-1}$ ,  $T_{\text{gas,max}} = 280 \text{ }^\circ\text{C}$ ) [41].

More information about the TTP and its influence in the GC shape that considers the masses and the thicknesses of the detector was showed by a further study of Stadtmann, Hranitzky and Brasik et. al. [40]. The typical temperature shift  $\Delta T$  and the corresponding time lag  $\Delta t$  for thin detectors were estimated as follows:

$$\Delta T \approx \frac{\beta \cdot m_{\text{chip}}}{A}, \quad (23)$$

$$\Delta t \approx \frac{m_{\text{chip}}}{A}, \quad (24)$$

with  $m_{\text{chip}}$  to be the mass of the detector. The GC deconvolution of the CGCD program by Stadtmann and Wilding [21] is an exemplary consideration of non-linearity.

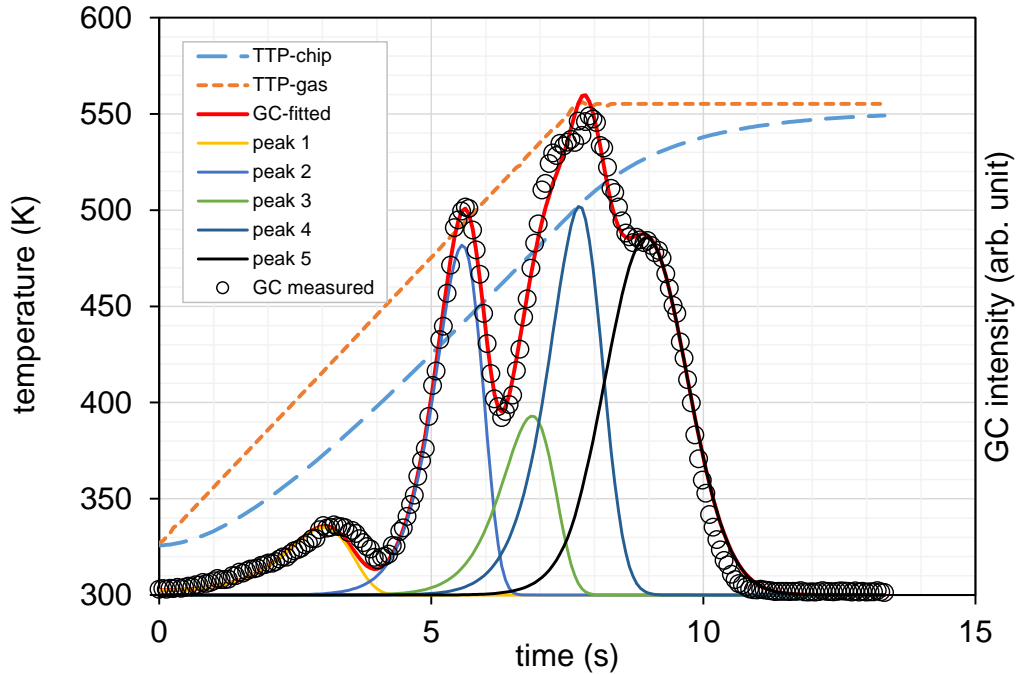


Figure 12: Example of a modelled GC with non-linear TTP, based on the analysis of a CGCD spreadsheet application using Microsoft Excel 2013, applied on GC measurement data [21].

### 3.5. Irradiation of TLDs

**TLD System 8800 internal irradiation** The TLD System 8800 includes a component for internal irradiation, a source of Sr-90. In routine application it is used as calibration source. In the PC program at first the reader anneals the TLD detectors. Then the detectors are irradiated to a dose of approximately 5 mSv. After that the detectors get read out immediately. The procedure makes it possible to get GCs with a short time interval between irradiation and readout. This lead to the characteristic calibration GCs.

**Dosimetry Laboratory (DEL)** The dosimetry laboratory (DEL) is an irradiation facility of Seibersdorf Laboratories. It is a secondary standard dosimetry laboratory (SSDL) which is traceable to a primary standard dosimetry laboratory (PSDL). [43] The DEL

is a laboratory maintaining primary and secondary standards in cooperation with the *Bundesamt für Eich- und Vermessungswesen* (BEV). The DEL consists of

- a panoramic irradiation facility (PIF),
- a reference irradiation facility (RIF),
- a teletherapy unit (TU) and
- five X-ray tubes.

Only the panoramic irradiation facility (PIF) was used for this study.

**Panoramic Irradiation Facility (PIF)** The panoramic irradiation facility (PIF) as shown in figure 13 consists of a circular segment stand made of transparent thermoplastic polymethyl and a transparent pipe with a stand for the source in the center of the cycle. All cards in the PIF have an equal distance of 1 m. When the irradiation starts, the source is injected with compressed air from a safe outside the irradiation chamber. There are four sources in the safe and they can be selected from outside of the chamber with a control system. All sources are  $^{137}\text{Cs}$  with well known half-lives and certified dose rates (in Air Kerma) by the BEV. Due to this the dose rate (and the activity) can be calculated for the date of irradiation. The selectable irradiation time is the second parameter to control the irradiation dose.

The irradiation procedure starts by selecting the source and adjusting the irradiation time. Afterwards the source is injected with air pressure, the irradiation expires its certain time and then the source is extracted over the pipe. The injection and the extraction time is considered in the calculation of the dose. As additional control measurement, the dose is observed by an ion chamber during the process. Several monitoring systems measure the dose and several cameras in the control room examine the procedure.

To guarantee the reproducibility of the dose the PIF irradiates with air KERMA  $K_a$  of about 5 mGy with an uncertainty of about 1 %. The PIF is designed for the irradiation of many cards per irradiation process. The circular segment stand allows the placement of up to 116 TLD cards into two rows.



Figure 13: Panoramic irradiation facility (PIF): TLD cards are placed in the circular segment stand. The irradiation source is injected through the transparent pipe. An ionising chamber is placed near the source to measure the dose rate.

### 3.6. Individual Calibration of TLD Cards

For all experiments the dosimeters consisted of two TL detectors. The calibration of the TLD Cards (so called "calibration dosimeters") was performed with the TLD Reader 8800.

The calibration started with an erase of the TL signal by annealing the TLDs with hot nitrogen gas. Then they immediately got irradiated with a Sr-90 source, encased in the TLD Reader 8800. The idea of this procedure was to set all readouts at the same individual dose. The deviations of the signals were considered with the calibration factor  $k$ , which had an average value of 1.0. These  $k$ -factors were the individual calibration factors from section 3.2.1: They considered the individual structures and interaction properties of every single crystal.

The principle of the calibration procedure is shown in Figure 14. Small samples of so called "reference dosimeters" (in the scheme called Reference Dos.) were added to the calibration process. All cards consisted of the same detectors of equal sizes. These reference dosimeters were preselected TLDs that showed average glow curves.

The calculation of the calibration factors was done as follows for all TLD crystal each:

$$AV = \frac{1}{N} \cdot \sum_{i=1}^N a_i$$
$$k_i = \frac{a_i}{AV} \tag{25}$$

$a_i$  values are the measured values of the TL signal in  $\mu\text{Sv}$ .  $AV$  is the average over the  $a_i$  values with  $N$  to be the number of measurements.  $k_i$  is an individual  $k$ -factor of one measurement. <sup>3</sup>

The calibration factors for the calibration dosimeters were calibrated based on the reference dosimeters and 10 % of every batch consisted of reference dosimeters.

---

<sup>3</sup>For this study the residual dose is not considered. The calibration and the irradiation were performed with a dose of 5 mSv, which is much higher than the background. The storage of the TLDs took place in a box made from lead, that guaranteed better shielding conditions.

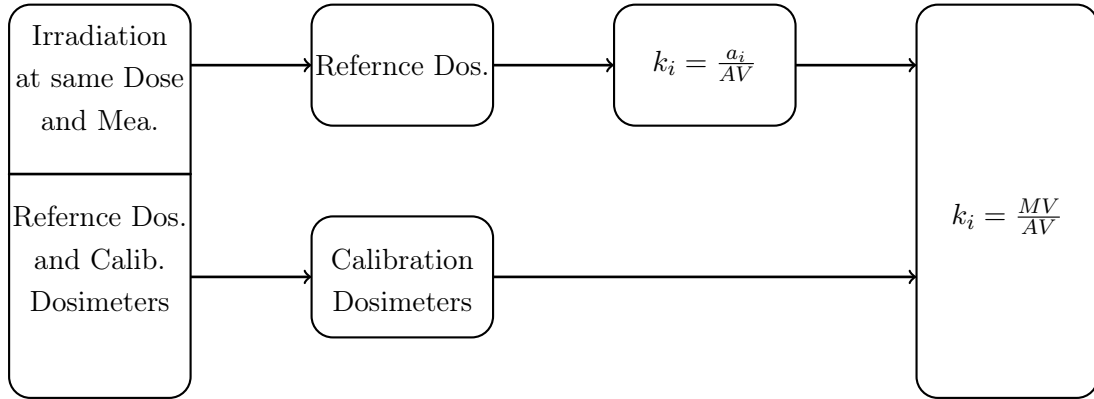


Figure 14: Scheme of the calibration procedure with  $MV$  as the measured value value. Mea. ... Measurements, Dos. ... Dosimeters, Calib. ... Calibration.

### 3.7. Simulation of Glow Curves

As mentioned in section 2.7.3 several methods to analyse glow curves have already been established. A program for GCDC with a spreadsheet application using Microsoft Excel 2013 was developed and introduced by Stadtmann and Wilding in 2017 [21]. It uses the graphic user interface of Microsoft Excel 2013 and the code was written in Visual Basic. The calculation is optimized for GCs from hot gas readers like the TLD Reader 8800. It considers the nonlinear conditions between the hot gas temperature and the chip temperature. The details of this non-linearities were described in section 3.4.1. The simulation model for the program is the first-order kinetic model, described in section 2.7.1. The program is also able to deconvolve the signal into five glow peaks and the linear heating profile is calculated as the real non-linear heating profile. The GCs resulted from the superposition (sum) of all individually calculated peaks.

The data points of measured GCs can be depicted in the program. With the selection of "good" fitting parameters, the simulated GC can be fitted onto the data points. A summary of fitted mean values and standard deviations for  $\log(s)$  of different heating rates (HR) with constant  $E_i$  values ( $E_{i,m_{fix}}$ ) were given in the publication of Stadtmann and Wilding [21]. It is possible to vary the trap energies  $E_i$ , the frequency factors  $s_i$  and the trap densities  $n_i$  of the five glow peaks. An example for a GC simulation is illustrated in figure 15.

In this study the GCDC program was used to vary the TTP and to have a look at the influence on the GC. After fitting the GC into the data points, the TTP can be varied in the program and thereupon the simulated curve changes. This technique was applied in the optimization of the TTP.

**Figure of merit** The figure of merit (FOM) is a central value in this program. The minimization of the FOM was used as a criterion to create adequate GC fits of the measurement data in the GCDC. It was introduced by Balian and Eddy in 1977. [44] A small FOM (smaller than 3 %) was aimed at in the calculations. The FOM is defined as

$$\text{FOM} = \frac{\sum_j |p_{N,j} - I_{\text{tot},j}|}{\sum_j I_{\text{tot},j}} \quad (26)$$

with  $p_{N,j} = \frac{p_j}{\sum_j p_j}$  the normed data point of the measured GC at channel  $j$  and  $I_{\text{tot},j}$  the total intensity of all deconvolved glow peaks, which is

$$I_{\text{tot},j} = \frac{\sum_i I_{ij}}{\sum_{i,j} I_{ij}}. \quad (27)$$

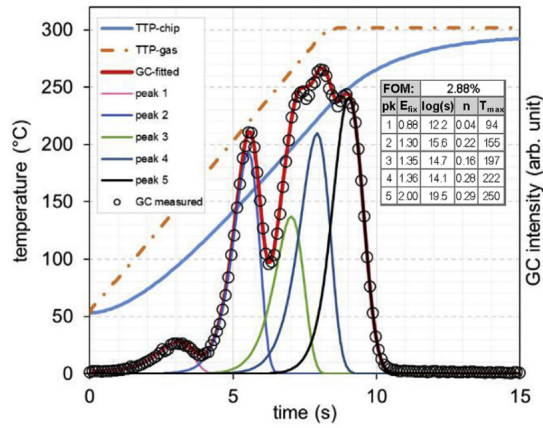


Figure 15: Fitted GC of detector thickness  $d = 0.38$  mm and a high gas heating rate  $30$  °C/s. Only two parameters  $\log(s_i)$  and  $n_i$  are fitted for all peaks, 2017 by Stadtmann and Wilding [21].

### 3.8. Fading Study

A fading study with several experiments has been performed over different time intervals of storing, irradiation and readout (see also figure 7). Harshaw TLD-100 dosimeters with two crystals were divided into batches of several equal treated cards for each point of time combination of  $t_1$  and  $t_2$ . Here  $t_1$  is defined as the pre-irradiation time, because during this time interval the sensitivity loss appears clearly in the measurements. And  $t_2$  is the post-irradiation time, which describes the signal loss after irradiation.

#### 3.8.1. Fading Experiments under Routine Conditions

On the one hand routine conditions were defined as readouts in typical time intervals in which usually TLDs got to the customer and back to the IMS. On the other hand the routine TTP was used, which is applied in the Dosimeterservice of Seibersdorf (table 4). For the fading experiments under routine conditions three separate fading experiments were performed. These experiments were classified with identification numbers (ID) A1, A2 and A3.

Here A1 was performed over a time period of three months with a special attention to the readout date. It resulted in monitoring periods of 64 permutations of time combinations of  $t_1$  and  $t_2$ . But only 37 permutations were different. For the A1 experiment, 37 batches were for each time combination considerable. The classified time combinations were shifted that way so read out of all cards could be done on one date to guarantee comparable results. This is schematically illustrated in figure 16.

This experiment depicts the typical monitoring period of one month: Usually such a routine consists of annealing the cards in the first four weeks, with a following utilization at the customers place for further four weeks and a final sent back and readout of an eventually irradiation exposure in the last four weeks.

Experiments A2 and A3 were performed over shorter time periods to collect data in these time intervals. The time periods in these experiments were important, because the shorter period times appear in the routine. The final readout again was shifted to one date.

The time periods of all fading experiments are listed in the matrix in table 5. All TLDs were stored at ambient temperature in a lead safe. For more details about the time combinations and the experimental plans to the fading experiments A1, A2 and A3 see the appendix in section A.2.1.

Table 4: Time-Temperature Profile of the Routine; for variables and the scheme of a TTP, see figure 10

Nr. / (s)	$t_{Ph}$ / (s)	$T_{Ph}$ / ( $^{\circ}C$ )	$t_{aq}$ / (s)	$\beta$ / ( $^{\circ}C/s$ )	$T_{max}$ / ( $^{\circ}C$ )
1	0	50	13.33	30	280

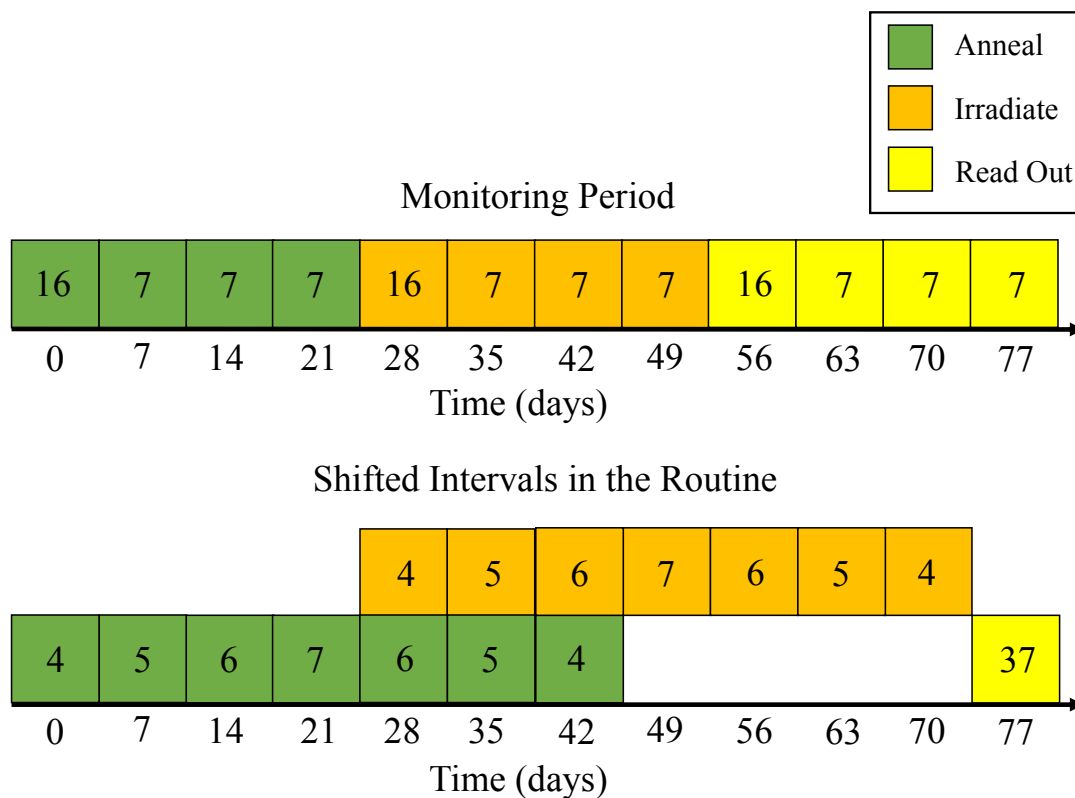


Figure 16: Scheme of the A1 fading experiment including the time intervals with and without the shift. The upper diagram shows the typical monitoring period for TLDs in the IMS of Seibersdorf Laboratories. The lower one shows the shifted experimentation plan. All intervals are shifted to a final readout on one single date. The number in the squares gives the number of batches, that had to be annealed, irradiated or read out (1 batch = 10 TLDs with the same time interval).

Table 5: Responses of the direct readout for the fading experiments A1, A3 and A4. The reference time interval is encircled.

Pre-irradiation time ...  $t_1$  / (days)

Post-irradiation time ...  $t_2$  / (days)

$t_1 \backslash t_2$	1	3	7	14	21	28	35	42	49	77
1	A2	A2	A2	A2						A1
3	A2	A2	A2	A2						
7	A2	A2	A2	A2	A3	A1,A2,A3	A1	A1	A1	
14	A2	A2	A2	A3	A1,A2,A3	A1	A1	A1	A1	
21			A3	A1,A2,A3	A1	A1	A1	A1	A1	
28			A1,A2,A3	A1	A1	A1	A1	A1	A1	
35			A1	A1	A1	A1	A1	A1		
42			A1	A1	A1	A1	A1			
49			A1	A1	A1	A1				

### 3.8.2. Fading Experiments with different TTPs

Another interesting question in the fading behavior of LiF:Mg,Ti is, whether the TTP has a significant influence on fading. Therefore, another fading experiment was performed. This fading experiment includes selective time intervals of the upper fading experiments A1 to A3 and the covers the same reference intervals. Additionally in this experiment seven TTPs are used which are listed in table 6. The scheme of the time intervals are depicted in table 7. For more details to this experiment see the appendix in section A.2.2.

Table 6: Time-Temperature Profiles (TTP) for the B fading experiment (\* A perheat was performed in an external furnace by  $T = 95 \text{ }^\circ\text{C}$  for 20 minutes in addition to the readout.)

Nr.	$t_{\text{Ph}} / (\text{s})$	$T_{\text{Ph}} / (^\circ\text{C})$	$t_{\text{aq}} / (\text{s})$	$\beta / (^\circ\text{C}/\text{s})$	$T_{\text{max}} / (^\circ\text{C})$
1	0	50	13.33	30	280
2	0*	50	13.33	30	280
3	5	140	13.33	30	280
4	5	120	13.33	30	280
5	0	50	13.33	25	280
6	0	50	13.33	30	300
7	0	50	13.33	25	300

Table 7: Time intervals of the B fading experiment  
 Pre-irradiation time ...  $t_1 / (\text{days})$   
 Post-irradiation time ...  $t_2 / (\text{days})$

$t_1 \backslash t_2$	0	7	14	21	28	35
1		x				
7	x	x	x		x	
14		x		x		
21			x			x
28		x			x	
35				x		
42			x			
49		x				

### 3.9. Readout-Optimization

**Influencing Factors and Parameters** The first investigation on the optimization of TTPs were performed with the measurement of GCs in the TLD Reader 8800. First of all the routine TTP was used to generate GCs with the internal radioactive source of the Harshaw TLD System 8800. Accordingly internal irradiation with a Sr-90 source was

performed and the GC was measured immediately. This ensured that the low energy peaks were detected. Due to this the TTPs were varied with the influencing parameters  $\beta$ ,  $T_{\max}$ ,  $T_{\text{Ph}}$ ,  $t_{\text{Ph}}$  and  $t_{\text{aq}}$ . As an output the parameters could be enclosed in ranges.

### 3.9.1. Criteria for the Optimization

In the following steps several TTPs were defined (see table 8) and measured. Then the measured GCs were evaluated with four criteria according to the information content. TTP 1 to TTP 5 was the first round of measurements and TTP 6 to TTP 8 was the second one according to an improvement of the first round. TTP 0 was the reference measurement of the routine TTP with the preheat in the furnace. The four criteria were defined as following:

- **Integral stability:** Over a wide range of measurements, the area under the curve was set to be complete and constant for each TTP. This criterion is independent to the peak-height maximum. It was possible to verify this circumstance with the GCDC program by Stadtmann and Wilding [21] or with a written Python<sup>TM</sup> script. For the detailed script see the appendix in section A.3.
- **Decrease of the low energy peaks:** Low intensities or vanishing of the low energy peaks are intended. In this section, this was a subjective criterion. In these two sections (section A.3.2 and 3.9.2), the GCDC program was modified to review it.
- **Shift of the GC:** One of the big problems of evaluating GCs is the shift of the curve according to the individual detector condition. In the GCDC Program it was possible to simulate and evaluate this with the shift parameter  $A$ . However, in this step it was a subjective criterion.
- **Duration of heating:** Time is of great value for the anneal of several thousands of TLDs every month. Under consideration of the upper criteria, the faster TTPs had to be preferred.

Table 8: Fit glow curves of the optimization process.

Nr.	Type	$t_1$ / days	$t_2$ / days
GC 1	"typical" calibration GC "	0	0
GC 2	short time signal loss in routine	14	2
GC 3	long time signal loss in routine	21	28

**Qualitative Analysis on one Glow Curve** In this section the potential of the GCDC program by Stadtmann and Wilding [21] was utilized to fulfil the criteria in section 3.9.1 in a qualitative way. With the "peak-modification" in the GCDC it was possible to variate two parameters at the same time, while others were to be kept constant. In this way it was possible to include the criteria for optimum values of the parameters. For the details about the peak modification in the GCDC-program see the appendix in section A.3.1. More details about the qualitative analysis on one GC is also in the appendix in section A.3.2.

### 3.9.2. Optimization Process

The qualitative analysis on one GC lead to an expansion in the method. A new analysis with 3 GCs was performed (see table 8). The modification of the GCDC program from section A.3.1 was applied.

The simulation was performed in a chronological process: First deconvolution of the GC 1, second vary the TTP parameters. If an optimized range could be defined for the parameters, GC 2 was simulated and at last GC 3. Finally optimal TTPs according to the simulation were reached. For more details to the optimization process see the appendix in section A.3.3.

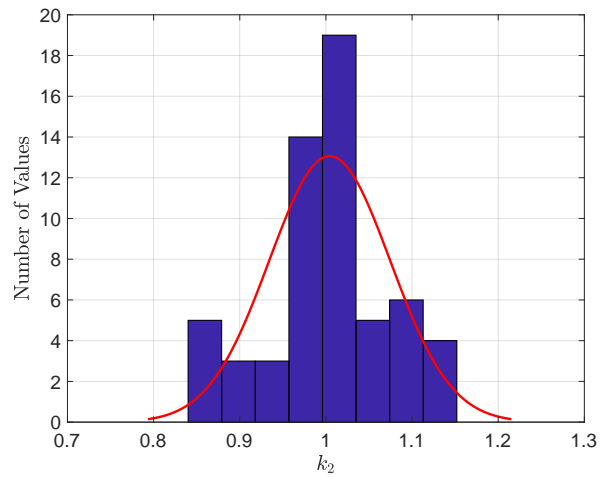
### 3.9.3. Validation of the optimum TTPs

To validate the theoretical assumptions 100 cards were used for each optimum TTP. According to this, all cards were annealed with the respective TTP. Four days later the TLDs were irradiated with 5 mSv in the DEL facility using the PIF. Finally the cards were read out in application of the separate TTP after a waiting time of ten days.

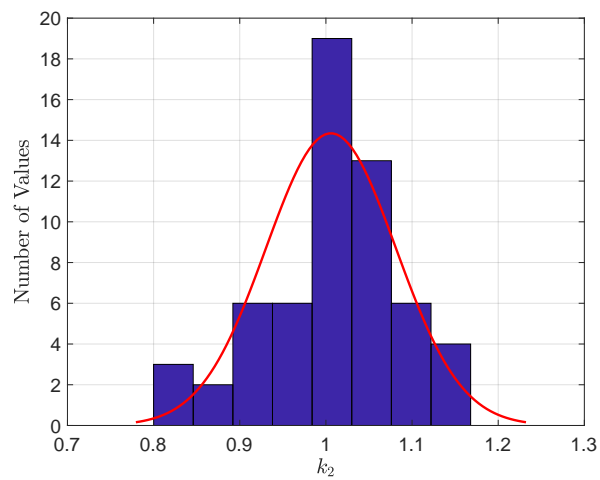
## 4. Results and Discussion

### 4.1. Individual Calibration

Before the experiments for the fading study and the optimization process started the individual calibration of the TLD cards was updated and compared as described in section 3.6.

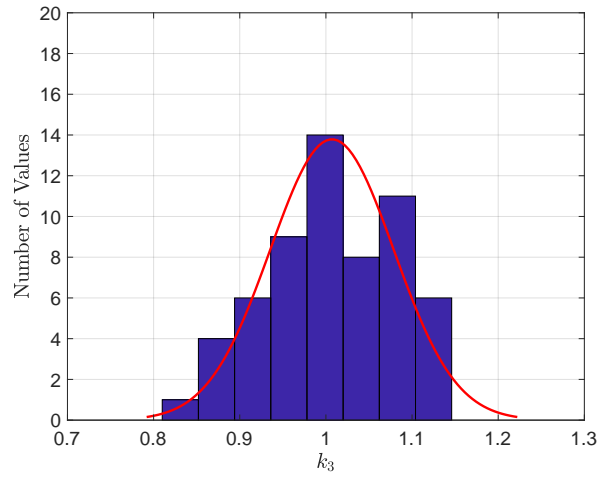


(a)  $k$  values of crystal at position 2 before calibration.

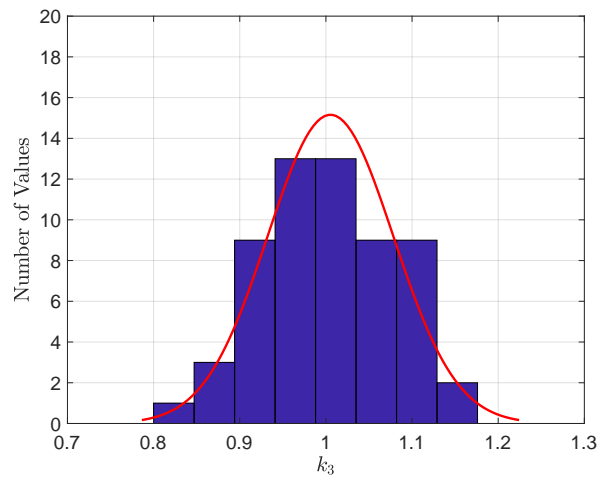


(b)  $k$  values of crystal at position 2 after calibration (update).

Figure 17: Deviation of  $k$  values for crystal 2



(a)  $k$  values of crystal at position 2 before calibration.



(b)  $k$  values of crystal 3 after calibration (update).

Figure 18: Deviation of  $k$  values for crystal 3

The averaged deviation for position 2 is 0.21 % and for position 3 is 0.24 %. Furthermore, the graphs do not show a significant pattern in the values, therefore randomness in the values was considered. Otherwise systematic influences would have been appeared in the measurement procedure (e. g. from the TLD Reader 8800 system).

## 4.2. Fading Study under Routine Conditions

The fading study under routine conditions was performed as described in section 3.8. Three separate experiments were compared to one matrix of relative responses for a direct readout TTP in the TLD Reader 8800 and a TTP with a preheat in an external furnace for 20 minutes by 95 °C. The median for each time combination is depicted.

### 4.2.1. Overlap Process and Experimental Setup

Every TLD card consists of two crystals, which were measured with two photomultipliers. This lead to the conclusion that the results of both positions had to be treated as two separate experiments.

For each position, the average of 5 cards was defined and the results of the two card positions were overlapped. Every experiment had the same reference time combination ( $t_1 = 21$  days and  $t_2 = 14$  days, i.e.,  $R_{21,14} = 1.0$ ). The relative responses were calculated as described in section 3.3. They were calculated with the reference time combination  $R_{21,14} = R_{\text{ref}}$ . The relative responses were adapted to the experiment with most information, which was experiment A1. Therefore, adaptation coefficients  $\alpha$  were introduced and relative responses from the element values of each measurement were calculated.

A lot of sources of uncertainty were to consider in the work with TLDs. One factor is that a TLD analysis with glow curves is always a relative evaluation, i.e., other GCs are chosen as reference, which are calibrated to well known dose values. However, in this fading study the results of two detector positions were to superimpose because of the readout consisting of two separate photomultiplier at the same time. Furthermore, three fading experiments were performed at three different times. An overlap process for the relative responses were elaborated for the comparison of all experiments.

$$R_i = \alpha \cdot EV \quad (28)$$

$$R_{t_1,t_2} = \frac{1}{N} \sum_{i=1}^N R_i \quad (29)$$

$R_{t_1,t_2}$  is the relative response of a single fading time combination,  $R_i$  is the relative response of a single measurement (a single GC),  $EV$  is the element value in nC,  $\alpha$  is the adaptation coefficient in nC<sup>-1</sup> and  $N$  is the number of measurements.

The defined adaptation coefficients  $\alpha$  were of great importance in the overlap process, because this procedure lead to more accurate values. Based on equation (28) the  $\alpha$ -coefficients of every time combination for every fading experiment was estimated. The results showed small standard deviations from 0.4 up to 0.7 %. For the A1 and A2 experiment the  $\alpha$ -coefficients were stable between 0.4 to 0.5 %. The  $\alpha$ -coefficient was multiplied with the single element values as described in equation (28). Moreover averages were built with the relative responses.

Table 9: Adaptation coefficients  $\alpha$  in  $\text{nC}^{-1}$  for each fading experiment.

ID	Experiment	$\alpha$ of Crystal 2	$\alpha$ of Crystal 3
A1	Direct Readout	$0.1892 \cdot 10^{-3}$	$0.2005 \cdot 10^{-3}$
A1	Preheat	$0.1956 \cdot 10^{-3}$	$0.2079 \cdot 10^{-3}$
A3	Direct Readout	$0.2047 \cdot 10^{-3}$	$0.2055 \cdot 10^{-3}$
A3	Preheat	$0.2160 \cdot 10^{-3}$	$0.2176 \cdot 10^{-3}$
A4	Direct Readout	$0.1987 \cdot 10^{-3}$	$0.2123 \cdot 10^{-3}$
A4	Preheat	$0.2088 \cdot 10^{-3}$	$0.2230 \cdot 10^{-3}$

#### 4.2.2. Relative Responses

The relative responses  $R_{t_1, t_2}$  for the fading experiments A1, A2 and A3 for the direct readout are listed in table 10 and for the preheat of 20 minutes at 95 °C with an external furnace in table 11.

Table 10: Relative responses  $R_{t_1, t_2}$  of the **direct readout** of fading experiments A1, A2 and A3.

The reference time combination is  $t_1 = 21$  days and  $t_2 = 14$  days and the data was normalized to 1.

Pre-irradiation time ...  $t_1$  / (days)

Post-irradiation time ...  $t_2$  / (days)

$t_1 \setminus t_2$	1	3	7	14	21	28	35	42	49	77
1	1,148	1,099	1,048	1,001						0,905
3	1,145	1,098	1,056	1,003						
7	1,133	1,102	1,058	1,011	0,997	0,983	0,982	0,968	0,949	
14	1,100	1,077	1,046	1,009	0,997	0,989	0,963	0,960	0,950	
21			1,019	<b>1,000</b>	0,983	0,974	0,954	0,946	0,964	
28			1,014	0,981	0,960	0,963	0,931	0,922	0,938	
35			0,994	0,965	0,935	0,945	0,911	0,920		
42			0,961	0,950	0,920	0,929	0,915			
49			0,959	0,929	0,921	0,914				

Table 11: Relative responses  $R_{t_1, t_2}$  of the **readout with preheat** of 20 minutes at 95 °C of fading experiments A1, A2 and A3.

The reference time combination is  $t_1 = 21$  days and  $t_2 = 14$  days and the data was normalized to 1.

Pre-irradiation time ...  $t_1$  / (days)

Post-irradiation time ...  $t_2$  / (days)

$t_1 \setminus t_2$	1	3	7	14	21	28	35	42	49
1	1,023	1,022	1,003	0,986					
3	1,030	1,037	1,024	0,996					
7	1,044	1,041	1,031	1,020	1,008	1,005	1,006	0,992	0,974
14	1,029	1,040	1,027	1,020	1,006	1,006	0,999	0,990	0,970
21			1,001	<b>1,000</b>	0,996	1,000	0,976	0,980	0,985
28			0,998	0,997	0,982	0,985	0,957	0,955	0,963
35			0,991	0,986	0,959	0,970	0,950	0,955	
42			0,967	0,959	0,939	0,951	0,940		
49			0,960	0,944	0,940	0,945			

As a result of the fading study there are two tables of relative responses  $R_{t_1, t_2}$  with the reference relative response  $R_{21, 14} = 1.0$ ; one consists of the result of the direct routine readout TTP (see table 10) and one consists of the routine TTP with preheat of 20 minutes at 95 °C in an external furnace (see table 11). The assumption from literature (see [26]) is that the fading effect is decreased by preheating of the TLDs. And indeed, that fact could be confirmed. The standard deviations  $\sigma$  for the direct readout are between 1.7 to 5.5 % for post-irradiation fading, while for the preheated TLDs the standard deviations  $\sigma$  are between 0.7 to 2.2 %.

Interesting here is that the preheat could not fully extinguish the fading behaviour. Another important part in the fading study is the pre-irradiation fading. In this study we were able to measure these influences. For the direct readout TTP the standard deviations  $\sigma$  are between 0.9 and 3.7 % and for the preheated TLDs they are between 0.8 and 2.8 %. It has to be mentioned that the standard deviation  $\sigma_{\max}$  of 3.7 % was the only significant higher value. The others have a standard deviation up to 2.8 %. So the decrease of the pre-irradiation fading influence was noticeable but not that high with the preheat.

Another alignment of the data lead to an interesting fact. In the diagonal direction of the tables, the data seemed to be very similar to each other. According to this assumption the data was aligned with the total time of  $t_{\text{tot}} = t_1 + t_2$  in lines and  $t_2$  in columns (see tables 12 and 13).

In the short total time of  $t_{\text{tot}} = 17$  days the standard deviation  $\sigma$  was then up to 5.0 % for the direct readout and 2.2 % for the preheat readout. It is considered that the variability of the TLD signal was of significant height in the first 17 days, because of the uncertainty in the reproducibility of the read out time combinations  $t_1$  and  $t_2$  in the first days, e.g., the longer the time interval is, the lower is the uncertainty of the interval itself. Therefore, the standard deviations  $\sigma$  of the time intervals over  $t_{\text{tot}} = 17$  days were calculated. The standard deviation  $\sigma$  of the direct readout is between 0.5 and 1.8 % and of the preheat readout the standard deviation  $\sigma$  is between 0.3 and 1.5 %. This results are indications of no significant difference in treatment with direct readout TTPs and a preheat readout TTP in routine time intervals.

Table 12: Relative responses  $R$  of the **direct readout** of fading experiments A1, A2 and A3.

The reference time combination is  $t_{\text{tot}} = 35$  days and  $t_2 = 14$  days and the data was normalized to 1.

Total time ...  $t_{\text{tot}}$  / (days)

Post-irradiation time ...  $t_2$  / (days)

$t_{\text{tot}} \setminus t_2$	1	3	7	14	21	28	35	42	49	77
2	1,148									
4	1,145	1,099								
6		1,098								
8	1,133		1,048							
10		1,102	1,056							
14			1,058							
15	1,100			1,001						
17		1,077		1,003						
21			1,046	1,011						
28			1,019	1,009	0,997					
35			1,014	<b>1,000</b>	0,997	0,983				
42			0,994	0,981	0,983	0,989	0,982			
49			0,961	0,965	0,960	0,974	0,963	0,968		
56			0,959	0,950	0,935	0,963	0,954	0,960	0,949	
63				0,929	0,920	0,945	0,931	0,946	0,950	
70					0,921	0,929	0,911	0,922	0,964	
77						0,914	0,915	0,920	0,938	
78										0,905

Table 13: Relative responses  $R_{t_1, t_2}$  of the **readout with preheat** of 20 minutes at 95 °C of fading experiments A1, A2 and A3.

The reference time combination is  $t_{\text{tot}} = 35$  days and  $t_2 = 14$  days and the data was normalized to 1.

Total time ...  $t_{\text{tot}}$  / (days)

Post-irradiation time ...  $t_2$  / (days)

$t_{\text{tot}} \backslash t_2$	1	3	7	14	21	28	35	42	49
2	1,023								
4	1,030	1,022							
6		1,037							
8	1,044		1,003						
10		1,041	1,024						
14			1,031						
15	1,029			0,986					
17		1,040		0,996					
21			1,027	1,020					
28			1,001	1,020	1,008				
35			0,998	<b>1,000</b>	1,006	1,005			
42			0,991	0,997	0,996	1,006	1,006		
49			0,967	0,986	0,982	1,000	0,999	0,992	
56			0,960	0,959	0,959	0,985	0,976	0,990	0,974
63				0,944	0,939	0,970	0,957	0,980	0,970
70					0,940	0,951	0,950	0,955	0,985
77						0,945	0,940	0,955	0,963

### 4.2.3. Representative Glow Curves

In the fading study all time periods of  $t_1$  and  $t_2$  consisted of ten measurements. Per each card there were two crystals, which were read out at the same time by two photomultipliers. The ten GCs had a similar structure and the method to find a representative GC in the measurement was the estimation of the median. According to a measurement of ten GCs, there was an upper- and an lower-median chosen, i.e., the two GCs in the middle, where the highest point of the GCs were located. The following procedure was performed to find the more representative one:

A center of all GCs was defined as the half distance between  $a$  and  $b$ , which is depicted in the figure 19 as point  $c$ . The highest peak on one GC, which was nearer to point  $c$  had to be the representative GC. Point  $a$  was located where a significant increase of the first GC starts and point  $b$  was where the last GC was so low that there is no significant decrease anymore. This method indicates a typical GC of the measurements.

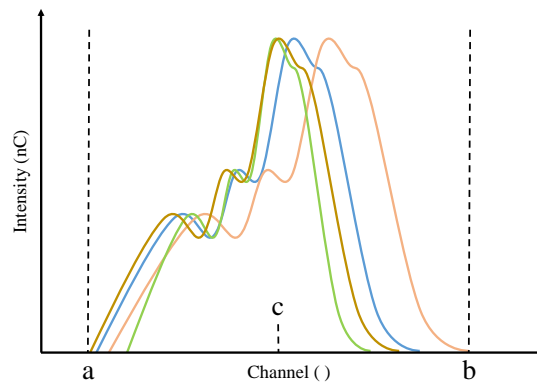


Figure 19: Defined Area of the estimation of the median. Here **a** is the startpoint and **b** is the endpoint.

**Median of the Glow Curves for Direct Readout** In the results from figure 20 to 28 for the direct readout TTP the low energy peaks 2 and 3 are decreasing with time according to their thermal instable states at room temperature [19].

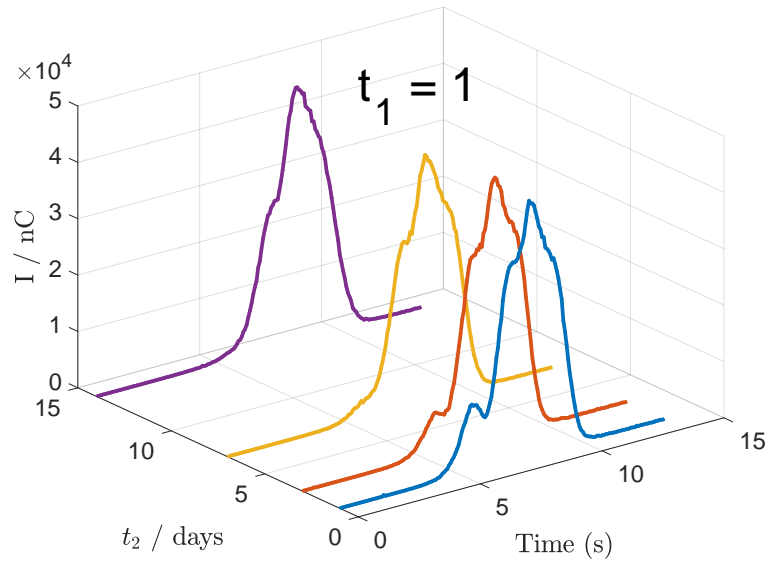


Figure 20: **Direct readout** median of GCs after  $t_1 = 1$  day of pre-irradiation fading time and several post-irradiation fading time intervals  $t_2 = \{ 1, 3, 7, 14 \}$  days.

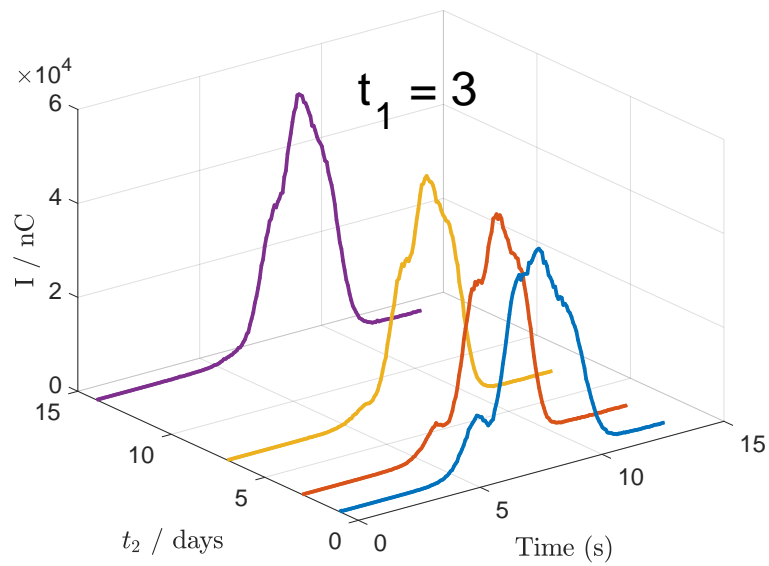


Figure 21: **Direct readout** median of GCs after  $t_1 = 3$  days pre-irradiation fading time and several post-irradiation fading time intervals  $t_2 = \{ 1, 3, 7, 14 \}$  days.

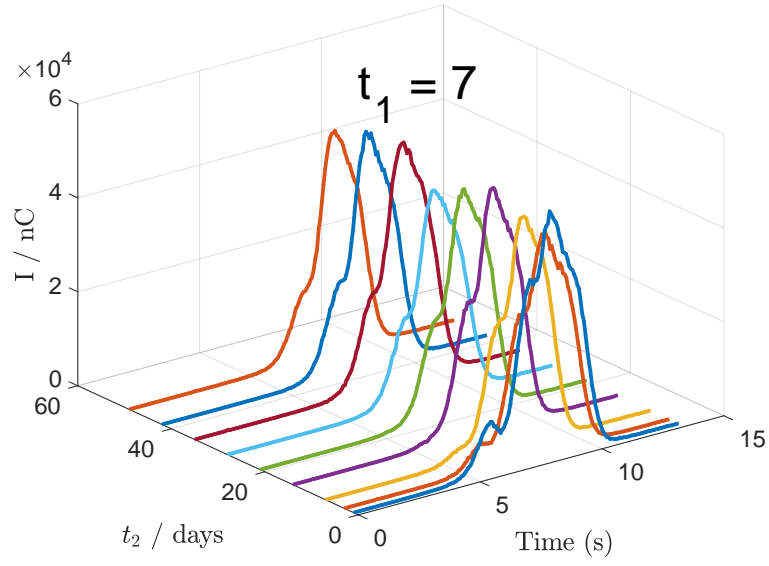


Figure 22: **Direct readout** median of GCs after  $t_1 = 7$  days pre-irradiation fading time and several post-irradiation fading time intervals  $t_2 = \{ 1, 3, 7, 14, 21, 28, 35, 42, 49 \}$  days.

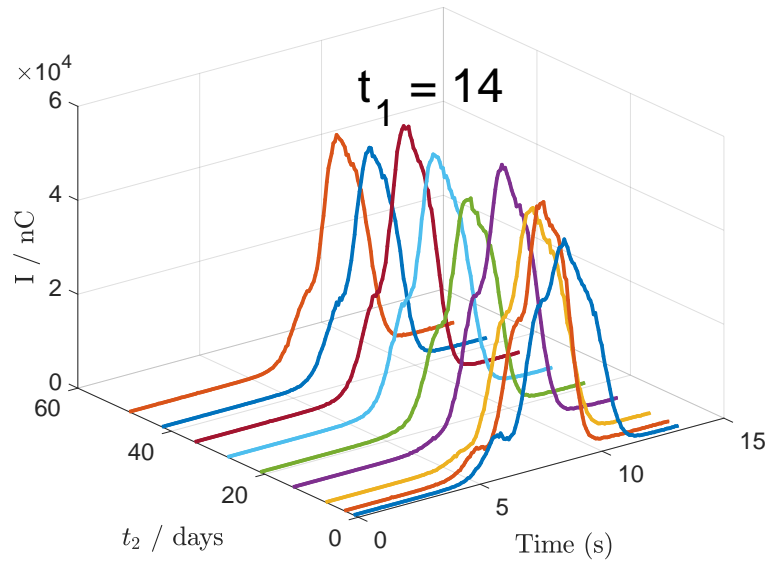


Figure 23: **Direct readout** median of GCs after  $t_1 = 14$  days pre-irradiation fading time and several post-irradiation fading time intervals  $t_2 = \{ 1, 3, 7, 14, 21, 28, 35, 42, 49 \}$  days.

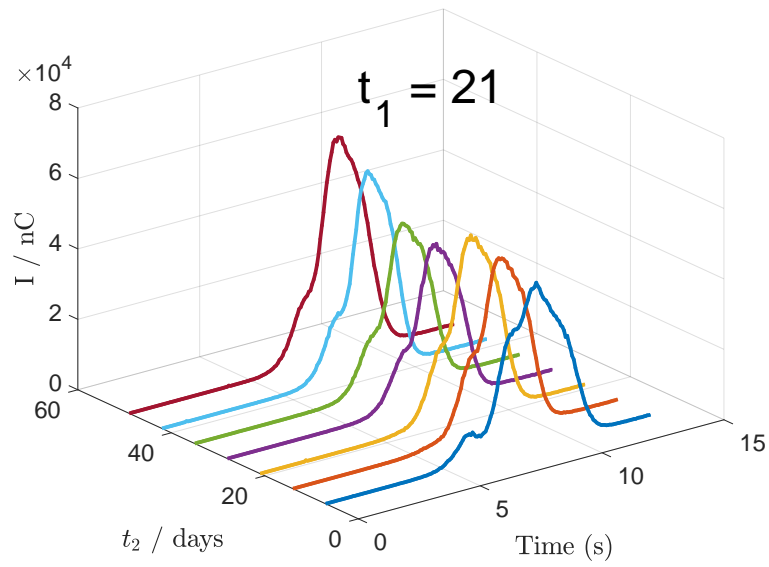


Figure 24: **Direct readout** median of GCs after  $t_1 = 21$  days pre-irradiation fading time and several post-irradiation fading time intervals  $t_2 = \{ 7, 14, 21, 28, 35, 42, 49 \}$  days.

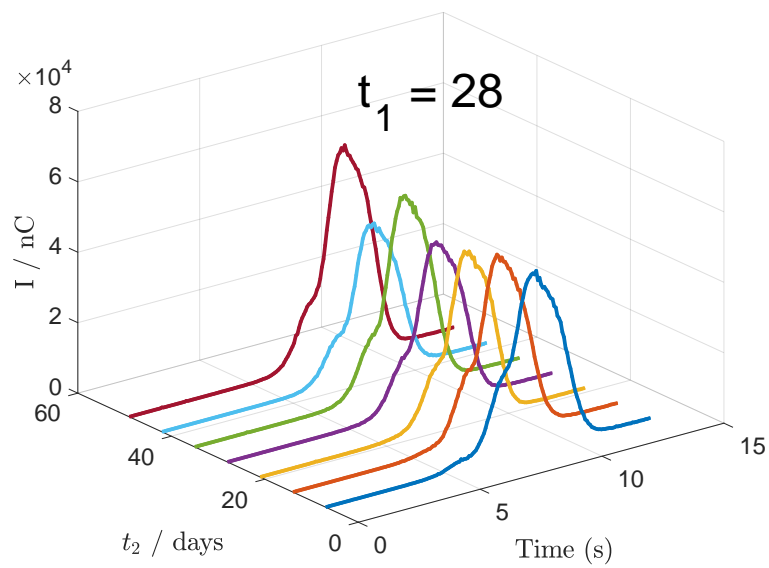


Figure 25: **Direct readout** median of GCs after  $t_1 = 28$  days pre-irradiation fading time and several post-irradiation fading time intervals  $t_2 = \{ 7, 14, 21, 28, 35, 42, 49 \}$  days.

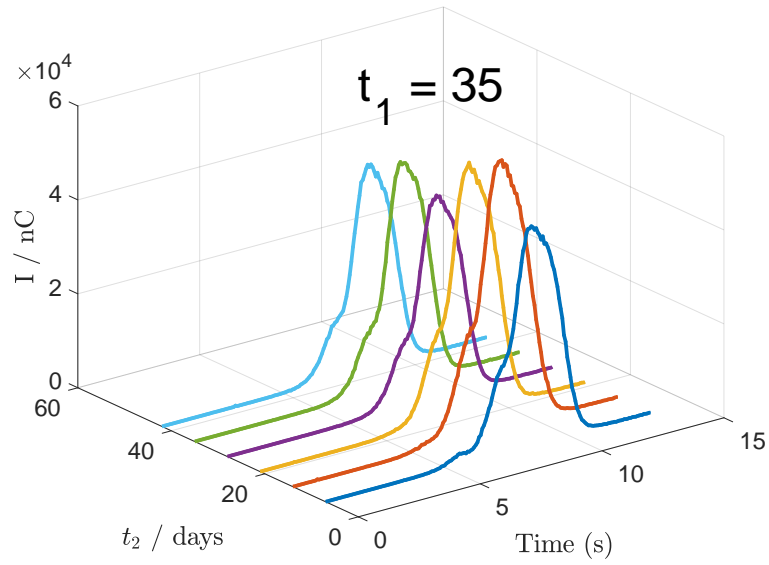


Figure 26: **Direct readout** median of GCs after  $t_1 = 35$  days pre-irradiation fading time and several post-irradiation fading time intervals  $t_2 = \{ 7, 14, 21, 28, 35, 42 \}$  days.

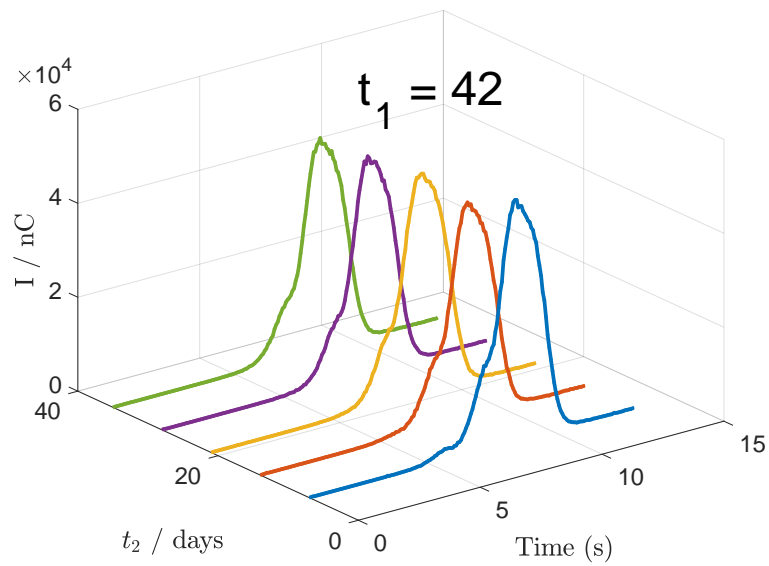


Figure 27: **Direct readout** median of GCs after  $t_1 = 42$  days pre-irradiation fading time and several post-irradiation fading time intervals  $t_2 = \{ 7, 14, 21, 28, 35 \}$  days.

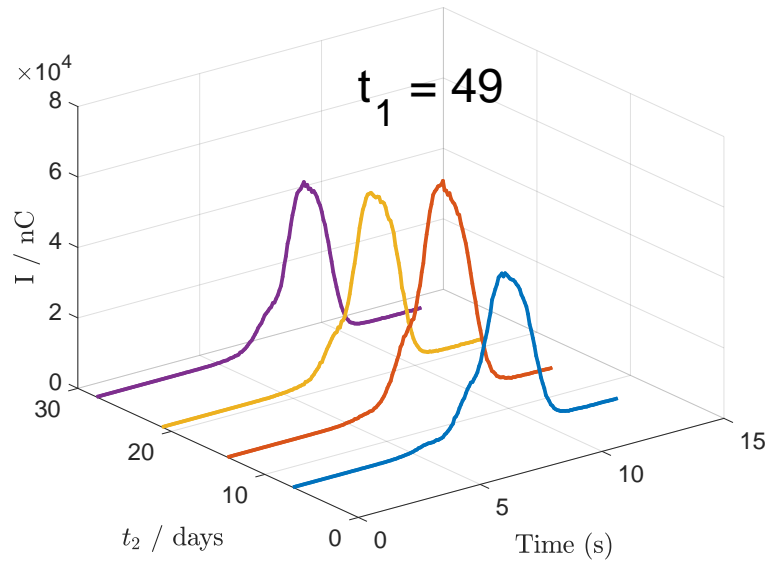


Figure 28: **Direct readout** median of GCs after  $t_1 = 49$  days pre-irradiation fading time and several post-irradiation fading time intervals  $t_2 = \{ 7, 14, 21, 28 \}$  days.

**Median of the Glow Curves Readout with Preheat** In the results from figure 29 to 37 there are no low energy peaks for the preheat readout TTP anymore. Peak 3 is a small part of the GC.

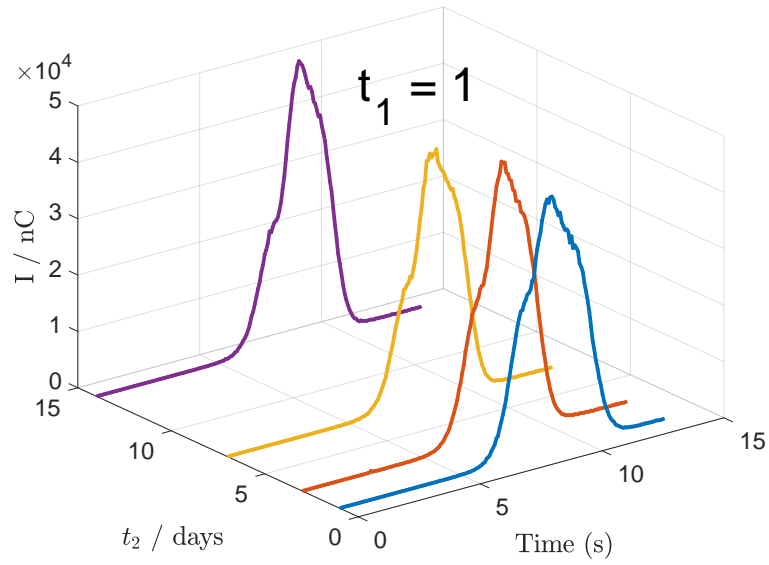


Figure 29: **Readout with Preheat:** Median of GCs after  $t_1 = 1$  day of pre-irradiation fading time and several post-irradiation fading time intervals  $t_2 = \{ 1, 3, 7, 14 \}$  days.

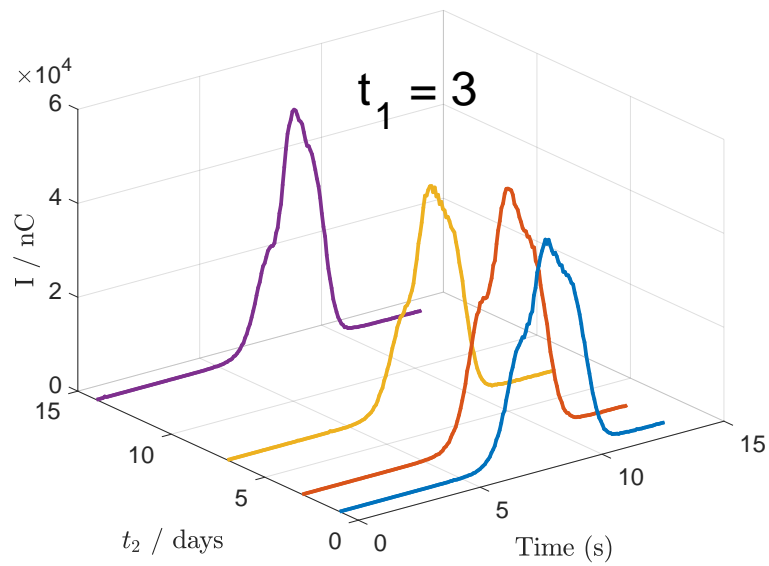


Figure 30: **Readout with Preheat:** Median of GCs after  $t_1 = 3$  days pre-irradiation fading time and several post-irradiation fading time intervals  $t_2 = \{ 1, 3, 7, 14 \}$  days.

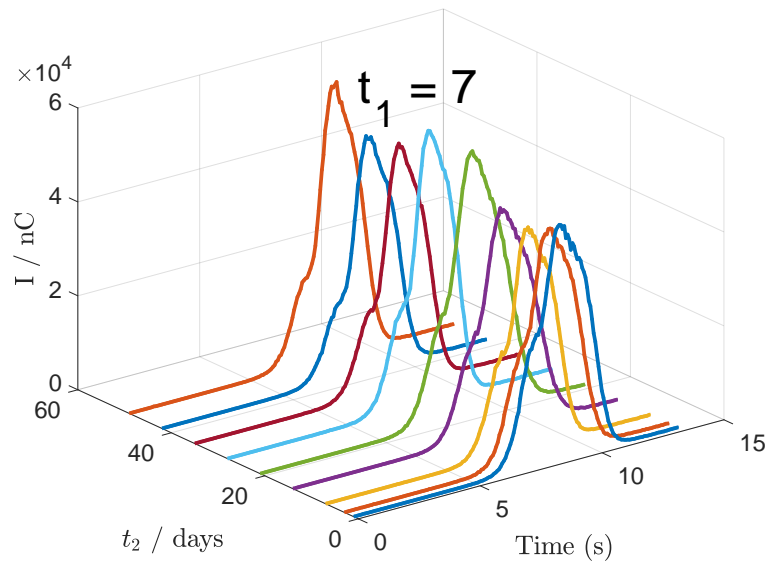


Figure 31: **Readout with Preheat:** Median of GCs after  $t_1 = 7$  days pre-irradiation fading time and several post-irradiation fading time intervals  $t_2 = \{ 1, 3, 7, 14, 21, 28, 35, 42, 49 \}$  days.

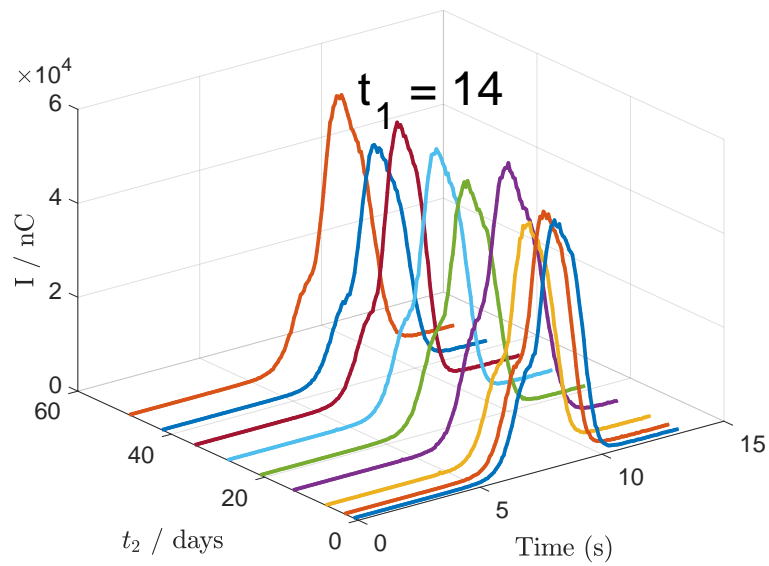


Figure 32: **Readout with Preheat:** Median of GCs after  $t_1 = 14$  days pre-irradiation fading time and several post-irradiation fading time intervals  $t_2 = \{ 1, 3, 7, 14, 21, 28, 35, 42, 49 \}$  days.

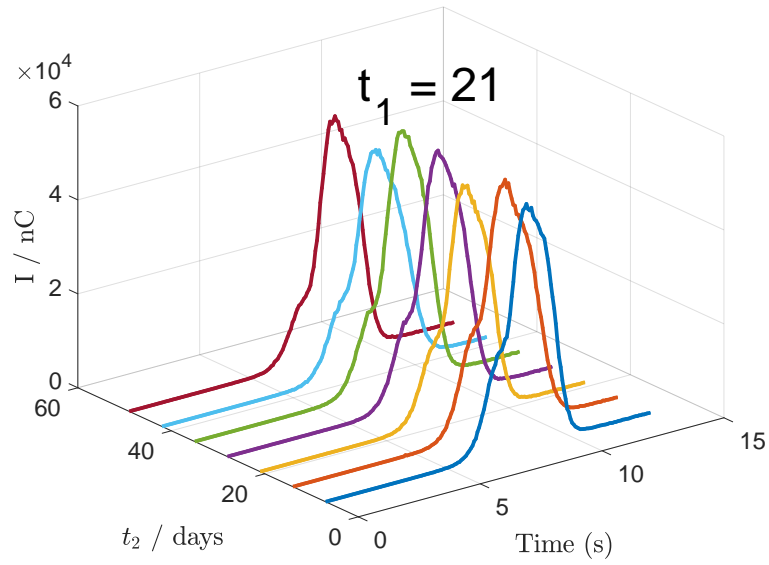


Figure 33: **Readout with Preheat:** Median of GCs after  $t_1 = 21$  days pre-irradiation fading time and several post-irradiation fading time intervals  $t_2 = \{ 7, 14, 21, 28, 35, 42, 49 \}$  days.

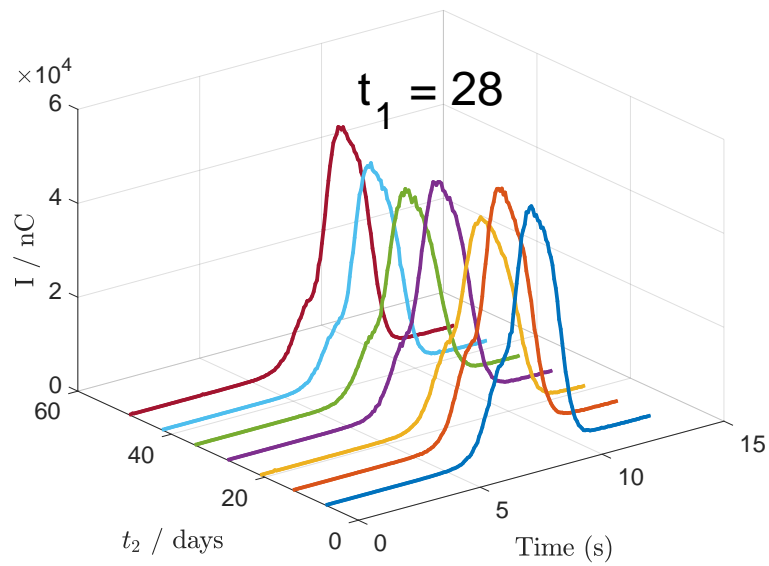


Figure 34: **Readout with Preheat:** Median of GCs after  $t_1 = 28$  days pre-irradiation fading time and several post-irradiation fading time intervals  $t_2 = \{ 7, 14, 21, 28, 35, 42, 49 \}$  days.

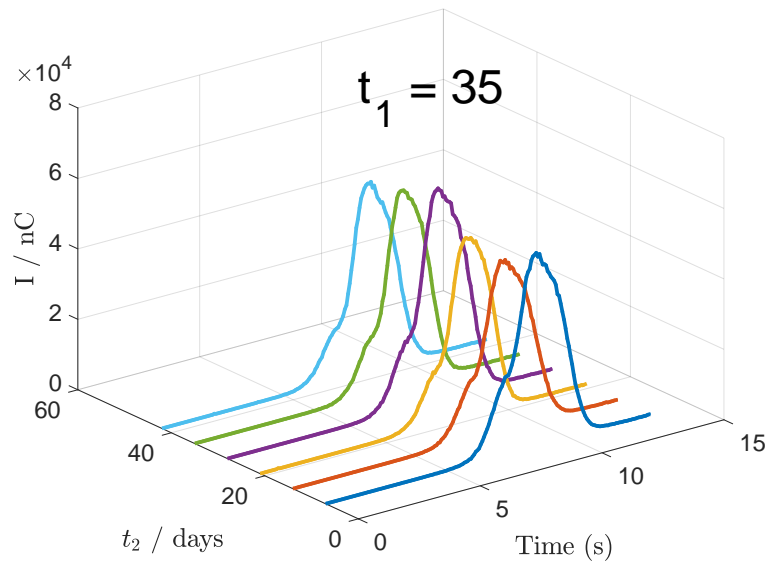


Figure 35: **Readout with Preheat:** Median of GCs after  $t_1 = 35$  days pre-irradiation fading time and several post-irradiation fading time intervals  $t_2 = \{ 7, 14, 21, 28, 35, 42 \}$  days.

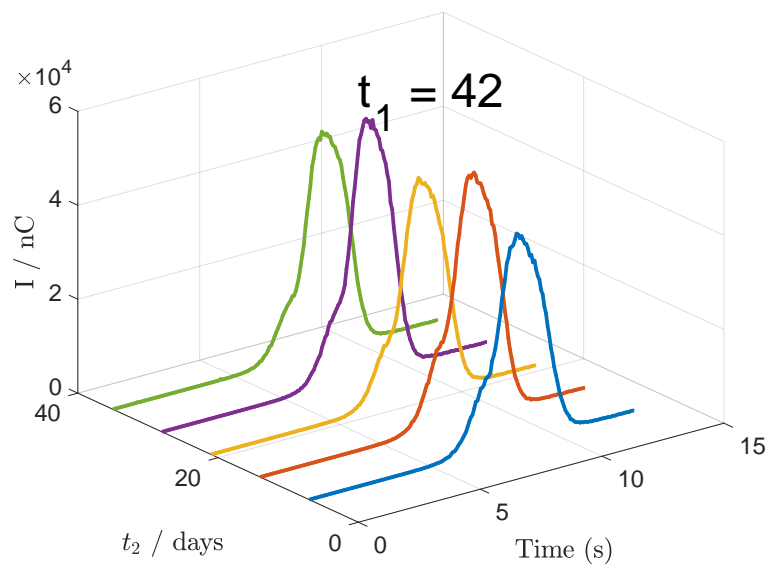


Figure 36: **Readout with Preheat:** Median of GCs after  $t_1 = 42$  days pre-irradiation fading time and several post-irradiation fading time intervals  $t_2 = \{ 7, 14, 21, 28, 35 \}$  days.

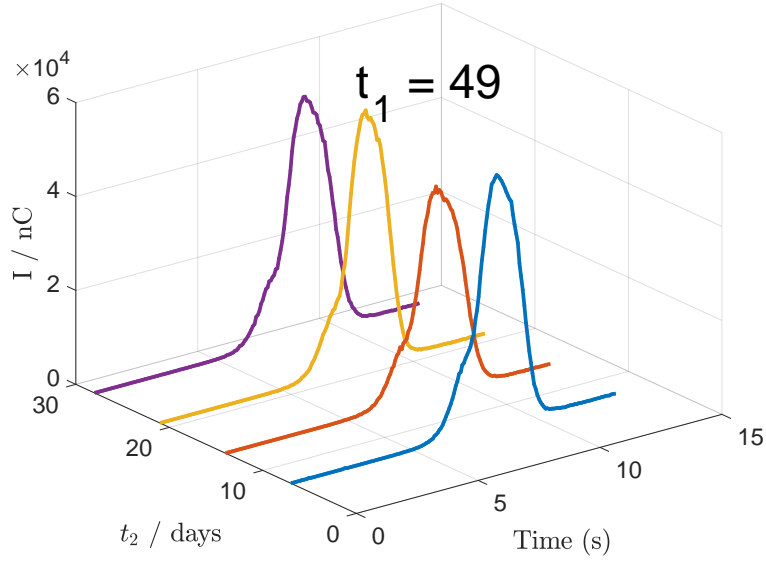


Figure 37: **Readout with Preheat:** Median of GCs after  $t_1 = 49$  days pre-irradiation fading time and several post-irradiation fading time intervals  $t_2 = \{ 7, 14, 21, 28 \}$  days.

### 4.3. Fading Function

For the direct readout and for the preheat readout two fading functions were estimated which describes the changes of the relative response  $R_{t_1, t_2}$  in a physically accurate way. Due to that it is possible to calculate the fading factors. Based on the relative responses  $R_{t_1, t_2}$  of tables 10 and 11, accurate parameters for the defined model function were found. Due to the physically assumed behaviour of the relative responses, the following general approach for the fading function  $F$  was used:

$$F(x) \propto K \cdot \exp[-z \cdot x] \quad (30)$$

with  $x$ ,  $K$  and  $z$  to be the parameters. Due to physical accuracy the sensitivity loss was assumed to occur over the whole time interval  $t_1 + t_2$ , because the breakdown of the low energy traps does not end after irradiation. The signal loss was approached over the time interval  $t_2$ . This lead to the following fading function:

$$F(t_1, t_2) = \kappa \cdot \exp[-\lambda \cdot (t_1 + t_2)] \cdot \exp[-\mu \cdot t_2] \quad (31)$$

with  $\kappa$  to be the reference factor,  $\lambda$  to be the sensitivity loss rate in  $s^{-1}$  and  $\mu$  to be the signal loss rate in  $s^{-1}$ . However, equation (31) could be rewritten, due to the

characteristics of the approach function (30):

$$F^*(t_1, t_2) = \kappa \cdot \exp[-\tau \cdot t_1] \cdot \exp[-\sigma \cdot t_2] \quad (32)$$

with  $\tau$  to be the pre-fading frequency in  $s^{-1}$  and  $\sigma$  to be the post-fading frequency in  $s^{-1}$ . Equations (31) and (32) are related by  $\tau = \lambda$  and  $\sigma = \lambda + \mu$ . Moreover  $F_{(t_1, t_2)} = F_{(t_1, t_2)}^*$ . The pre-irradiation time  $t_1$  and the post-irradiation time  $t_2$  were excellent parameters for the depiction of the routine times, which were applied in the experiments of this study. However, the only variable that is known in a monitoring service is the total time interval  $t_{\text{tot}} = t_1 + t_2$ . One fading function for the direct readout and one fading function for the preheat readout were calculated.

With the approach of equation (32), a least square fitting procedure was applied to find adequate parameters. They are listed in table 14.

Table 14: Parameters of the approach function (32),

- $\kappa / [ ]$  ... reference factor,
- $\tau / \text{days}^{-1}$  ... pre fading frequency,
- $\sigma / \text{days}^{-1}$  ... post fading frequency.

	Direct Readout	Preheat Readout
$\kappa$	1.1031	1.0393
$\tau$	0.0025	0.0015
$\sigma$	0.0026	0.0008

Based on the parameters in table 14, two simplifications were taken for adequate empirical fading functions:

- $\nu_\tau = \tau = \sigma$  is the fading frequency for the direct readout.
- $\nu_\tau = \tau = 2 \cdot \sigma$  is the fading frequency for the preheat readout.

**Direct Readout** The formula for the fading function is

$$F(t_1, t_2) = \kappa \cdot \exp[-\nu_\tau \cdot (t_1 + t_2)].$$

Then  $t_{\text{tot}}$  was inserted and  $\nu_\tau$  was inverted. The new variable is a time constant of fading  $t_{C, \text{direct}}$  with the equation

$$F(t_{\text{tot}}, \kappa, t_{C, \text{direct}}) = \kappa \cdot \exp\left[-\frac{t_{\text{tot}}}{t_{C, \text{direct}}}\right].$$

The final empirical function for the direct readout is

$$F(t_{\text{tot}}) = 1.1032 \cdot \exp \left[ -\frac{t_{\text{tot}}}{387.5 \text{ days}} \right] \quad (33)$$

with  $\kappa = 1.1032$  and  $t_{C,\text{direct}} = 387.5$  days.

Table 15: Relative responses  $R_{t_1,t_2}$  of the direct readout of fading function (33).  
Pre-irradiation time ...  $t_1$  / (days)  
Post-irradiation time ...  $t_2$  / (days)

<b>t1 \ t2</b>	<b>1</b>	<b>3</b>	<b>7</b>	<b>14</b>	<b>21</b>	<b>28</b>	<b>35</b>	<b>42</b>	<b>49</b>	<b>77</b>
<b>1</b>	1,098	1,092	1,081	1,061						0,902
<b>3</b>	1,092	1,086	1,075	1,056						
<b>7</b>	1,081	1,075	1,064	1,045	1,026	1,008	0,990	0,972	0,955	
<b>14</b>	1,061	1,056	1,045	1,026	1,008	0,990	0,972	0,955	0,938	
<b>21</b>			1,026	<b>1,008</b>	0,990	0,972	0,955	0,938	0,921	
<b>28</b>			1,008	0,990	0,972	0,955	0,938	0,921	0,904	
<b>35</b>			0,990	0,972	0,955	0,938	0,921	0,904		
<b>42</b>			0,972	0,955	0,938	0,921	0,904			
<b>49</b>			0,955	0,938	0,921	0,904				

Table 16: Differences to the relative responses  $R_{t_1,t_2}$  of the direct readout between the measured data and the data from the fading function (33).  
Pre-irradiation time ...  $t_1$  / (days)  
Post-irradiation time ...  $t_2$  / (days)

<b>t1 \ t2</b>	<b>1</b>	<b>3</b>	<b>7</b>	<b>14</b>	<b>21</b>	<b>28</b>	<b>35</b>	<b>42</b>	<b>49</b>	<b>77</b>
<b>1</b>	5,0%	0,7%	3,2%	6,0%						0,3%
<b>3</b>	5,3%	1,2%	1,9%	5,3%						
<b>7</b>	5,2%	2,7%	0,6%	3,4%	2,9%	2,5%	0,7%	0,4%	0,6%	
<b>14</b>	3,9%	2,1%	0,1%	1,7%	1,1%	0,0%	0,9%	0,6%	1,2%	
<b>21</b>			0,7%	0,8%	0,7%	0,2%	0,1%	0,8%	4,3%	
<b>28</b>			0,6%	0,9%	1,2%	0,8%	0,6%	0,1%	3,4%	
<b>35</b>			0,4%	0,8%	2,0%	0,7%	1,0%	1,5%		
<b>42</b>			1,1%	0,5%	1,8%	0,8%	1,0%			
<b>49</b>			0,4%	0,9%	0,0%	0,9%				

**Direct Readout Improvement** The relative responses  $R_{t_1, t_2}$  of fading function (33) differs from the measured ones in average about 1.6 %. The short time combinations (shorter than 17 days) differs in average about 3.5 % and the maximum difference is about 6.0 %. This could be improved with the following approach for the fading function:

$$F(t_{\text{tot}}, \kappa_1, \kappa_2, t_{C,1}, t_{C,2}) = \kappa_1 \cdot \exp \left[ -\frac{t_{\text{tot}}}{t_{C,1}} \right] + \kappa_2 \cdot \exp \left[ -\frac{t_{\text{tot}}}{t_{C,2}} \right]$$

The final empirical function for the direct readout is

$$F(t_{\text{tot}}) = 1.0641 \cdot \exp \left[ -\frac{t_{\text{tot}}}{512.1 \text{ days}} \right] + 0.1091 \cdot \exp \left[ -\frac{t_{\text{tot}}}{8.2 \text{ days}} \right] \quad (34)$$

with  $\kappa_1 = 1.0641$ ,  $\kappa_2 = 0.1091$ ,  $t_{C,1} = 512.1$  days and  $t_{C,2} = 8.2$  days.

The new equation (34) differs from the measured ones in average about 1.3 %. For short days (shorter than 17 days) equation (34) differs in average about 3.0 % and the maximum difference is about 5.0 %.

Table 17: Relative responses  $R_{t_1, t_2}$  of the direct readout of fading function (34).  
 Pre-irradiation time ...  $t_1$  / (days)  
 Post-irradiation time ...  $t_2$  / (days)

$t_1 \setminus t_2$	1	3	7	14	21	28	35	42	49	77
1	1,146	1,123	1,089	1,051						0,914
3	1,123	1,104	1,076	1,043						
7	1,089	1,076	1,055	1,030	1,011	0,995	0,981	0,967	0,954	
14	1,051	1,043	1,030	1,011	0,995	0,981	0,967	0,954	0,941	
21			1,011	0,995	0,981	0,967	0,954	0,941	0,928	
28			0,995	0,981	0,967	0,954	0,941	0,928	0,916	
35			0,981	0,967	0,954	0,941	0,928	0,916		
42			0,967	0,954	0,941	0,928	0,916			
49			0,954	0,941	0,928	0,916				

Table 18: Differences to the relative responses of the direct readout between the measured data and the data from the fading function (34).  
 Pre-irradiation time ...  $t_1$  / (days)  
 Post-irradiation time ...  $t_2$  / (days)

$t_1 \setminus t_2$	1	3	7	14	21	28	35	42	49	77
1	0,2%	2,4%	4,0%	5,0%						0,8%
3	2,2%	0,6%	2,0%	4,0%						
7	4,4%	2,6%	0,3%	1,8%	1,4%	1,3%	0,1%	0,1%	0,5%	
14	4,9%	3,4%	1,6%	0,2%	0,2%	0,8%	0,4%	0,6%	0,9%	
21			0,8%	0,5%	0,2%	0,7%	0,0%	0,5%	3,6%	
28			1,8%	0,0%	0,7%	0,9%	1,0%	0,6%	2,3%	
35			1,3%	0,3%	1,9%	0,4%	1,8%	0,4%		
42			0,6%	0,4%	2,1%	0,1%	0,1%			
49			0,5%	1,2%	0,8%	0,2%				

**Preheat Readout** The formula for the fading function is

$$F(t_1, t_2) = \kappa \cdot \exp \left[ -\nu_\tau \cdot \left( t_1 + \frac{t_2}{2} \right) \right].$$

Then  $t_{\text{tot}}$  was inserted and  $\nu_\tau$  was inverted and the factor  $3/4$  was implemented into a

new variable. The new variable is a time constant of fading  $t_{C,\text{preheat}}$  with the equation

$$F(t_{\text{tot}}) = \kappa \cdot \exp \left[ -\frac{t_{\text{tot}}}{t_{C,\text{preheat}}} \right].$$

The final empirical function for the preheat readout is

$$F(t_{\text{tot}}) = 1.0393 \cdot \exp \left[ -\frac{t_{\text{tot}}}{867.9 \text{ days}} \right] \quad (35)$$

with  $\kappa = 1.0393$  and  $t_{C,\text{preheat}} = 867.9$  days.

Table 19: Relative responses  $R_{t_1,t_2}$  of the preheat readout of fading function (33).

Pre-irradiation time ...  $t_1$  / (days)

Post-irradiation time ...  $t_2$  / (days)

<b>t1 \ t2</b>	<b>1</b>	<b>3</b>	<b>7</b>	<b>14</b>	<b>21</b>	<b>28</b>	<b>35</b>	<b>42</b>	<b>49</b>
<b>1</b>	1,037	1,035	1,030	1,022					
<b>3</b>	1,035	1,032	1,027	1,019					
<b>7</b>	1,030	1,027	1,023	1,014	1,006	0,998	0,990	0,982	0,974
<b>14</b>	1,022	1,019	1,014	1,006	0,998	0,990	0,982	0,974	0,967
<b>21</b>			1,006	<b>0,998</b>	0,990	0,982	0,974	0,967	0,959
<b>28</b>			0,998	0,990	0,982	0,974	0,967	0,959	0,951
<b>35</b>			0,990	0,982	0,974	0,967	0,959	0,951	
<b>42</b>			0,982	0,974	0,967	0,959	0,951	0,943	
<b>49</b>			0,974	0,967	0,959	0,951			

Table 15 and table 19 shows the calculated relative responses from the fading functions. The differences to the measurement values were listed in table 16 for the direct readout and in table 20 for the preheat readout.

Table 20: Differences to the relative responses  $R_{t_1, t_2}$  of the preheat readout between the measured data and the data from the fading function (33).

Pre-irradiation time ...  $t_1$  / (days)

Post-irradiation time ...  $t_2$  / (days)

$t_1 \setminus t_2$	1	3	7	14	21	28	35	42	49
1	1,4%	1,3%	2,7%	3,5%					
3	0,5%	0,5%	0,3%	2,4%					
7	1,4%	1,4%	0,8%	0,6%	0,2%	0,7%	1,6%	1,0%	0,0%
14	0,8%	2,1%	1,2%	1,4%	0,8%	1,5%	1,7%	1,6%	0,3%
21			0,5%	0,2%	0,6%	1,8%	0,2%	1,4%	2,6%
28			0,1%	0,7%	0,0%	1,1%	0,9%	0,3%	1,2%
35			0,0%	0,4%	1,5%	0,3%	0,9%	0,4%	
42			1,5%	1,5%	2,7%	0,8%	1,1%		
49			1,4%	2,2%	1,8%	0,6%			

**Fit of the fading function** The relative responses with the fit of the fading functions are depicted in figure 38 for the direct readout and in figure 39 for the preheat readout.

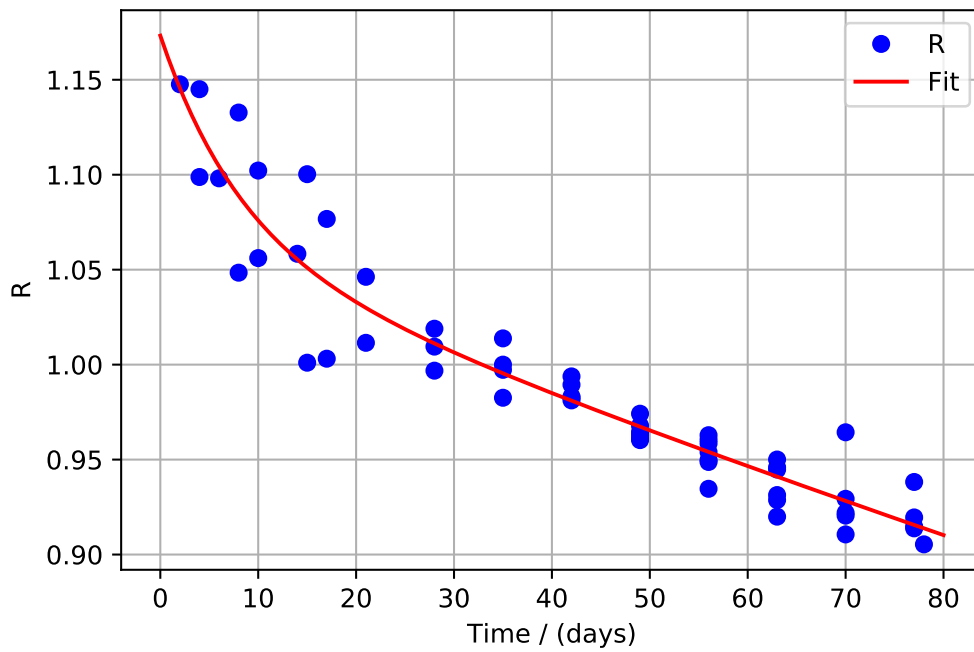


Figure 38: Fit of the fading function over the relative response data for the direct readout.  
*R*... Relative responses,  
 Time / (days) ... total time intervals.

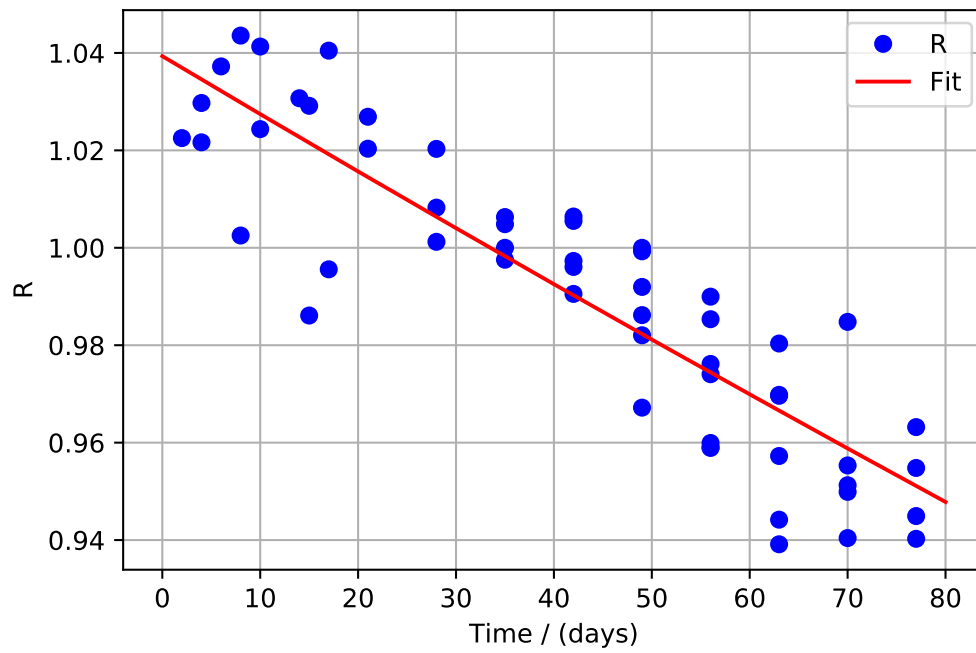


Figure 39: Fit of the fading function over the relative response data for the preheat readout.

$R$ ... Relative responses,  
 Time / (days) ... total time intervals.

Usually the time intervals  $t_1$  and  $t_2$  were not known in a monitoring service. Due to that, equations with the total time  $t_{\text{tot}}$  were applied. Based on the knowledge from the first fit of equation (32) with parameters  $t_1$  and  $t_2$  it was possible to get the first empirical parameters from the measurement data. The upper two simplifications in the formulas lead to accurate fading functions which deviations do not significantly differ from more complex equations. Furthermore, the second simplification indicates that the post irradiation fading is only half as high as the pre irradiation fading after the full anneal of the low energy peaks. Moreover, it is possible to decrease the uncertainty with these two equations in the routine, because they only depends on the total time interval  $t_{\text{tot}}$ , because in praxis the irradiation date is not known, or the irradiation did not occur on a specific date - continuous irradiation.

For the direct readout two approaches for the fading function were performed. The first function (33) differs from the measured ones in average about 1.6 %. The second function (34) differs from the measured ones in average about 1.3 %. The second approach led to a better fit of the time combinations shorter than 17 days. Furthermore, for time combinations longer than 17 days the function was improved from 1.1 % to 0.8 %.

For the readout with preheat the fading function from equation (35) was used. The relative responses  $R_{t_1,t_2}$ , calculated with (37), differs from the measured ones with an average of 1.5 % at short times (shorter than 17 days). At normal routine times (longer than 17 days) the relative responses  $R_{t_1,t_2}$ , calculated with (37), differs from the measured ones with an average of 1.0 %. The whole relative responses from the measurements differs from the calculated ones with an average of 1.1 %.

## 4.4. Fading Study with different TTPs

### 4.4.1. Fading B

The experiment B, which is described in section 3.8.2, lead to relative responses of a sample in the time matrix for different TTPs (table 6). These responses were superposed with the solution time matrices (see tables 10 and 11) of the routine fading experiment. This was necessary because of the time depending conditions of the system (noise of the photomultiplier, high voltage, temperature, sensitivity, ...). As a result it was possible to calculate a time matrix as the solution of the sample, based on the previous fading experiments.

The results from the fading study under routine conditions were the starting point for the overlap of the measured samples. Several adaptation coefficients  $\alpha$  were introduced and they were also used to calculate the overlapped relative responses from the sample of all time intervals. This experiment aimed to find out if it was possible to calculate the whole table of relative responses  $R_{t_1,t_2}$  out of a sample of relative responses with a special TTP and the information of the routine TTP.

The two TTPs with and without preheat linked this experiment and the previous fading experiment. Due to this, the adaptation coefficients were defined:

Table 21: Adaptation coefficients  $\alpha$  of fading experiment B, direct readout and preheat.  
Adaptation coefficient ...  $\alpha / \text{nC}^{-1}$

ID	Experiment	$\alpha$ of Crystal 2	$\alpha$ of Crystal 3
B	Direct Readout (TTP 2)	$0.2011 \cdot 10^{-3}$	$0.1990 \cdot 10^{-3}$
B	Preheat (TTP 1)	$0.2117 \cdot 10^{-3}$	$0.2084 \cdot 10^{-3}$

These adaptation coefficients were used to estimate the relative responses from the element values of each individual crystal and they were averaged to one response value for each time combination.

The relative responses  $R_{t_1, t_2}$  from table 10 and table 11 were supposed to be the same. Most experimental conditions were the same, like the time combinations and the TTPs. But influences in the Harshaw TLD Reader 8800 like the calibration of the photomultiplier led to small differences of in the values of the relative responses  $R_{t_1, t_2}$ . The values of the direct readout differed to a maximum of 0.033 with an average deviation of 0.016. The values of the preheat readout differed to a maximum of 0.029 with an average deviation of 0.009.

Table 22: Relative responses  $R_{t_1, t_2}$  of the **direct readout** with TTP 1 of the fading experiment B  
Pre-irradiation time ...  $t_1 /$  (days)  
Post-irradiation time ...  $t_2 /$  (days)

<b>t1 \ t2</b>	<b>1</b>	<b>7</b>	<b>14</b>	<b>21</b>	<b>28</b>	<b>35</b>
<b>1</b>		1,035				
<b>7</b>	1,149	1,042	1,012		0,968	
<b>14</b>		1,037		0,975		
<b>21</b>			<b>1,000</b>			0,939
<b>28</b>		0,980			0,937	
<b>35</b>				0,935		
<b>42</b>			0,924			
<b>49</b>		0,934				

Table 23: Relative responses  $R_{t_1, t_2}$  of the **preheat readout** with TTP 2 of the fading experiment B

Pre-irradiation time ...  $t_1$  / (days)

Post-irradiation time ...  $t_2$  / (days)

<b>t1 \ t2</b>	<b>1</b>	<b>7</b>	<b>14</b>	<b>21</b>	<b>28</b>	<b>35</b>
<b>1</b>		1,011				
<b>7</b>	1,055	1,047	1,032		0,997	
<b>14</b>		1,056		1,004		
<b>21</b>			1,000			0,980
<b>28</b>		0,996			0,977	
<b>35</b>				0,954		
<b>42</b>			0,950			
<b>49</b>		0,953				

For TTP 3 to 7 of table 6, adaptation coefficients were estimated.

Table 24: Adaptation coefficients  $\alpha$  of the fading experiment B, TTP 3 to 7.

Adaptation coefficient ...  $\alpha$  /  $\text{nC}^{-1}$

TTP Nr.	$\alpha$ of Crystal 2	$\alpha$ of Crystal 3
3	$0.8680 \cdot 10^{-2}$	$0.7816 \cdot 10^{-2}$
4	$0.8909 \cdot 10^{-2}$	$0.8183 \cdot 10^{-2}$
5	$0.9006 \cdot 10^{-2}$	$0.8140 \cdot 10^{-2}$
6	$0.8965 \cdot 10^{-2}$	$0.8071 \cdot 10^{-2}$
7	$0.9030 \cdot 10^{-2}$	$0.8133 \cdot 10^{-2}$

These adaptation coefficients were used to estimate the relative responses from the element values of each individual crystal and they were averaged to one relative response value for each time combination.

Table 25: Relative responses  $R_{t_1, t_2}$  of TTP 3 of the fading experiment B  
 Pre-irradiation time ...  $t_1$  / (dyas)  
 Post-irradiation time ...  $t_2$  / (days)

t1 \ t2	1	7	14	21	28	35
1		1,039				
7	1,111	1,036	1,023		0,989	
14		1,040		1,000		
21			1,000			0,954
28		0,991			0,943	
35				0,932		
42			0,937			
49		0,947				

Table 26: Relative responses  $R_{t_1, t_2}$  of TTP 4 of the fading experiment B  
 Pre-irradiation time ...  $t_1$  / (dyas)  
 Post-irradiation time ...  $t_2$  / (days)

t1 \ t2	1	7	14	21	28	35
1		1,041				
7	1,141	1,067	1,024		0,975	
14		1,045		0,992		
21			1,000			0,957
28		1,007			0,953	
35				0,943		
42			0,940			
49		0,958				

Table 27: Relative responses  $R_{t_1, t_2}$  of TTP 5 of the fading experiment B  
 Pre-irradiation time ...  $t_1$  / (dyas)  
 Post-irradiation time ...  $t_2$  / (days))

t1 \ t2	1	7	14	21	28	35
1		1,042				
7	1,155	1,066	1,021		0,985	
14		1,048		0,991		
21			1,000			0,959
28		1,001			0,948	
35				0,932		
42			0,935			
49		0,940				

Table 28: Relative responses  $R_{t_1, t_2}$  of TTP 6 of the fading experiment B  
 Pre-irradiation time ...  $t_1$  / (dyas)  
 Post-irradiation time ...  $t_2$  / (days))

t1 \ t2	1	7	14	21	28	35
1		1,050				
7	1,148	1,058	1,035		0,985	
14		1,046		0,991		
21			1,000			0,954
28		1,013			0,960	
35				0,945		
42			0,942			
49		0,945				

Table 29: Relative responses  $R_{t_1, t_2}$  of TTP 7 of the fading experiment B  
 Pre-irradiation time ...  $t_1$  / (dyas)  
 Post-irradiation time ...  $t_2$  / (days))

<b>t1 \ t2</b>	<b>1</b>	<b>7</b>	<b>14</b>	<b>21</b>	<b>28</b>	<b>35</b>
<b>1</b>		1,045				
<b>7</b>	1,156	1,052	1,026		0,984	
<b>14</b>		1,053		0,979		
<b>21</b>			1,000			0,955
<b>28</b>		1,000			0,954	
<b>35</b>				0,938		
<b>42</b>			0,938			
<b>49</b>		0,952				

Samples of relative responses were measured in batches of 10 TL cards each. The first two TTPs were the same as measured in experiment A (see tables 10 and 11). Due to that a comparison on the fading behavior is possible. The color-scale is at highest at 1.15 (green) and at lowest at 0.91 (red). As already discussed in 4.2, fading decreases due to the preheat in the furnace, because peaks 1 and 2 could be fully distinguished. The TTPs 3 and 4 were TTPs with a preheat in the hot gas reader. But in this experiment, fading was not significantly reduced. The reason is that the low energy peaks could not get fully annealed at short time combinations. The TTPs 5, 6 and 7 were without any preheat and have the same fading characteristics like TTP 1 with an direct readout. Summing up this observations lead to two notes. On the one hand fading without any preheat does not depend on the chosen TTP. On the other hand if the low energy peaks were fully annealed, fading would decrease significantly.

Table 30: Several Time-Temperature Profiles for the evaluation of GCs.

TTP Nr.	$t_{Ph}$ / (s)	$T_{Ph}$ / ( $^{\circ}C$ )	$t_{aq}$ / (s)	$\beta$ / ( $^{\circ}C/s$ )	$T_{max}$ / ( $^{\circ}C$ )
1	0	50	13.33	30	280
8	3	150	13.33	30	285
9	5	145	13.33	30	285
10	7	150	13.33	28	290
11	5	155	13.33	28	290
12	5	160	13.33	28	290
13	5	160	13.33	25	290
14	5	160	13.33	22	290
15	7	160	13.33	25	290

## 4.5. Readout-Optimization

### 4.5.1. Analysis of Glow Curves with different TTPs

Several GCs were measured with the TLD Reader 8800 internal irradiation tool. They are listed in table 30. Examples of these calibration GCs are depicted in figures 40 to 48.

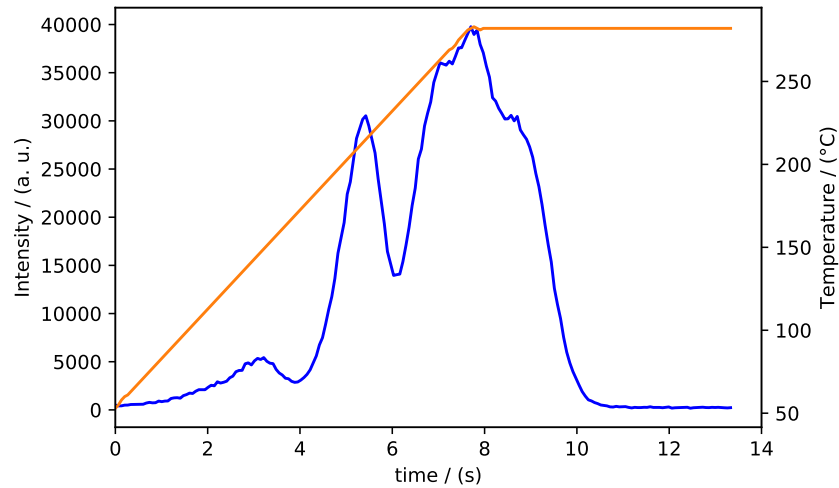


Figure 40: Measured calibration GC with TTP 1 from table 30.

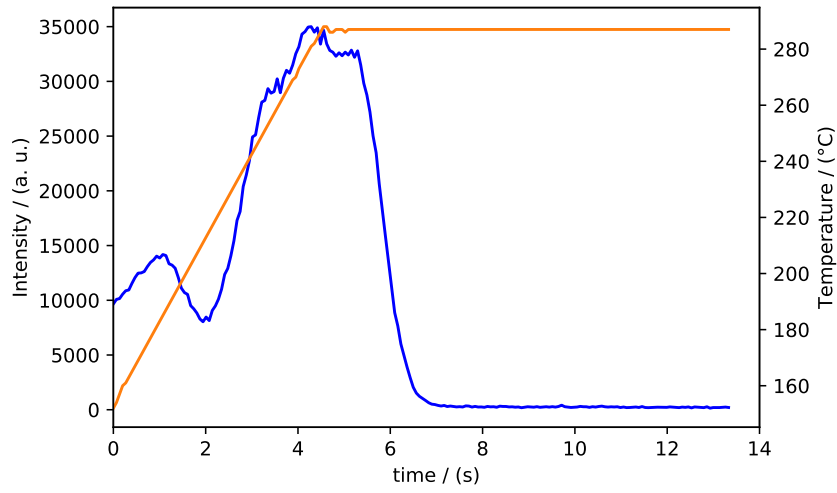


Figure 41: Measured calibration GC with TTP 8 from table 30.

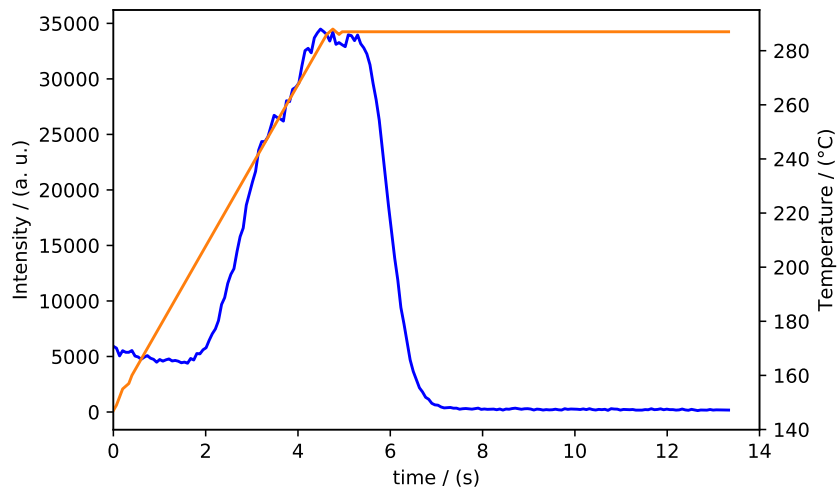


Figure 42: Measured calibration GC with TTP 9 from table 30.

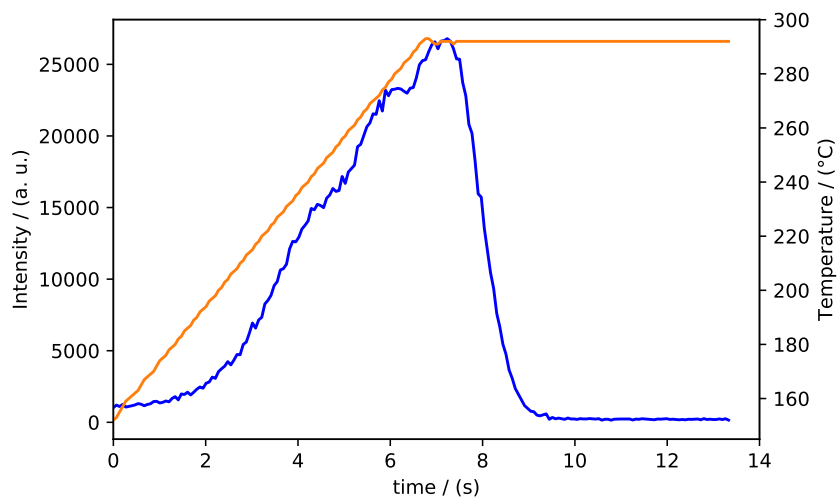


Figure 43: Measured calibration GC with TTP 10 from table 30.

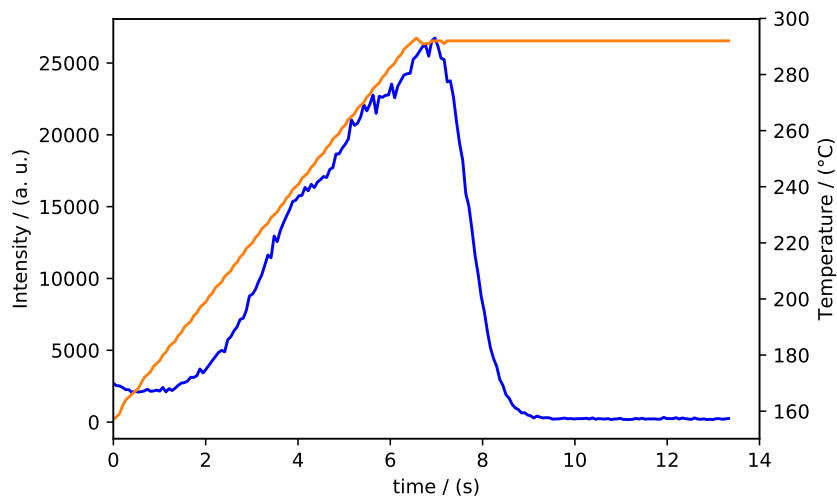


Figure 44: Measured calibration GC with TTP 11 from table 30.

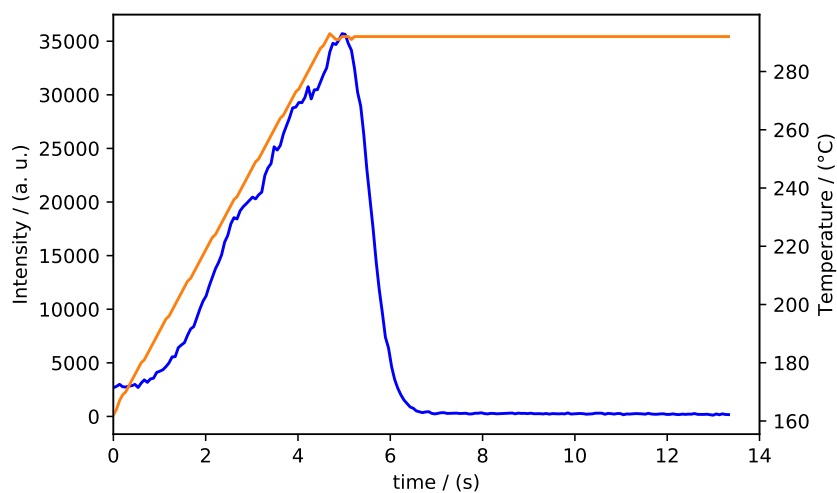


Figure 45: Measured calibration GC with TTP 12 from table 30.

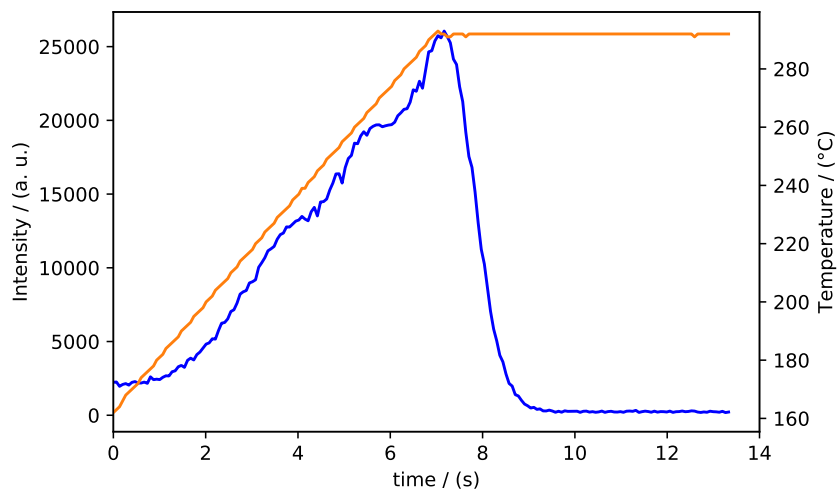


Figure 46: Measured calibration GC with TTP 13 from table 30.

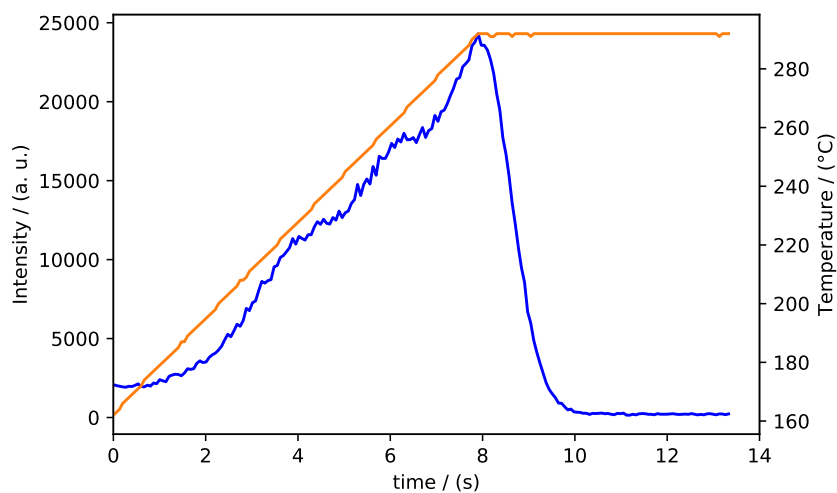


Figure 47: Measured calibration GC with TTP 14 from table 30.

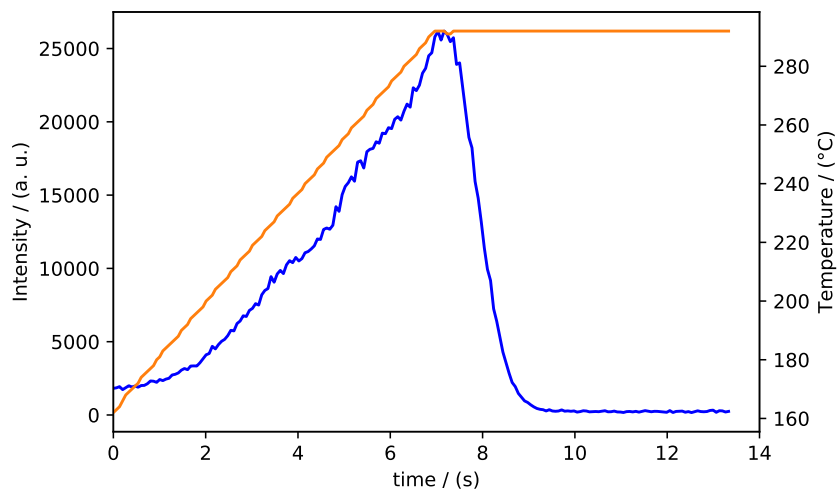


Figure 48: Measured calibration GC with TTP 15 from table 30.

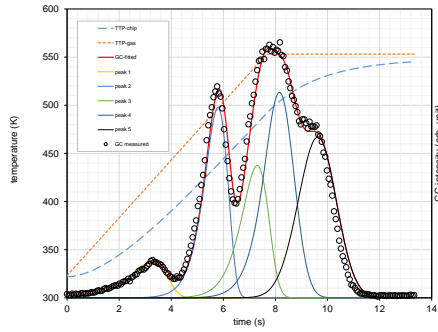
#### 4.5.2. Optimized TTPs

In the readout optimization process three optimal TTPs were found. The TTPs have the following configurations: TTP 1 consists of no preheat, TTP 16 performs the preheat of peak 1 and 2, and TTP 17 performs the preheat of peak 1 to 3. There the TTPs were listed in table 31. Representative simulated GCs, are depicted in figures 49, 50 and 51. As a result there is no significant difference in the quality of the GC according to the glow peaks, when the heating rate  $\beta$  and maximum temperature  $T_{\max}$  are varied. The experience from the praxis lead to several assumptions: At first the highest heating rate causes a faster readout. Due to a minimum IR-part in the GC the optimum of the maximum temperature was at 280 °C.

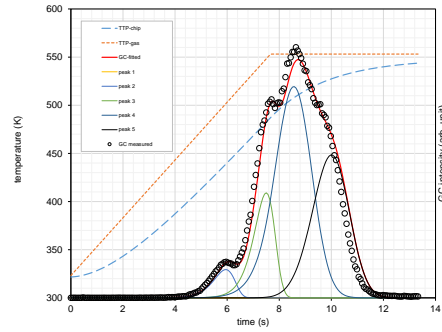
Table 31: Optimized Time-Temperature Profiles with the GCDC Simulation.

TTP Nr.	$t_{\text{Ph}}$ / (s)	$T_{\text{Ph}}$ / (°C)	$t_{\text{aq}}$ / (s)	$\beta$ / (°C/s)	$T_{\text{max}}$ / (°C)
1	0	50	13.33	30	280
16	5	160	10	30	280
17	5	190	10	30	280

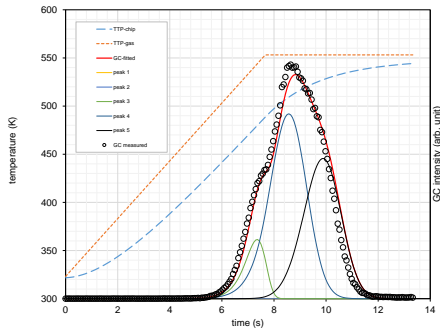
As a result of a several step optimization process with the CGCD-program these three TTPs turned out to be "optimal". During the simulation procedure it was focused to find the optimal TTPs with and without a hot gas preheat. Furthermore the quality of the simulated GCs was checked by the FOM (see 3.7), which has to be  $< 3\%$ , for all GCs. Finally three TTPs were found to be optimal; one with all glow peaks, one with glow peaks 3, 4 and 5, and one with glow peaks 4 and 5. These three TTPs were picked as base for the validation.



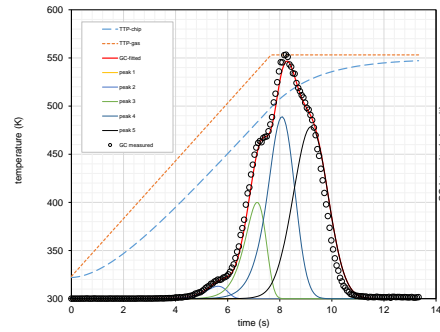
(a) Calibration GC



(b) Short time fading GC



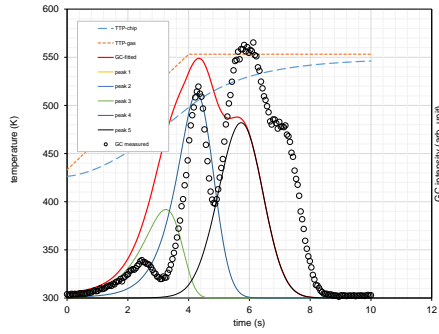
(c) Long time fading GC 1



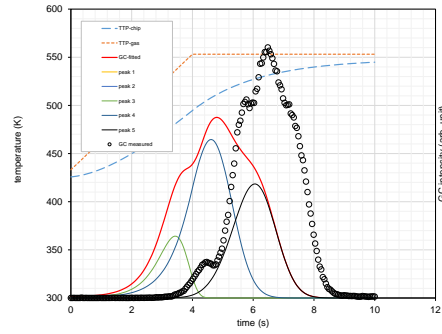
(d) Long time fading GC 2

Figure 49: Simulated GC with GCDC. The fit (red curve) of the GC is based on the measurement with TTP 1 and the FOM is  $\leq 2\%$ . The points depict the measured-GC, which was the starting GC for the simulation. The simulated TTP is the Nr. 1 from table 31. Here the measurement does not differ that much, due to the fact that the simulation TTP was the measurement TTP. The gaussian peaks under the GC are the deconvolved glow peaks. Here all peaks are visible.

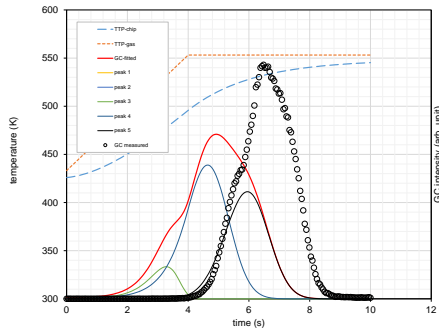
time / s,  
Intensity / [a.u.],  
temperature / K.



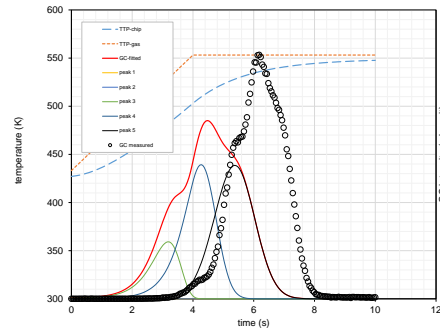
(a) Calibration GC



(b) Short time fading GC



(c) Long time fading GC 1



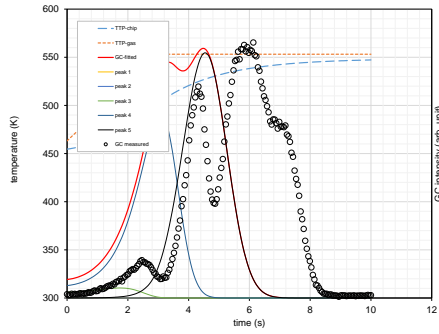
(d) Long time fading GC 2

Figure 50: Simulated GC with GDCD. The fit (red curve) of the GC is based on the measurement with TTP 1 and the FOM is  $\leq 2\%$ . The points depict the measured-GC, which was the starting GC for the simulation. The simulated TTP is the Nr. 16 from table 31. The gaussian peaks under the GC are the deconvolved glow peaks. Here peaks 3 to 5 are visible.

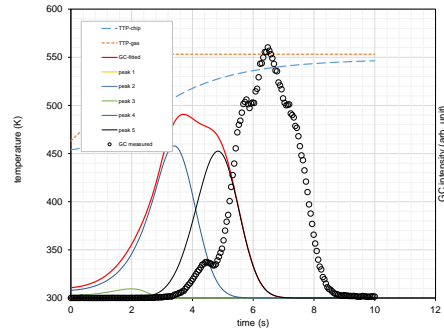
time / s,

Intensity / [a.u.],

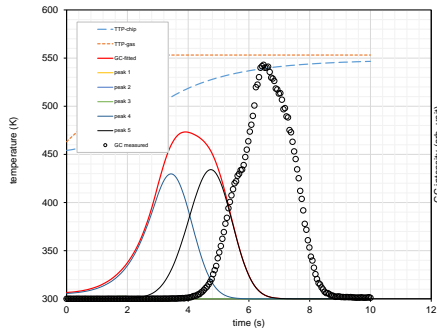
temperature / K.



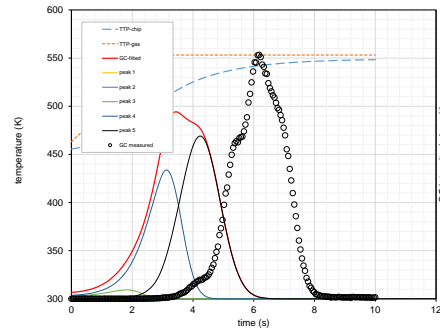
(a) Calibration GC



(b) Short time fading GC



(c) Long time fading GC 1



(d) Long time fading GC 2

Figure 51: Simulated GC with GCDC. The fit (red curve) of the GC is based on the measurement with TTP 1 and the FOM is  $\leq 2\%$ . The points depict the measured-GC, which was the starting GC for the simulation. The simulated TTP is the Nr. 17 from table 31. The gaussian peaks under the GC are the deconvolved glow peaks. Here only peaks 4 to 5 are visible.

time / s,  
Intensity / [a.u.],  
temperature / K.

Table 32: Measured optimized Time-Temperature Profiles.

TTP Nr.	$t_{Ph}$ / (s)	$T_{Ph}$ / ( $^{\circ}\text{C}$ )	$t_{aq}$ / (s)	$\beta$ / ( $^{\circ}\text{C}/\text{s}$ )	$T_{max}$ / ( $^{\circ}\text{C}$ )	Note
1	0	50	13.33	30	280	Simulated optimum TTP
16	5	160	10	30	280	Simulated optimum TTP
17	5	190	10	30	280	Simulated optimum TTP
18	0	50	13.33	25	280	like TTP 1, lower $\beta$
19	15	160	10	30	280	like TTP 16, higher $t_{Ph}$
20	15	190	10	30	280	like TTP 17, higher $t_{Ph}$

#### 4.6. Validation of new TTPs

The three optimal TTPs were compared in one experiment. As described in section 3.9.3, 100 TLD cards for each TTP were annealed, irradiated and read out with the respective TTP. This led to a database of 200 GCs. Comparing these GCs a representative GC for each TTP was chosen. They are depicted in figures 52 to 57 and the measured responses are grouped in block diagrams in figures 58 and 59. The time combination for this experiment was  $t_1 = 4$  days and  $t_2 = 10$  days.

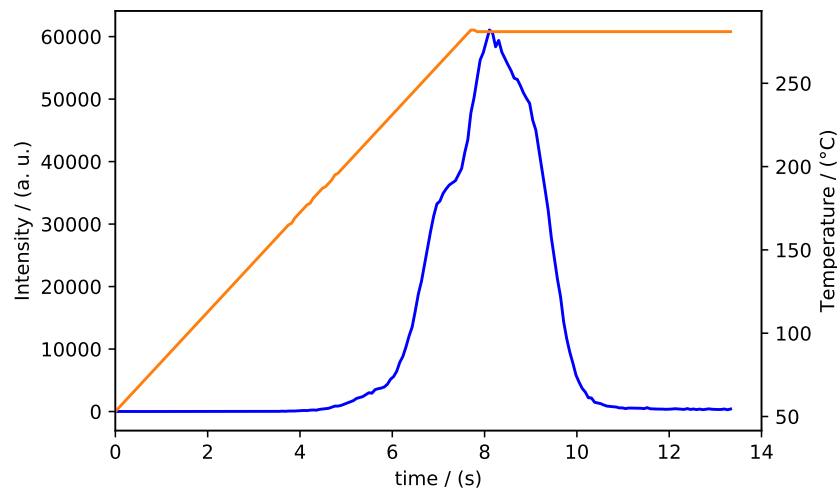


Figure 52: Measured GC with optimized TTP 1 from table 32.

The relative standard-deviations for each TTP are listed in table 33.

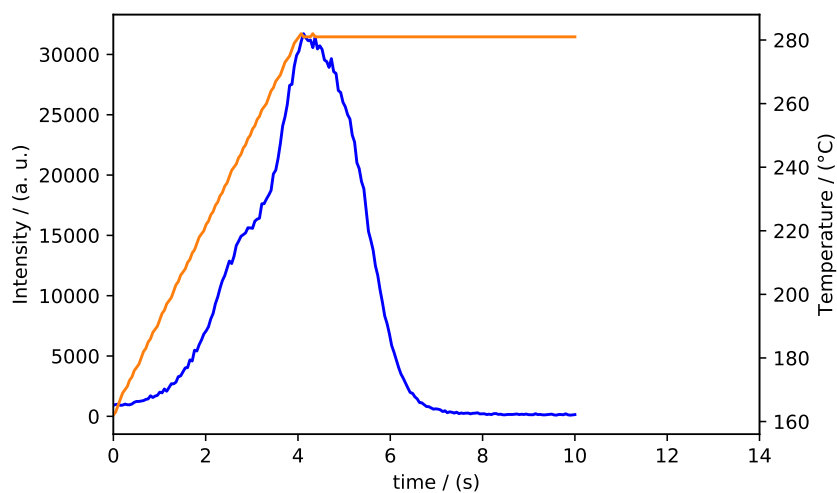


Figure 53: Measured GC with optimized TTP 16 from table 32.

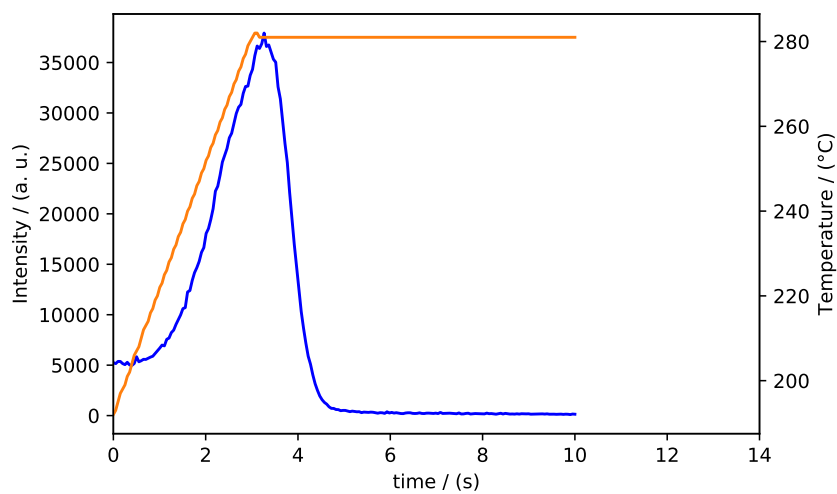


Figure 54: Measured GC with optimized TTP 17 from table 32.

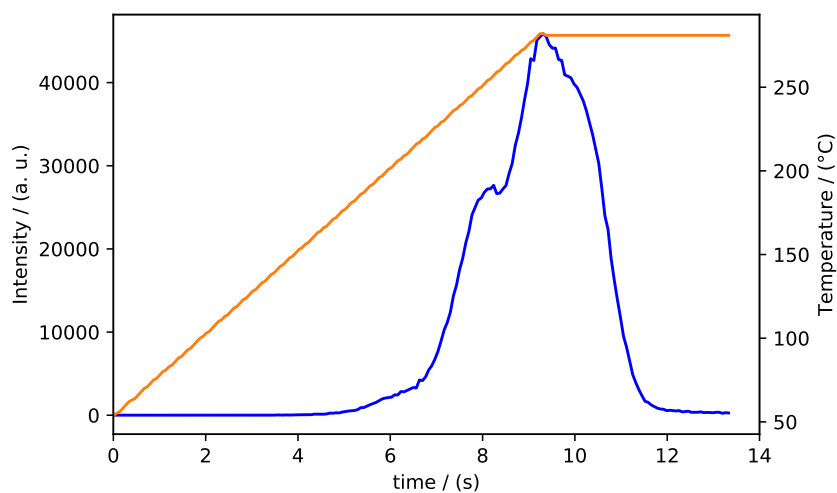


Figure 55: Measured GC with optimized TTP 18 from table 32.

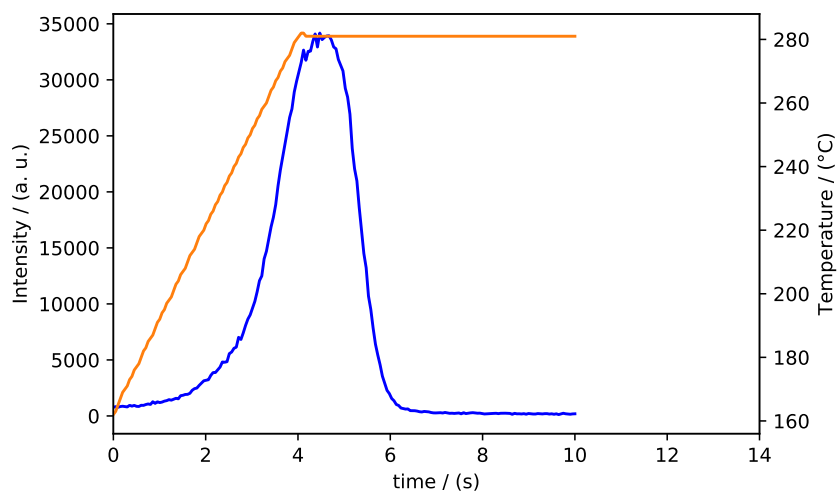


Figure 56: Measured GC with optimized TTP 19 from table 32.

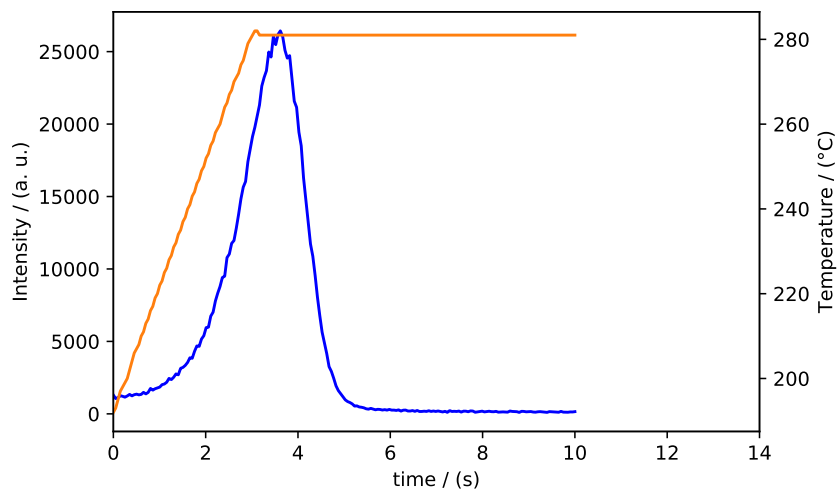


Figure 57: Measured GC with optimized TTP 20 from table 32.

Table 33: Relative standard-deviations from the optimized Time-Temperature Profiles,  
 $\sigma_2 \dots$  Relative standard-deviation of detector 2,  
 $\sigma_3 \dots$  Relative standard-deviation of detector 3.

TTP Nr.	$\sigma_2 / \%$	$\sigma_3 / \%$
1	1.97	1.52
16	1.65	1.37
17	3.21	2.38
18	1.44	1.46
19	2.45	2.39
20	4.60	4.95

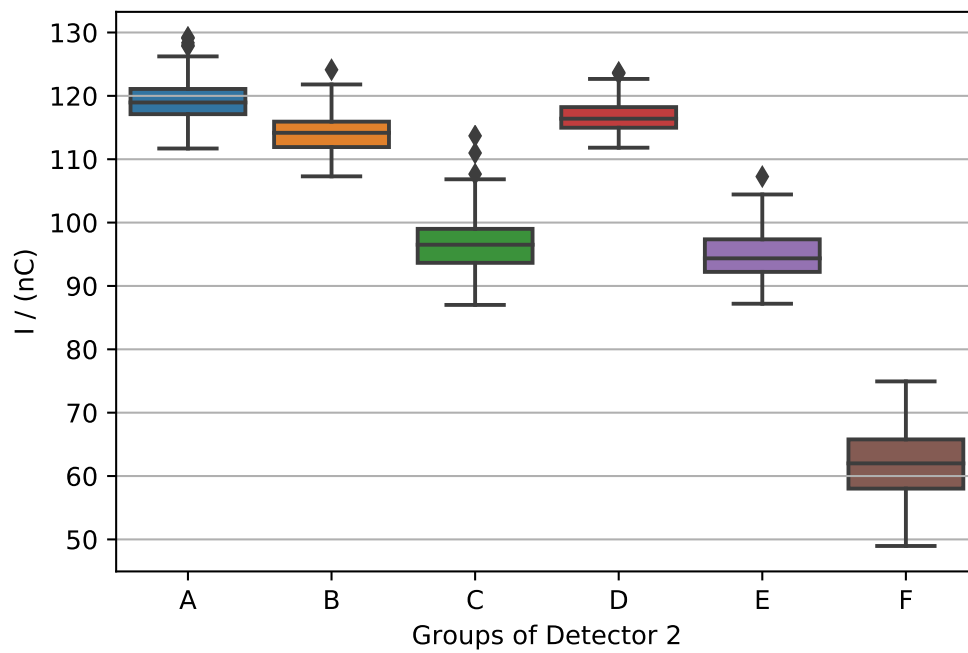


Figure 58: Block diagram of the measurements from detector 2 (TTPs from table 32):

- TTP 1 ... Groupe A
- TTP 16 ... Groupe B
- TTP 17 ... Groupe C
- TTP 18 ... Groupe D
- TTP 19 ... Groupe E
- TTP 20 ... Groupe F
- $I / \text{nC}$  ... TL-Signal.

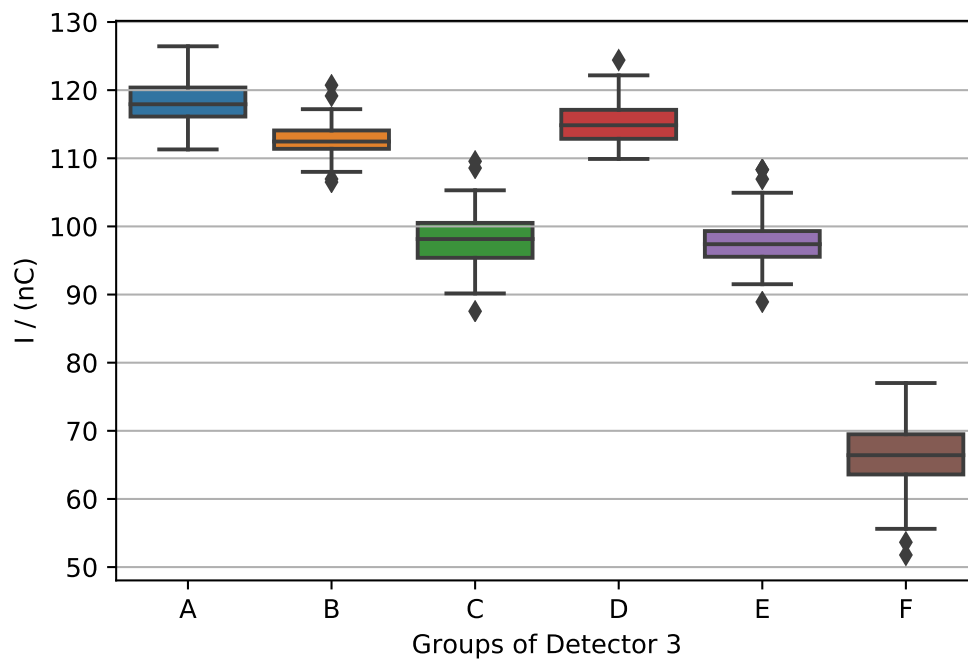


Figure 59: Block diagram of the measurements from detector 3 (TTPs from table 32):

- TTP 1 ... Groupe A
- TTP 16 ... Groupe B
- TTP 17 ... Groupe C
- TTP 18 ... Groupe D
- TTP 19 ... Groupe E
- TTP 20 ... Groupe F
- $I / \text{nC}$  ... TL-Signal.

The relative standard-deviations of the three optimum TTPs and three more with little variations were measured. TTP 18 is similar to TTP 1, but had a lower heating rate, TTPs 19 and 20 are similar to TTPs 16 and 17, but with longer preheat times  $t_{ph}$ . As a main result of this experiment the standard deviations for the measurement of TTPs 1, 2 and 4 turned out small ( $< 2\%$ ). Due to the higher uncertainty to measure just peak 4 and 5 in TTP 3 and 6, the standard deviations increased slightly. At TTP 5, a longer preheat leads to an uncontrolled annealing of fractions of peak 3. It turned out that the best standard deviation belongs to TTP 4, which was the routine TTP with a lower heating rate. This indicates that lower heating rates lead to lower deviations. Furthermore the block diagrams visualize the low deviations in TTP 1 and TTP 2.

## 5. Conclusion

Thermoluminescence dosimetry with LiF:Mg,Ti detectors is one of the most common methods for passive dosimetry in monitoring services.[14] Their advantage is that they produce tissue equivalent responses, they are easy to handle, whether the detectors are encased in cards or in chips for ring dosimeters. The readout process is quick and TLD has a wide measurement range. However, two aspects of dosimetry with LiF:Mg,Ti were studied, according to the measurement of the TL-signal and the handling with the responses:

**Fading of the signal and the sensitivity over time** The fading in LiF:Mg,Ti is an influencing problem and leads to higher uncertainties. It is separated into two phenomena. The pre-irradiation-fading is characterized by the spontaneous collapse of the energy traps in the crystal. This happens at storage temperature before irradiation and is called the sensitivity loss. The post-irradiation-fading appears after irradiation due to the loss of low energy electrons, e.g., the low energy peaks 1, 2 and 3 fades faster. This is called the signal loss.

Coming along with the problem a fading study was performed for several months. This includes three separate experiments under routine conditions of the IMS at Seibersdorf Laboratories. The routine condition was specified as follows: Different routine conditions according to defined time-combinations of  $t_1$  and  $t_2$  were selected for pre- and post-irradiation time respectively. As a result to this study, tables of relative responses for each pre- and post-irradiation time combination were calculated based on the responses and the individual correction factors for each crystal (see tables 10 and 11). Furthermore, the measurements were performed with the readout of two different fast readout TTPs at the end of each experiment. These TTPs have high heating rates  $\beta$ . The TTP 1 from table 6 is provided with a direct readout of the established TTP in the hot gas reader (the Harshaw TLD reader 8800). This represents an experiment, where all peaks fade over time. The TTP 2 from table 6 is provided with a preheat in an external furnace at 95 °C for 20 minutes. This represents an experiment, where peaks one and two were extinguished before the other peaks fade over time. Additionally in a second fading study, samples of time combinations were performed with different fast readout TTPs. Furthermore, for the established TTPs the following fading functions with and without a preheat were calculated:

**TTP with direct readout:**

$$F(t_{\text{tot}}) = 1.0641 \cdot \exp \left[ -\frac{t_{\text{tot}}}{512.1 \text{ days}} \right] + 0.1091 \cdot \exp \left[ -\frac{t_{\text{tot}}}{8.2 \text{ days}} \right] \quad (36)$$

with the parameters  $\kappa_1 = 1.0641$ ,  $\kappa_2 = 0.1091$ , and the time constants  $t_{C,1} = 512.1$  days

and  $t_{C,2} = 8.2$  days. The reference time combination was  $t_1 = 21$  days and  $t_2 = 14$  days. The relative responses  $R_{t_1,t_2}$ , calculated with equation (36), differs from the measured ones with an average of 1.3 %.

**TTP with preheat:**

$$F(t_{\text{tot}}) = 1.0393 \cdot \exp \left[ -\frac{t_{\text{tot}}}{867.9 \text{ days}} \right] \quad (37)$$

with the parameter  $\kappa = 1.0393$  and the time constant  $t_{C,\text{preheat}} = 867.9$  days of fading. The reference time combination was  $t_1 = 21$  days and  $t_2 = 14$  days. The relative responses  $R_{t_1,t_2}$ , calculated with equation (37), differs from the measured ones with an average of 1.1 %.

The fading study with the estimation of a high number of relative responses  $R_{t_1,t_2}$  for several time combinations of  $t_1$  and  $t_2$  and several fast readout TTPs led to the following conclusions and recommendations:

- Defining a fading factor for the dose calculation would be an accurate way to handle with fading. It is a relative response  $R_{t_1,t_2}$ , based on the data from the fading study and the fading functions (36) and (37). This would significantly decrease the uncertainty of the fading component in the dose calculation.
- Both fading functions are good approximations for the measured relative responses  $R_{t_1,t_2}$ . The fading function in equation (36) could be used for other fast readout TTPs, if the applied TTP does not perform a preheat. The fading function in 37 could be used for other fast readout TTPs, if the applied TTP fully extinguish the peaks 1 and 2. At longer time between the anneal and the readout, a lower uncertainty is given. The advantage of these fading functions is that they do not explicit depend on  $t_1$  and  $t_2$ . They only depend on the total time between the anneal and the readout  $t_{\text{tot}} = t_1 + t_2$ , which is always known in an IMS.

**Optimization of the routine readout:** A stable and reproducible glow curve is the most important requirement of TLD. The time-temperature profile has a high influence on the signal qualities. Furthermore the preheat of a crystal influences the fading behaviour - especially when peaks 1 and 2 are fully annealed. It is of great value to find a TTP with stable, reproducible and fast readout GCs for several thousand readouts every month. This lead to the use of higher heating rates  $\beta$  and due to that, non-linearities in the real detector TTP occur.

An optimization of the TTP was performed. The irradiation-tool of the Harshaw TLD System 8800 has been used to vary the TTPs with the same dose of irradiation. Then a GCDC-program was used to simulate several GCs - with the aim to find optimal TTPs. The computerised simulation and the experimental validation yielded in three optimal

TTPs. TTP 1 is the routine TTP without the external furnace, TTP 16 is the preheat TTP, where peaks 1 and 2 were annealed, and TTP 18 is similar to TTP 1 but has a lower heating rate with a lower deviation of the element values in nano Coulomb. According to the results of the optimization process, conclusions and recommendations for an readout optimization could be done:

- It would be useful to exclude the preheat of the TLDs in the external furnace. The annealing of the low energy peaks is the main advantage of the furnace, because of its tendency to decrease the fading. On one hand this could also be handled with a fading function, which result is an accurate fading factor. On the other hand this could be handled with a preheat in the Harshaw TLD Reader 8800, as shown in table 34 with TTP 16. Furthermore, it turned out that fading in routine time combinations showed no significant difference with and without preheat (see tables 12 and 13).
- Based on the results, the three TTPs given in table 34 turned out as optimal. All GCs were stable and there always was a full readout guaranteed. Fast and full-signal readouts would be accomplished by considering one or more of the explained recommendations. In addition all three TTPs are suitable for the readout system of a monitoring service.

Table 34: Optimized Time-Temperature Profiles.

Nr.	$t_{Ph}$ / (s)	$T_{Ph}$ / ( $^{\circ}C$ )	$t_{aq}$ / (s)	$\beta$ / ( $^{\circ}C/s$ )	$T_{max}$ / ( $^{\circ}C$ )
1	0	50	13.33	30	280
16	5	160	10	30	280
18	0	50	13.33	25	280

## References

- [1] IAEA. *Glossary - draft 2016 revision* (2016).
- [2] H. KRIEGER. *Grundlagen der Strahlungsphysik und des Strahlenschutzes*. Lehrbuch. Springer Spektrum, Berlin, Heidelberg, 5. auflage [überarbeitete und aktualisierte] Auflage, 2017.  
doi:10.1007/978-3-662-55760-0
- [3] M. WANNENMACHER, J. DEBUS, F. WENZ. *Strahlentherapie*. Springer (2006).
- [4] E. PICHL. *Lecture Script "Applied Radiation Physics", Nr. PHT.711UF - Graz University of Technology* (2017).
- [5] ICRP. *Recombinations of the International Commission on Radiation Protection*. ICRP (2007a) Publication 103 (2007).
- [6] ICRU. *Quantities and Units in radiation protection dosimetry*. ICRU Report 60 (1999).
- [7] ICRU. *Fundamental Quantities and Units for Ionizing Radiation*. ICRU Report 85 (Bethesda, MD: ICRU) (2011).
- [8] N. PETOUSSI-HENSS, CO. *Conversion Coefficients for Radiological Protection Quantities for External Radiation Exposures*. ICRP Publication 116 (2012).
- [9] ICRU. *Quantities and Units in radiation protection dosimetry*. ICRU Report 51 (1993).
- [10] H. STADTMANN. *Dose Quantities in Radiation Protection and Dosimeter Calibration*. *Radiation protection dosimetry* **96** (2001) 21.  
doi:10.1093/oxfordjournals.rpd.a006584
- [11] ICRP. *ICRP Statement on Tissue Reactions/Early and Late Effects of Radiation in Normal Tissue and Organs - Threshold Dose for Tissue Reactions in a Radiation Protection Context*. ICRP (2007b) Publication 118 (2007).
- [12] IEC. *Radiation protection instrumentation - Measurement of personal dose equivalent  $H_p(10)$  and  $H_p(0.07)$  for X, gamma, neutron and beta radiations - Direct reading personal dose equivalent meters and monitors*. International Standard IEC 61526 (2005).
- [13] IEC. *Radiation protection instrumentation - Passive integration dosimetry systems for environmental and personal monitoring*. International Standard IEC 62387-1 (2007).
- [14] H. STADTMANN, A. MCWHAN, T. GRIMBERGEN, CO. *Eurados Report 2018-01*. Eurados Publication (2018).

- [15] IEC. *Thermoluminescence dosimetry systems for personal and environmental monitoring*. International Standard IEC 61066 (2006).
- [16] A. F. MACKINLAY. *Thermoluminescence dosimetry*. Medical physics handbooks. Hilger, Bristol, 1981.
- [17] R. BOYLE. *Experiments and considerations touching colors* (1664).
- [18] R. CHEN, Y. KIRSH. *Analysis of Thermally Stimulated Processes*. Pergamon Press, Oxford (1981).
- [19] L. Z. LUO. *Extensive fade study of Harshaw LiF TLD materials*. Radiation Measurements **43** (2008) 365.  
doi:10.1016/j.radmeas.2007.11.069
- [20] S. W. S. MACKEEVER, M. MOSCOVITCH, P. D. TOWNSEND. *Thermoluminescence dosimetry materials: Properties and uses*. Nuclear Technology Publ, Ashford Kent, 1995.
- [21] H. STADTMANN, G. WILDING. *Glow curve deconvolution for the routine readout of LiF:Mg,Ti thermoluminescent detectors*. Radiation Measurements **106** (2017) 278.  
doi:10.1016/j.radmeas.2017.03.008
- [22] J. T. RANDALL, M. H. F. WILKINS. *Phosphorescence and electron traps: I. the study of trap distributions*. Proc. R. Soc. London **A184** (1945a) 366–389.
- [23] Y. WEIZMANN, Y. HOROWITZ, L. OSTER, D. YOUSSEAN, A. HOROWITZ. *Mixed-order kinetic analysis of the glow curve characteristics of single crystal LiF:Mg,Ti as a function of Ti concentration*. Radiation protection dosimetry **84** (1999) 047.
- [24] R. VISOCEKAS. *La Luminescence de la Calcite apres Irradiation Cathodique: TL et Luminescence par Effect Tunnel*. PhD Thesis, Universite Pierre et Marie Curie, Paris (1978).
- [25] R. TEMPLER. *The Localised Transition Model of Anomalous Fading*. Radiation protection dosimetry **17** (1986) 493.
- [26] Y. S. HOROWITZ, M. MOSCOVITCH. *Highlights and pitfalls of 20 years of application of computerised glow curve analysis to thermoluminescence research and dosimetry*. Radiation protection dosimetry **153** (2013) 1.  
doi:10.1093/rpd/ncs242
- [27] C. FURETTA. *Handbook of thermoluminescence*. World Scientific Pub. Co, Singapore and Hackensack, N.J, 2010.
- [28] C. FURETTA, M. PROKIC, R. SALAMON, CO. *Dosimetric characteristics of tissue equivalent thermoluminescent solid TL detectors based on lithium borate*. Nuclear Instruments and Methods in Physics Research Section A: Accelerators, Spectrometers, Detectors and Associated Equipment (2001) 411.

- [29] THERMOFISCHERSCIENTIFIC. *Product Overview - Materials and Assemblies for Thermoluminescence Dosimetry* (2007).
- [30] TLDPOLAND. *TLD Poland - Products* (2019).
- [31] S. DOREMUS, G. HIGGINS. *Pre-Irradiation Fade and Post-Irradiation Fade for LiF:Mg,Ti TLD-600, TLD-700, as a Function of Time* .
- [32] B. BURGKHARDT, E. PIESCH. *Fading Characteristics...* .
- [33] R. A. VASILACHE, S. TA<sup>ˆ</sup>NASE-NICOLA, R. TIRON. *Characteristics of TLD-100 fading and its influence on the calibration of personal dosimeters* .
- [34] B. BEN SHACHAR, Y. S. HOROWITZ. *Long-Term Fading of Peak 5 in TLD-100 using Computerised Glow Curve Deconvolution (CGCD) and Thermal Peak Isolation Technique* .
- [35] J. GULBIN, G. DE PLANQUE. *An Investigation of Field Fading in LiF (TLD-700) in an Environmental Monitoring Programme* .
- [36] R. VISOCEKAS, T. CEVA, C. MARTI, F. LEFAUCHEUX, M. C. ROBERT. *Tunneling processes in afterglow of calcite*. *Physica Status Solidi* **35** (1976) 315.
- [37] M. MOSCOVITCH. *A TLD System Based on Gas Heating with Linear Time-Temperature Profile* .
- [38] Y. S. HOROWITZ, L. OSTER, H. DATZ, M. MARGALLOT. *Some dosimetric characteristics of the high temperature TL in LiF:Mg,Ti (TLD-100)*. *Radiation Measurements* **43** (2008) 203.  
doi:10.1016/j.radmeas.2007.09.022
- [39] G. WILDING, H. STADTMANN, W. SPRENGEL. *Improvement of the TLD dose calculation by application of an individual residual dose correction*. *Radiation Measurements* **106** (2017) 273.  
doi:10.1016/j.radmeas.2017.03.039
- [40] H. STADTMANN, C. HRANITZKY, N. BRASIK. *Study of real time temperature profiles in routine TLD read out—influences of detector thickness and heating rate on glow curve shape*. *Radiation protection dosimetry* **119** (2006) 310.  
doi:10.1093/rpd/nci655
- [41] H. STADTMANN, A. DELGADO, J. M. G MEZ-ROS. *Study of Real Heating Profiles in Routine TLD Readout: Influences of Temperature Lags and Non-linearities in the Heating Profiles on the Glow Curve Shape*. *Radiation protection dosimetry* **101** (2002) 141.  
doi:10.1093/oxfordjournals.rpd.a005955
- [42] J. VAN DIJK, F. BUSSCHER. *The Zero Signal and Glow Curves of Bare LiF:Mg,Ti Detectors in a Hot Gas TLD System*. *Radiation protection dosimetry* **101** (2002) 059.

- [43] IAEA. *SSDL Network Charter*. IAEA (2018).
- [44] H. BALIAN, N. EDDY. *Figure of Merit (FOM), an improved criterion over the normalized chi-squared test for assessing the goodness-of-fit of gamma ray spectral peaks*. *Nuclear Instruments and Methods* **145** (1977) 389.

## A. Appendix

### A.1. Time-Temperature Profiles of the Experiments

Table 35: Time-Temperature Profiles of the Experiments. Overview of all TTPs used in this work. (\* A preheat was performed in an external furnace by  $T = 95 \text{ }^\circ\text{C}$  for 20 minutes in addition to the readout.)

TTP Nr. / (s)	$t_{\text{Ph}}$ / (s)	$T_{\text{Ph}}$ / ( $^\circ\text{C}$ )	$t_{\text{aq}}$ / (s)	$\beta$ / ( $^\circ\text{C}/\text{s}$ )	$T_{\text{max}}$ / ( $^\circ\text{C}$ )	Tables
1	0	50	13.33	30	280	4, 6, 30, 31, 32, 34
2	0 *	50	13.33	30	280	6
3	5	140	13.33	30	280	6
4	5	120	13.33	30	280	6
5	0	50	13.33	25	280	6
6	0	50	13.33	30	300	6
7	0	50	13.33	25	300	6
8	3	150	13.33	30	285	30
9	5	145	13.33	30	285	30
10	7	150	13.33	28	290	30
11	5	155	13.33	28	290	30
12	5	160	13.33	28	290	30
13	5	160	13.33	25	290	30
14	5	160	13.33	22	290	30
15	7	160	13.33	25	290	30
16	5	160	10	30	280	31, 32, 34
17	5	190	10	30	280	31, 32
18	0	50	13.33	25	280	32, 34
19	15	160	10	30	280	32
20	15	190	10	30	280	32

## A.2. Additional Details to the Fading Study

### A.2.1. Fading Study under Routine Conditions

**Experiment A1** The readout of the experiment was performed with the established TTP. 5 TLDs of each batch were directly read out in the hot-gas reader and 5 TLDs of each batch were preheated in a furnace for 20 minutes at a temperature of 95 °C. Additionally, after the whole readout the TLDs were calibrated.

Table 36: Time-Temperature Profile of the Routine; for variables and the scheme of a TTP, see figure 10.

$t_{Ph} / (s)$	$T_{Ph} / (°C)$	$t_{aq} / (s)$	$\beta / (°C/s)$	$T_{max} / (°C)$
0	50	13.33	30	280

Table 37: Response time combinations for the A1 fading experiment according to time combinations as seen in figure 7,  
Pre-irradiation time ...  $t_1 / (days)$ ,  
Post-irradiation time ...  $t_2 / (days)$ .

$t_1 \backslash t_2$	0	7	14	21	28	35	42	49
0		x						
7	x				x	x	x	x
14				x	x	x	x	x
21			x	x	x	x	x	x
28		x	x	x	x	x	x	x
35		x	x	x	x	x	x	
42		x	x	x	x	x		
49		x	x	x	x			

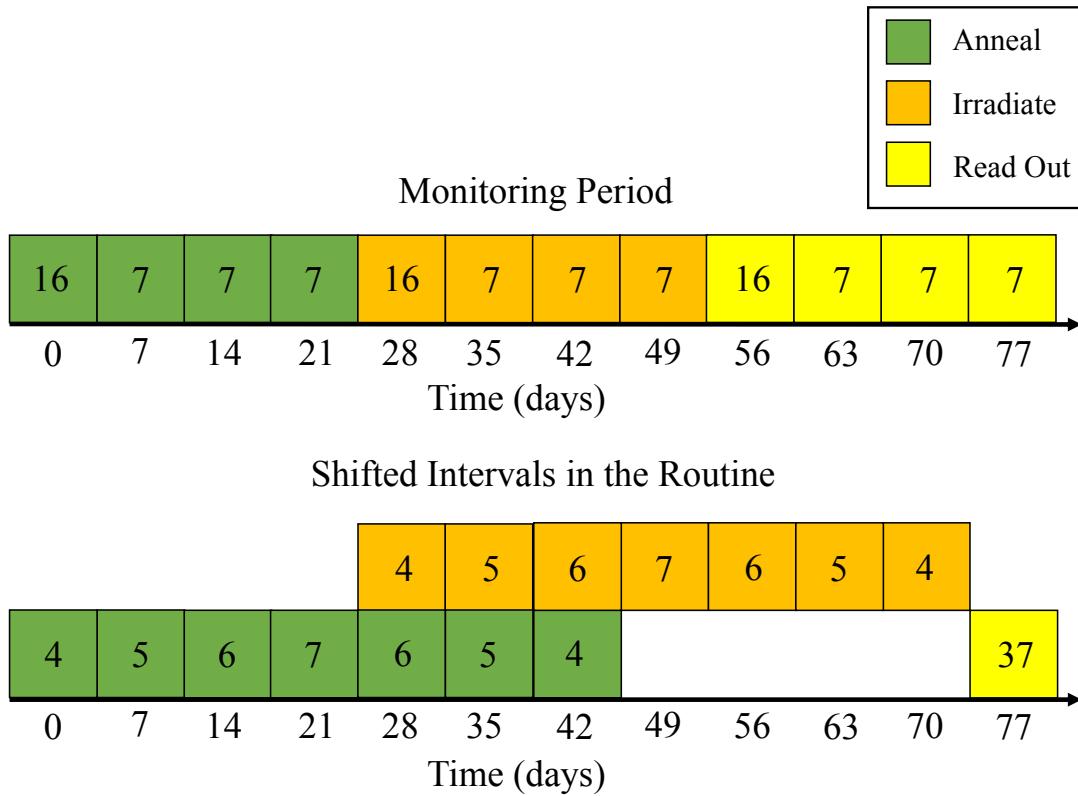


Figure 60: Scheme of the **A1 fading experiment** including the time combinations with and without the shift. The upper diagram shows the typical monitoring period for TLDs in the IMS of Seibersdorf Laboratories. The lower one shows the shifted experimentation plan. All combinations are shifted to a final readout on one single date. The number in the squares gives the number of batches, that had to be annealed, irradiated or read out (1 batch = 10 TLDs with the same time combination).

**Experiment A2** The following short-time fading experiment of about 34 days (approximately one month) was performed to fill the upper triangle of the matrix in table 37. In addition one to three day intervals were taken into account. In table 38 there is a matrix of time combinations for pre- and post-irradiation time. The scheme shows the shift to one readout date (figure 61). According to the fading behavior, reference combinations were defined. In all fading experiments these combinations were measured. In the A2 fading experiment, batches for each time combination of 5 TLDs were used, 5 for a direct readout by the TLD Reader 8800 and 5 with a preheat in the furnace for 20 minutes at a temperature of 95 °C. Additionally, after the whole readout the TLDs were calibrated.

Table 38: Time combinations of A2 fading experiment,  
 Pre-irradiation time ...  $t_1$  / (days),  
 Post-irradiation time ...  $t_2$  / (days).

$t_1 \backslash t_2$	1	3	7	14	21	28
1	x	x	x	x		
3	x	x	x	x		
7	x	x	x	x		x
14	x	x	x		x	
21				x		
28			x			

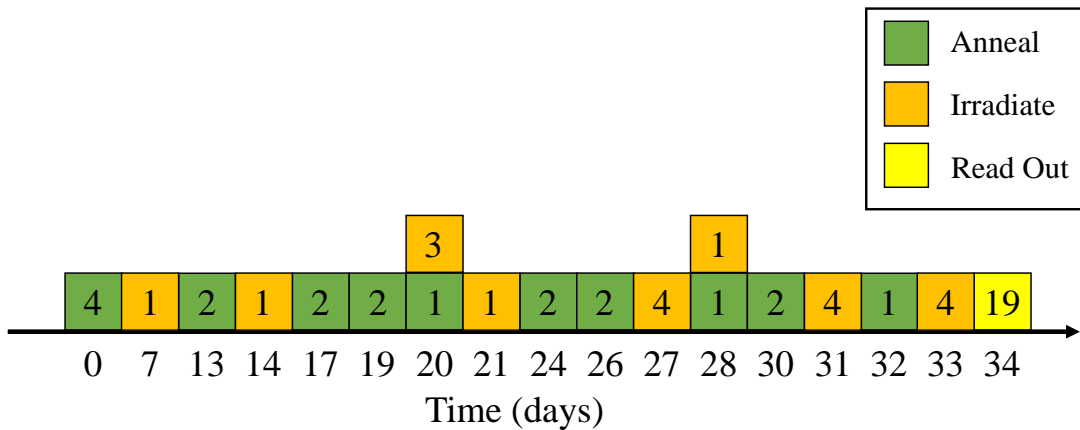


Figure 61: Scheme for the **A2 fading experiment** of the time combinations and the experimental procedure. All combinations were shifted in a way that the readout was on one date. The number in the squares gives the number of batches, that had to be annealed, irradiated or read out (1 batch = 10 TLDs with the same time combinations).

**Experiment A3** Unfortunately three combination batches were not annealed on the necessary date. These values were estimated within a five weeks fading experiment. The references were the same. The matrix for this experiment is depicted in table 39 and the scheme in figure 62. Batches for each time combination of 5 TLDs were used, 5 for a direct read on the TLD Reader 8800 and 5 with a preheat in an external furnace for 20 minutes at a temperature of 95 °C.

Table 39: Time combinations of A3 fading experiment,  
 Pre-irradiation time ...  $t_1$  / (days),  
 Post-irradiation time ...  $t_2$  / (days).

$t_1 \backslash t_2$	7	14	21	28
7			x	x
14		x	x	
21	x	x		
28	x			

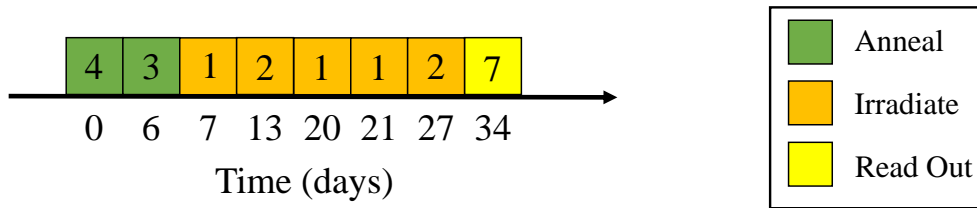


Figure 62: Scheme for the **A3 fading experiment** of the time combinations and the experimental procedure. All combinations are shifted in a way that the read-out was on one date. The number in the squares gives the number of batches, that had to be annealed, irradiated or read out (1 batch = 10 TLDs with the same time combinations).

### A.2.2. Fading Study with different TTPs

**Experiment B** Several time combinations of the upper fading study were selected with the same reference combinations. Batches of 35 TLDs for each time combination were taken for seven TTPs for the readout at the end. Two of them were the routine TTPs with and without any preheat, to compare the fading behavior of the other TTPs. The different TTPs were listed in table 6, the scheme of the time combinations was depicted in figure 40 and the matrix of the time combinations was depicted in figure 63.

Table 40: Time intervals of the B fading experiment

Pre-irradiation time ...  $t_1$  / (days)

Post-irradiation time ...  $t_2$  / (days)

$t_1 \backslash t_2$	0	7	14	21	28	35
1		x				
7	x	x	x		x	
14		x		x		
21			x			x
28		x			x	
35				x		
42			x			
49		x				

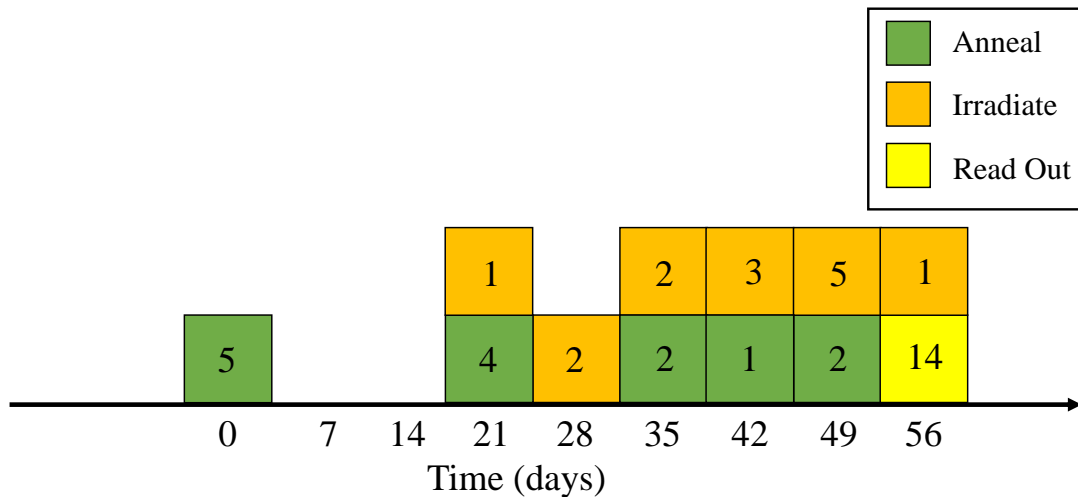


Figure 63: Scheme for the **B fading experiment** of the time combinations and the experimental procedure. All combinations were shifted in a way that the readout was on one date. The number in the squares gives the number of batches, that had to be annealed, irradiated or read out (1 batch = 10 TLDs with the same time combinations).

### A.3. Additional Details to the Readout-Optimization

**Python<sup>TM</sup> script for the calculation of the area under the GC** This Python<sup>TM</sup> script performs the calculation of the area under one or several GCs. The input file is a TXT-file with 200 points of a recorded GC (y-vector) for each row. The input variable  $a$  is the last row in the TXT-file, which should be evaluated with the program, e.g., the program evaluates GCs from row zero to row  $a$ . The second input variable  $b$  is the number of the row for the x-vector of the GC.

The script performs an interpolation of the 200 GC-points and calculates the area under the curve. With that information it is possible to estimate, whether the GC-area under the curve is stable for several TLDs. The TLDs were irradiated with the same dose and read out in the Harshaw TLD Reader 8800 with one specific TTP.

```
# -*- coding: utf-8 -*-
"""
Created on Tue Dec 4 08:41:01 2018

@author: Sorger David
"""

import numpy as np
import matplotlib.pyplot as plt
from scipy.interpolate import interp1d
import scipy.integrate as integral
```

```

## Input START
a = 12 #GC from row 0 to a are evaluated. a is the end and we need txt
      #files
      #as input which start with the intensity vectors of the GC and
      #end with
      #the x vector.
b = -1 #x-Vector
## Input End

## Import Data
A = A.astype(np.float)

Area = np.zeros((a))
Er_area = np.zeros((a))

for z in range(0, a):

    x = A[b,:]
    x_inter = np.linspace(x[0],x[-1],600)

    y = A[z,:]

##Normation fo GC
    y_norm = np.zeros((200))

    for i in range(0, 200):
        y_norm[i] = y[i] / sum(y)

#### Interpolation with cubic spline and numerical integration START

    f = interp1d(x,y,kind='linear')
    In = integral.quad(f,x[0],x[-1])

    f_norm = interp1d(x,y_norm,kind='linear')
    In_norm = integral.quad(f_norm,x[0],x[-1])

#### Interpolation with cubic spline and numerical integration END

#### Plot of GC START

    plt.plot(x,y,'go',linewidth=2)
    plt.plot(x_inter,f(x_inter),'r-',linewidth=2)
    plt.xlabel('time / (s)')
    plt.ylabel('I / (nC)')
    plt.xlim(0, 14)
    plt.grid(True)
    plt.legend(('Measurement', 'Cubic Spline'))
    plt.show()

    plt.plot(x,y_norm,'go',linewidth=2)
    plt.plot(x_inter,f_norm(x_inter),'r-',linewidth=2)
    plt.xlabel('time / (s)')
    plt.ylabel('I / (a.u.)')

```

```

plt.xlim(0, 14)
plt.grid(True)
plt.legend(('Measurement', 'Cubic Spline'))
#plt.savefig('GlowCurve_303549.pdf')
plt.show()
print('Area = ', In[0], 'pm', In[1])
print('Area normed = ', In_norm[0], 'pm', In_norm[1])

Area[z] = In_norm[0]*10**3
Er_area[z] = In_norm[1]*10**3

#### Plot of GC END

points = np.linspace(1,a,a)
Mean_area = np.mean(Area)

stand = np.sqrt(1/(a-1) * sum((Area - Mean_area)**2))
stand_rel = stand / Mean_area * 100
maxi_stand = max(Area - Mean_area) / Mean_area * 100

#plt.errorbar(points, Area, yerr=stand, fmt='o', linewidth=1)
plt.plot(points,Area,'go',linewidth=4)
plt.plot([1,a],[Mean_area,Mean_area], 'r',linewidth=2)
plt.title('Variance = ' + str(round(stand_rel,4)) + '%, Mean Area = ' +
          str(round(Mean_area,4)) + ', Max.
          Abw. = ' + str(round(maxi_stand,4)) +
          '%')

#plt.plot(points,Er_area,'ro',linewidth=2)
plt.xlabel('Points')
plt.ylabel('Area / (area unit)')
plt.xlim(0, 14)
plt.grid(True)
plt.legend(('Area under the curve', 'Average Area',))
plt.savefig('TTP_8.pdf')
plt.show()

X = np.zeros((2,a))
X[0] = Area
X[1] = stand_rel

np.savetxt('TTP_8.txt', X, fmt='%.18e', delimiter=' ', newline='\n',
          header='Relative Area / (area unit)
          Variance / (%)', footer='',
          comments='# ', encoding=None)

```

### A.3.1. Peak-Modification in the GCDC Program

A modification in the GCDC program was performed to get qualitative assessments of the GC by making qualitative assessments of the glow peaks.

The program calculated a fit onto the measurement data and estimated 200 values for every peak (200 channels).  $I$  was defined as the intensity of the TL signal of the GC,  $I_i$  as the calculated intensity of peak  $i$  and  $I_{ij}$  as the calculated intensity at peak  $i$  by channel  $j$ .

$$I = \sum_{i,j} I_{ij} \quad (38)$$

Then the normalized intensities were estimated to make general assessments.

$$P_{ij} = \frac{I_{ij}}{I} \quad (39)$$

$$P_i = \sum_j P_{ij} \quad (40)$$

$P_{ij}$  is defined as the normalized value of the intensity at peak  $i$  by channel  $j$ ,  $P_i$  to be the normalized value of the intensity at peak  $i$  and

$$P = \sum_i P_i = 1.0. \quad (41)$$

In addition to the calculation of the  $P_i$  values, the function "TABLE()" in MS Excel™ was used to variate two parameters at the same time; an example is depicted in figure 64.

$T_{Ph}$

$t_{Ph}$

Peak 3	$T_{Ph}$	$t_{Ph}$						
9,65E-02	165	167,5	170	172,5	175	177,5	180	
-3	13,1%	12,5%	11,7%	10,9%	9,9%	8,8%	7,6%	
-4	12,2%	11,4%	10,4%	9,4%	8,3%	7,0%	5,8%	
-5	11,3%	10,3%	9,3%	8,1%	6,9%	5,6%	4,4%	
-6	10,4%	9,4%	8,2%	7,0%	5,7%	4,5%	3,3%	
-7	9,6%	8,5%	7,3%	6,0%	4,7%	3,5%	2,5%	
Peak 4	$T_{Ph}$	$t_{Ph}$						
3,70E-01	165	167,5	170	172,5	175	177,5	180	
-3	36,4%	36,5%	36,7%	36,8%	36,9%	37,0%	37,0%	
-4	36,6%	36,8%	36,9%	37,0%	37,0%	37,0%	36,8%	
-5	36,8%	36,9%	37,0%	37,1%	37,0%	36,9%	36,5%	
-6	36,9%	37,0%	37,1%	37,1%	36,9%	36,6%	36,1%	
-7	37,0%	37,1%	37,1%	37,0%	36,8%	36,3%	35,5%	
Peak 5	$T_{Ph}$	$t_{Ph}$						
5,33E-01	165	167,5	170	172,5	175	177,5	180	
-3	50,3%	50,9%	51,6%	52,3%	53,2%	54,2%	55,4%	
-4	51,1%	51,8%	52,7%	53,6%	54,7%	56,0%	57,4%	
-5	51,9%	52,7%	53,7%	54,8%	56,1%	57,5%	59,1%	
-6	52,6%	53,6%	54,7%	55,9%	57,3%	58,9%	60,6%	
-7	53,3%	54,4%	55,6%	57,0%	58,5%	60,2%	62,0%	

Figure 64: Example of the variation of TTP parameters. The preheat temperature  $T_{Ph}$  was varied in steps of 2.5 between 165 °C and 180 °C. The preheat time  $t_{Ph}$  was varied in steps of 1 between 3 s and 7 s. The values in the table were negative, due to program intern conventions. In the matrix the possible peak proportion values on the total GC  $n$  in % are depicted. It gives the information of the peak intensities with the applied parameters.

### A.3.2. Qualitative Analysis on one Glow Curve

One GC was measured and fitted with the deconvolution. Then the fit was modified by changing the TTP parameters, starting from adequate default values. The analysis was performed as follows:

- Preheat:  $T_{\max} = 290^{\circ}\text{C}$ ,  $t_{\text{aq}} = 10$  s,  $\beta = 28^{\circ}\text{C/s}$  (all default values). The preheat temperature and the preheat time was varied.
- Variation of  $T_{\max}$  and  $\beta$ : Improved values for  $T_{\text{Ph}}$  and  $t_{\text{Ph}}$  and the default value for  $t_{\text{aq}} = 10$  were used.
- Variation of the experimental parameter  $A$  (see equation (21)) and  $t_{\text{aq}}$ : Improved values for  $T_{\text{Ph}}$ ,  $t_{\text{Ph}}$ ,  $T_{\max}$  and  $\beta$  were used.
- Preheat: The preheat parameters were optimized with the further optimized values.

Table 41: First **Starting Parameters** of the simulation, based on the fitting of calibration glow curves,  
 Shift Parameter ...  $A$  / s,  
 Trap energy ...  $E$  / eV,  
 Logarithmic frequency factor ...  $\log(s)$  /  $\log(\text{s}^{-1})$ ,  
 Peak proportion on the GC ...  $n$  / %,  
 Maximum temperature ...  $T_{\max}$  /  $^{\circ}\text{C}$ .

FOM:			A:	1,77
pk	E	log(s)/E	n	$T_{\max}$
1	0,82	13,8	0,06	159
2	1,35	11,7	0,21	159
3	1,38	10,8	0,12	202
4	1,53	10,2	0,26	229
5	1,84	9,6	0,35	253

### A.3.3. Optimization Process

The deconvolution and the evaluation was performed as follows:

1. Based on the knowledge of the previous experiments, a starting interval with the following parameters could be defined:  $\beta = [22, 30]^{\circ}\text{C/s}$ ,  $T_{\max} = [275, 295]^{\circ}\text{C}$ ,  $T_{\text{Ph}} = 50, [110, 190]^{\circ}\text{C}$ ,  $t_{\text{Ph}} = [3, 15]$  s and  $t_{\text{aq}} = [6, 15]$  s.
2. Analysis of GC1: At first a "typical" calibration GC was deconvolved. The kinetic parameters (fit parameters) are listed in table 42. To make an accurate fit of GC 1 the kinetic parameters could be fixed for the simulation, or varied. Two fitting simulations were carried out; the first one with variable  $E_1$ ,  $E_2$ ,  $E_4$ ,  $E_5$ ,  $\log(s_3)$ ,

- $\log(s_4)$ ,  $\log(s_5)$ ,  $n_3$ ,  $n_4$  and  $n_5$ ; and the second one with variable  $E_3$ ,  $E_4$ ,  $E_5$ ,  $\log(s_3)$ ,  $\log(s_4)$ ,  $\log(s_5)$ ,  $n_3$ ,  $n_4$  and  $n_5$ .
3. Analysis of GC1: Two parameters were varied at the same time while the other parameters were kept constant. This procedure was carried out for several times. The spectra could be enclosed:  $\beta = [25, 30]^\circ\text{C/s}$ ,  $T_{\max} = [275, 285]^\circ\text{C}$ ,  $T_{\text{Ph}} = 50, [160, 200]^\circ\text{C}$ ,  $t_{\text{Ph}} = [5, 13.33]$  s and  $t_{\text{aq}} = [10, 15]$  s.
  4. Analysis of GC2: A short interval GC was deconvolved. The kinetic parameters are listed in table 43. The first fitting simulation was performed with the variable parameters  $E_2$ ,  $E_3$ ,  $E_4$ ,  $E_5$ ,  $\log(s_2)$ ,  $\log(s_5)$ ,  $n_1$ ,  $n_2$ ,  $n_3$  and  $n_4$ . The second one had the same variable parameters, except of  $n_4$ ; in this simulation  $n_5$  was a variable parameter.
  5. Analysis of GC2: Two parameters were varied at the same time while the other parameters were kept constant. This procedure was carried out for several times.  $t_{\text{aq}}$  was limited to 10 s and 13.33 s. Several simulations were performed with these parameters. The heating rate was limited to the optimum value of  $30^\circ\text{C/s}$ . The maximum temperature was limited to the optimum value of  $280^\circ\text{C}$ . For the preheat parameters it was possible to fully extinguish the low energy peaks. Peak 1 and 2 were extinguished with  $t_{\text{Ph}} = 5$  s and  $T_{\text{Ph}} = 160^\circ\text{C}$ . Peak 1, 2 and 3 were extinguished, but the optimum values were not found at this point. So the spectra was  $T_{\text{Ph}} = [190, 200]^\circ\text{C}$ ,  $t_{\text{Ph}} = [5, 10]$  s.
  6. Analysis of GC3: A "typical" routine GC was deconvolved. The kinetic parameters are listed in table 44. One fitting simulation was carried out. The variable parameters were  $E_3$ ,  $E_4$ ,  $E_5$ ,  $\log(s_2)$ ,  $\log(s_3)$ ,  $\log(s_4)$ ,  $n_2$ ,  $n_3$ ,  $n_4$  and  $n_5$ .
  7. Analysis of GC3: Two parameters were varied at the same time while the other parameters were kept constant. This procedure was carried out for several times. For the preheat parameters the low energy peaks could be fully extinguished. The optimum for a TTP without any preheat was found. In addition an optimum TTP with an extinction of peaks 1 and 2 and the extinction of peaks 1, 2 and 3 with a preheat has been found.
  8. Finally the TTPs were verified in the simulation with several routine and calibration GCs.

Table 42: Kinetic parameters of GC1.

Shift Parameter ...  $A$  / s,  
 Trap energy ...  $E$  / eV,  
 Logarithmic frequency factor ...  $\log(s)$  /  $\log(s^{-1})$ ,  
 Peak proportion on the GC ...  $n$  / %,  
 Maximum temperature ...  $T_{\max}$  / °C.

<b>FOM:</b>		2,94%	<b>A:</b>	2,04
<b>pk</b>	<b>E</b>	<b>log(s)/E</b>	<b>n</b>	<b>T<sub>max</sub></b>
1	0,76	13,8	0,06	99
2	1,33	11,7	0,21	165
3	1,87	10,7	0,05	207
4	1,04	10,2	0,41	225
5	2,39	9,6	0,28	254

Table 43: Kinetic parameters of GC2.

Shift Parameter ...  $A$  / s,  
 Trap energy ...  $E$  / eV,  
 Logarithmic frequency factor ...  $\log(s)$  /  $\log(s^{-1})$ ,  
 Peak proportion on the GC ...  $n$  / %,  
 Maximum temperature ...  $T_{\max}$  / °C.

<b>FOM:</b>		2,48%	<b>A:</b>	2,38
<b>pk</b>	<b>E</b>	<b>log(s)/E</b>	<b>n</b>	<b>T<sub>max</sub></b>
1	0,76	13,8	0,00	
2	1,40	11,8	0,04	164
3	1,89	10,7	0,15	206
4	1,55	10,2	0,33	228
5	2,00	9,7	0,47	248

Table 44: Kinetic parameters of GC3.

Shift Parameter ...  $A$  / s,

Trap energy ...  $E$  / eV,

Logarithmic frequency factor ...  $\log(s)$  /  $\log(s^{-1})$ ,

Peak proportion on the GC ...  $n$  / %,

Maximum temperature ...  $T_{\max}$  / °C.

<b>FOM:</b>		1,62%	<b>A:</b>	2,52
<b>pk</b>	<b>E</b>	<b>log(s)/E</b>	<b>n</b>	<b>T<sub>max</sub></b>
1	0,76	13,8	0,00	
2	1,40	11,2	0,00	
3	1,60	10,9	0,10	201
4	1,97	10,1	0,25	230
5	1,77	9,7	0,65	245

## B. Abbreviations

CGCD	Computerised Glow Curve Deconvolution
DEL	Dosimetry Laboratory Seibersdorf
FOM	Figure of Merit
GC	Glow Curve
Gy	Gray
IAEA	International Atomic Energy Agency
ICRP	International Commission on Radiation Protection
ICRU	International Commission on Radiation Units and Measurements
IMS	Individual Monitoring Service
PIF	Panoramic Irradiation Facility
PMT	Photomultiplier tube
ROI	Range of Interest
TL	Thermoluminescence
TLD	Thermoluminescence Dosimeter
TTP	Time-Temperature-Profile
SL	Seibersdorf Laboratories
SSDL	Secondary standard dosimetry laboratory
Sv	Sievert